DYNAMIC ANALYSIS OF JACK-UPS

comparison of simulations with field-measurements

by A.W. Kraak

Final thesis, June 1990

Hydraulic Engineering Group
Faculty of Civil Engineering
Delft University of Technology

in co-operation with:

Hydro-dynamics group
LRP/3
Shell Research B.V.
Rijswijk

PREFACE

The study presented in this report has been carried out as final thesis work for the Department of Civil Engineering of the Delft University of Technology. All the work has taken place at the research laboratory of Shell at Rijswijk (KSEPL), but supervision has been obtained from KSEPL as well as the TU Delft. I would like to thank all people who have contributed to this work and especially:
Ali Anatürk and Peter Tromans of LRP3 for their supervision during my stay at KSEPL and Prof. dr. ir. J.A. Battjes, ir. M.W.J.W. Dijkman and W.W. Massie M.Sc. for their support from the TU Delft.

Arie Kraak
Rijswijk, June 1990

SUMMARY

Jack-up offshore structures have a natural period which lies in the high frequency tail of the spectra of North Sea storm waves. This tail has significant energy and the jack-up may experience significant dynamic response.

Data have become available from field measurements of the dynamic behaviour of the Maersk Guardian jack-up rig. These data have been compared to simulations performed with Shell's time domain dynamic analysis program 'DYNAL'. A simplified model of the Maersk Guardian has been developed, and has been used in the simulations under environmental conditions similar to those during the measurements.

A comparison has been made between the simulated and the measured deck accelerations and leg forces, by examining spectra and time histories. The results of the simulations were in reasonably good agreement with the measurements. Further research on the damping, the deck to leg connection and the foundation stiffness is desirable.

CONTENTS

1. INTRODUCTION

Jack-up platforms are in operation on a wide scale, generally in shallow water (less than 100 meters depth). A jack-up is distinguished from fixed structures, such as jackets, by the relative ease with which it can be moved from one location to another. The deck of the jack-up can be raised or lowered relative to its legs by means of the jacking mechanism (fig. 1 and 10). The deck is at its lowest position during transport and floats like a ship (fig 3). The legs of the jack-up are moved downward during installation until they touch the bottom of the sea. Further jacking raises the deck out of the water. When it has reached its working height the deck will be clamped to the legs.

Tanks at the deck are temporary filled with water before the jack-up will be operative, to preload the foundation and ensure a certain bearing capacity of the ground.

Since the legs of a jack-up are only connected to each other by the deck, the stiffness of a jack-up is relatively small compared to that of a jacket structure. The lowest natural frequency of a jack-up platform is typically in the high frequency tail of the water surface elevation spectrum of storms. This tail has significant energy and thus causes dynamic response of the jack-up platform.

Several computer programs are available for the estimation of the dynamic behaviour of jack-ups. The most sophisticated program available at Shell is DYNAL which performs non-linear, time-domain, dynamic analysis under three-dimensional wave loading.

Shell and Exxon have performed field-measurements of the dynamic response of a jack-up platform which makes it possible to test the dynamic analysis models in DYNAL with the measured dynamic behaviour.

The aim of the present study is to perform such a comparison and to develop an accurate model which may be used for the analysis of extreme sea conditions. However, some restrictions have to be considered:

- the data on which this comparison is based are obtained from measurements in relatively mild sea conditions, which may make any subsequent application to extremes questionable,
- the comparison is made for measurements for only one storm and one particular jack-up.

This report will discuss the following steps:

- a description of the jack-up Maersk-Guardian and the measurement programme as performed by Shell and Exxon;
- a short description of the main features of the DYNAL program;
- a general description of the main input-parameters required for the DYNAL program;
- a description of the model of the Maersk-Guardian and the three-dimensional wave loading model;
- a sensitivity analysis of the model;
- a comparison of the measured and predicted global responses of the jack-up;
- some conclusions and remarks on the next steps to be taken.

2. SURVEY OF THE JACK-UP AND THE MEASUREMENTS

2.1. DESCRIPTION OF THE MAERSK GUARDIAN

The Maersk Guardian and its sister 'Maersk Giant' are independent three leg, self elevating, cantilever, jack-up, drilling rigs of the Hitachi Zosen design. The total mass of the deck is approximately 16.000 tons while the legs have a mass of about 1.600 tons each.

Some dimensions are:

Length overall	: 84,6 m
Width overall	: 90,0 m
Length of legs	: 156,8 m

Some weather/design criteria are:

Water depth	: 106,7 m
Wind speed	: 45,0 m/s (87 knots)
Leg penetration	: 5,0 m
Current (surface)	: 0,8 m/s
Air gap	: 21,0 m

2.2. NORTH SEA JACK-UP MEASUREMENTS ON MAERSK GUARDIAN

During the winter of 1988-1989 field measurements were made on the Maersk Guardian jack-up rig, located at Silver Pit Block 44/26-D, in the southern North Sea. This measurement programme was carried out by Exxon Production Research Co. (EPR), for Shell Expro, operator of the Shell/Esso joint fields in the U.K. sector of the North Sea.

The Maersk Guardian at the Silver Pit location was situated on a firm sandy bottom in 70,1 m (230 ft) water. Data each were collected during four interesting storms. The main features of these storms have been listed in table 1.
The maximum individual wave height measured is about 6,1 m (20 ft) which is significantly less than the design wave of 18,3 m (60 ft).

All data segments have a duration of one hour with a sample frequency of 2 Hz. Strain gages were installed at chord members (6 gages per chord) to obtain axial forces, while strain gages at brace members were used to obtain shear forces (2 gages per brace member). All data was reviewed to assure the data was free of noise. The strain gages were typically accurate to within 2 percent. For more information on the data processing and the measurements see ref. 1.

The quantities obtained directly from measurements on the jack-up were (see fig. 5 and 6):

- axial leg forces, using strain gages on chords in bay 7 and 19;
- shear forces in the legs near the deck-leg connection, using strain gages on braces in bay 19 and 23;
- deck accelerations, using two accelerometers located on the deck, both measuring two accelerations in mutual perpendicular directions.
- current velocity, using two current meters, both measuring in two horizontal directions;
- wave height, using wave sensors at two locations on the deck;
- wind speed and direction, using the anemometer at top of the derrick.

These quantities have been stored on records which were available at KSEPL. A Fortran program has been written which prepares the input for an existing program which produces plots of time histories and spectra.

The lowest natural frequencies of the jack-up can be estimated from the deck acceleration spectra. Fig. 7 shows the measured surface elevation spectrum in combination with the acceleration spectrum of the bow in x and in y direction. Three different frequencies may be distinguished in the spectra. The first frequency corresponds to the dominant peak of the surface elevation spectrum, while the other frequencies correspond to natural frequencies of the structure. Since at the bow the y direction is normal to motion generated by rotation it is obvious that the second frequency corresponds to a bending mode, while that the third frequency corresponds to a torsional mode.

Besides the estimation of the natural frequencies, some estimate of the damping ratio may be made from the response spectra as well. This will be discussed in appendix A6.

3. DESCRIPTION OF SHELL'S DYNAMIC ANALYSIS MODEL DYNAL III

3.1. GENERAL FEATURES

DYNAL III is the third generation of a computer program for the dynamic and static analysis of three-dimensional offshore structures. Several dynamic loads can be applied to the structure including seismic loads, wave loads or any other user defined periodic load. The real structure is represented by a multi degree-of-freedom system for which the dynamic response is governed by the following coupled differential equations of motion:

$$[M] \{\ddot{U}\} + [C] \{\dot{U}\} + [K] \{U\} = \{F(t)\}$$

[M] = mass matrix
[C] = damping matrix
[K] = stiffness matrix
{U} = displacement vector
{F(t)} = applied load vector

DYNAL simplifies the solution of the equations of motion by ignoring the off diagonal mass terms in the mass-matrix.

For wave or other time varying loading three solution methods are available:

1. static response in the time domain
2. modal superposition in the time domain
3. modal dynamic with static correction in the time domain (=mode acceleration method)

1. Static response:

Dynamic effects are not taken into account; the (quasi)static response is calculated at every time step that the force is evaluated.

2. Modal superposition:

The dynamic response of the multi degree-of-freedom system is analysed by uncoupling the coupled differential equations. Each uncoupled single degree-of-freedom equation corresponds to a mode shape and a natural frequency. The total response is the sum of these vibration modes. For large offshore structures it is expensive and impractical to include all the modes in the solution. The global response however is determined by only the first few (lower frequency) modes. Therefore only a few modes of vibration are used in the total solution. However, higher modes may be important for calculation of local deformation patterns and thus local stresses.

3. Modal dynamic with static correction

This method is available to improve the pure modal superposition especially for the calculation of local stresses. In a system vibrating at low frequencies the higher frequency modes will not contribute to the inertia and damping forces. The response of the higher modes is thus essentially static. By using first the pure modal superposition method the inertia forces are calculated and added to the applied forces. After that an improved displacement pattern of the structure is calculated from a straightforward static analysis.

DYNAL is a program which requires two, major, user-defined inputs. The first is the description of the structure (structural model), including proper joints, joint connecting members, extra masses, foundation stiffness, and leg to hull stiffness The second is the description of the environmental conditions (sea-state model), including water-depth, wave heights and current-velocities, wind-loads and other environmental conditions affecting the behaviour of the structure, such as loads due to the operation of the offshore platform.

3.2. STRUCTURAL MODEL

3.2.1 Introduction

The structure will be modelled by defining joints and members connecting these joints. DYNAL distinguishes members which carry wave loads (wave load members) and members which do not (structural members). The latter contribute only to the stiffness and mass of the structure while the first only contribute to the loading. In some cases the two types can be combined into one carrying wave load as well as contributing to the mass and stiffness of the structure.

3.2.2. Members

structural members

There are three basic types of structural member available:

1. circular members
2. non-circular members
3. shim or pseudo members

The first tupe is defined by its diameter and wall-thickness while the second one is defined by its cross-sectional area, shear area, and moments of inertia, bending as well as torsional. The third member type only transmits forces by means of a spring from one joint to the other. The shim type has a zero length and transmits forces only in a horizontal plane (global x and y directions), employing a user-given spring stiffness. The pseudo member type transmits forces as well as moments in all directions (rotational as well as translational) employing user-given spring stiffnesses.

fluid loading members

Fluid loading members have no weight associated with them, and only carry wave loading. The properties of these members can be given as a diameter for a circular cylinder or as projected area per unit length and volume per unit length parallel to the member axis in case of non-circular members. The projected area is assumed to be independent of the direction of flow-attack. Marine growth thickness can be specified and will increase the diameter in the first case and initiate the use of rough Morison coefficients. For non-circular members the user has to estimate the increment of the projected area and volume due to marine growth.

3.2.3. Joints

Three types of joints can be distinguished:

1. standard joint
2. fixed boundary joint
3. spring supported boundary joint

A standard joint has six degrees of freedom (x-,y- and z- translations and rotations about the x-,y- and z-axis). For a fixed boundary joint, the number of degrees of freedom can be constrained for each joint by fixing one or more global degrees of freedom. Spring supported boundary joints are constrained by springs that restrain the movement in the global coordinate system.

3.2.4. Mass

There are two ways to deal with the lumping of the masses, which can be combined. The first one involves the lumping of the masses at the joints and is performed by the program itself; while the second option involves applying user calculated (extra) masses at the joints. In the first case

DYNAL lumps the mass and calculates the mass inertia about the joint by considering one half of the mass of all members incident on the joint plus the user given extra mass and mass inertia at that joint. The actual mass lumped is the mass of the steel, mass of the water enclosed in the member, added or virtual mass and the mass due to marine growth on the member. In the second case all members are assumed to have zero mass and the lumping of the masses and moments of inertia mentioned above should be pre-calculated by the user.

3.2.5. Damping

Structural damping is assumed to be viscous and is specified as the fraction of the critical damping for each normal mode. For three-dimensional random wave analysis hydrodynamic damping can also be accounted for by using relative velocities, that is by including the structure motion in Morison's wave force equation.

3.3. SEA STATE MODEL

3.3.1. Introduction

The second major input is the description of the sea state for the calculation of the wave kinematics required to obtain fluid forces from Morison's equation.

3.3.2. Waveloading models

In DYNAL it is possible to analyze the structure under two-dimensional regular wave loading or under three-dimensional, irregular, random wave loading. In the first case wave kinematics are calculated using a periodic wave theory (Stokes' fifth order, Airy or Chappelear's wave theory).

In the second case wave kinematics input has to be calculated by a separate program called DYNSCRN which uses its module GENERATE to calculate random wave kinematics from a user-defined directional surface elevation spectrum.

The module GENERATE gives wave kinematics up to the mean water level (MWL). However, the kinematics in the crests, above the MWL, are very significant for the wave force calculation. Thus DYNAL has several options for estimating the kinematics in the wave crests: linear extrapolation, vertical extrapolation and the so called delta stretching. The latter option is an empirical extension of the theoretical wave kinematics to the free surface (see fig 8).

From the calculated wave kinematics DYNAL calculates the force distribution on the structure using the Morison equation with user given drag and inertia coefficients, including relative velocities if required.

3.4. DESCRIPTION OF 'GENERATE'

3.4.1. Introduction

GENERATE is a program which generates wave kinematics that match an irregular random sea surface. The program needs as input the physical form of the structure, that is the joints and the members connecting these joints, a three-dimensional grid which covers that part of the sea where wave kinematics should be calculated, a wave spectrum and information on the current.

A special feature of the program is the ability to generate wave kinematics and/or surface elevations in the time domain such that they fit a measured wave kinematic and/or surface elevation record. This so called conditioned simulation can be used instead of an ordinary time domain generation of wave kinematics.

3.4.2. 'GENERATE' input

joints and members

The joints and members have been defined for the DYNAL input and may be used for the GENERATE input as well.

grid

The accuracy of the description of the sea state is directly related to the number of grid points used. The largest forces acting on the structure occur where the water particle velocities and accelerations are largest; that is near the sea surface. Moreover, the kinematics have their steepest gradients near the surface. Thus the grid point spacing should decrease from mudline to water surface. GENERATE deletes superfluous grid points to minimize the number of points at which kinematics have to be calculated.

wave spectrum

GENERATE has several options for the wave spectrum. A user-defined one-dimensional or two-dimensional frequency spectrum can be used as input or the default Pierson-Moskowitch or JONSWAP frequency spectrum in combination with one of the default directional spreading functions (Von Mises spreading, cosine power spreading and wrapped normal spreading). All functions are dependent on frequency and angle with respect to the central direction. The central direction angle may also differ for different frequencies.

The user-defined one-dimensional frequency spectrum can also be used in combination with the default spreading functions.

If there is a current at mean water level, GENERATE may account for the Doppler shift by assuming that the input frequency spectrum is specified in a reference frame, moving with the current (shift = off), or in a fixed reference frame (shift = on).

3.4.3. 'GENERATE' simulation techniques

introduction

Two different simulation techniques may be distinguished: the so called conditioned simulation technique and the 'ordinary' time domain simulations. The conditioned simulation technique is more time consuming and more input is required, but is likely to give more accurate results.

simple time domain simulations

In a simple time domain wave simulation, the program uses inverse Fast Fourier transformation of the surface elevation spectrum to determine wave amplitudes for each frequency; it simulates an irregular wave surface and wave kinematics by summation of the different contributions with random phases for each contribution. The kinematics as generated in a simple time domain simulation always have the constraint that the frequency spectrum of the simulated sea must match the frequency spectrum used as input. The wave kinematics generated in this way are calculated in the time domain for each grid point and stored internally for use as input to the DYNAL program.

conditioned simulations

In conditioned simulation techniques, the program uses information on a measured variable to improve its random simulation of the sea surface. When at certain grid points wave kinematic records are available from, for example, measurements, GENERATE has the ability to use this time record as a constraint (condition the variable) for the simulated kinematics. GENERATE tries to minimize the error between the simulated kinematics and the conditioned kinematics at these particular points.

An abstract of the theoretical background is given in appendix A4.

4. A (SIMPLIFIED) MODEL OF THE MAERSK GUARDIAN JACK-UP

The major inputs described above will be discussed here as they have been formulated for the Maersk Guardian jack-up. First an overview of the structural model will be given and then of the sea state model.

4.1. A STRUCTURAL MODEL OF THE MAERSK GUARDIAN

4.1.1. Introduction

The DYNAL program is expected to give the most accurate results when the model is closest to the real construction. However, it is necessary and desirable to simplify the model such that it will give proper results at minimal costs. Thus some simplifications of the structure will be made by lumping properties (such as leg stiffness, and resistance to wave motion) without losing too much information. This model will still be suitable for comparisons of the global dynamic behaviour of the structure such as motion of the deck, overturning moment, base shear, and axial forces in a leg.

A sketch of the model described on the next pages is given in fig. 18. The origin of the global x and y axis is situated in the centre of gravity of the triangle corresponding to the three legs. (see fig. 6)

4.1.2. Modelling of the legs

The Maersk Guardian is a three-legged structure. Each leg is composed of three vertical (or chord) members, called corner posts, connected by horizontal and diagonal brace members. As shown in fig. 9 each leg forms 32 bays and there is the typical spud can at the bottom. Each bay (see fig. 4 and 14) has three horizontal brace members, six diagonal brace members and three vertical corner posts.

structural members:

In the structural model each bay is replaced by a single beam with equivalent stiffnesses. Thus each leg will be modelled by 32 joints connected by these equivalent beams. Because of this method of lumping stiffnesses, the mass of the steel and the added mass of this equivalent beam are not necessarily the same as those of the original bay. Therefore it is necessary to calculate the lumped mass (steel and added mass) of each bay and add this as (extra) mass at each joint. The mass of the equivalent beam should then be treated as zero in DYNAL.

mass lumping:

In the computation of the lumped mass per bay the following contributions have been estimated:

- mass of the steel.
- added mass (see appendix A2).
- marine growth has been neglected as a contribute to mass as well as member diameter increment. However, it is specified for members below mean water level to initiate the use of the rough Morison coefficients.

An overview of the masses computed per bay is given in table 2.

additional forces

- buoyancy (members are considered to have no water in them and buoyancy has been calculated as an extra force acting upward).
- other additional loading such as wind loading will be omitted in the model

stiffness lumping

For each bay an equivalent cross-sectional area, shear area as well as equivalent bending stiffnesses and torsion stiffness have been calculated. For the overview of the quantities of the stiffnesses and the formulations used, see appendix A3 and table 3.

The hydrodynamic loads on the equivalent beam will differ from those on the original bay. Fortunately DYNAL makes it possible to distinguish structural members having no wave loading and non-structural members carrying wave loading only. This feature will be used in the present model.

wave loading members:

The Morison equation is used by DYNAL for the computation of the forces on a bay due to fluid motion. For a circular cylinder, with a fluid velocity u and an acceleration $\dot{u}$ perpendicular to the member axis the equation has the form:

$$\frac{F}{\text{unit length}} = B\, u\, |u| + A\, \dot{u} ,$$

$B = 0.5\ \rho\ Cd\ D$

$A = 0.25\ \rho\ \pi\ D^2\ Cm$

ρ = density of (sea)water

Cd = drag coefficient

D = cylinder diameter

Cm = inertia coefficient

To obtain the formula for an equivalent beam it is necessary that the contributions of all members in one bay are lumped to one contribution for that equivalent beam. One bay is constructed of two different types of members, namely the corner post (with disturbing racks) and the circular brace members. Due to the racks the corner post will always be considered as smooth. The brace member however can be rough or not depending on the

marine-growth profile. To keep this distinction, one single bay will be represented by two equivalent beams. One carrying the wave force of the corner posts and the other that of the brace members. Because of the different orientation of the brace members and the racks, some approximations have to be made; these lead to the following formulae for lumped coefficients B and A (see appendix A5):

corner post:

$$Bcp = \sum_{i=1}^{3} AREAcp_i Cd\ \rho,$$

$$Acp = \sum_{i=1}^{3} VOLUMEcp_i Cm\ \rho,$$

$AREAcp_i$ = area per unit length

$VOLUMEcp_i$ = volume per unit length

i = cornerpost number

brace members:

$$Bbm = \left\{ \sum_{i=1}^{12} 0.5\ \rho\ Cd\ Di\ (1 - \sin^2\phi i\ \cos^2\psi i)^{3/2} Li \right\} / Lb$$

$$Abm = \left\{ \sum_{i=1}^{12} 0.25\ \rho\ Cm\ Di^2\ (1 - \sin^2\phi i\ \cos^2\psi i)\ Li \right\} / Lb$$

i = member number i

Di = diameter of member i

Li = length of member i

ϕi = orientation of member i (see fig. 14)

ψi = orientation with respect to flow direction (see fig. 14)

Lb = height of one bay

4.1.3. Modelling of the deck

The deck will be considered as infinitely stiff compared to the legs. Again the deck members will be treated in DYNAL as having no weight and the mass of the deck will be added as extra masses at the deck joints.
The position of the lumped deck masses in the horizontal plane does not influence significantly the estimation of natural period corresponding to the first bending modes. If all the mass of the deck is lumped at the centre of gravity of the deck, the natural period is less than 1,0 percent lower than if all the mass is lumped at the three corners of the deck.
The natural period of the first torsion mode however is in the latter case more than 57 percent larger. The deck mass will be lumped in such a way that the estimated natural period of the first torsion mode will be equal to the measured value of 3,45 seconds.

If all the mass is lumped at the highest joint (joint #1024) then the bending mode period is less than 4 percent larger than if all the mass is lumped at the lowest deck joint (joint #1014)

The gravity load from the hull mass is not equally distributed over the three legs (table 4), hence the centre of gravity is eccentric. This eccentricity is about 2,5 cm in the positive x direction and about 21,2 cm in the negative y direction.

This eccentricity has been modelled by an un-equal distribution of the masses at the three joints which correspond with the three corners of the deck (joint 1091, 1092 and 1093). An overview of the lumped deck masses and the member properties is given in table 5.

4.1.4. Leg/deck and leg/soil connections

Both the stiffness of the foundation or leg/soil connection and the stiffness of the connection between the legs and the hull influence significantly the natural period of the structure. It is desirable, because of this influence, to have accurate data on both stiffnesses and to have an accurate model of both connections. Because of the lack of data on these stiffnesses and the non-linear behaviour of soil, the modelling is problematic. On the other hand these stiffnesses are among the major parameters which can be manipulated in order to achieve the correct natural periods.

foundation stiffness

The leg-to-soil connection has been modelled as a hinge with freedom of rotation in the x-z plane and the y-z plane in combination with a linear rotational spring presenting the leg/soil stiffness. This is a spring supported boundary joint with zero translation and zero rotation about the vertical axis (only global x and y rotations possible).

In DYNAL it is not possible to model a non-linear soil behaviour, therefore a linear spring will be used. The translation stiffness will be assumed to be infinite. The rotation stiffness follows from a model for circular, infinitely stiff plates (see appendix A7) and leads to a rotational spring stiffness in the range of:

$K_\theta = 0,6*10^8-1,8*10^8$ [kNm/rad]

leg/hull stiffness

The leg-to-deck connection (fig. 2 and 10) is composed of three guides (lower, middle and upper guide) transmitting forces in a horizontal plane only and the clamps transmitting horizontal, vertical forces and moments. The lower and upper guide are modelled as two pseudo-members with zero stiffness except for a specified stiffness in the global x and y directions. The middle guide and the clamps are modelled as one pseudo member with specified stiffnesses in all directions (translation and rotation).

The stiffness of the leg/hull connection arises from two sources. The first is the capacity to resist bending moments in the legs by the clamps. These clamps have clamp teeth (fig. 10) which transmit vertical forces (one in opposite direction to the other) to the corner posts and thus cause a drop in the moment distribution. The second is the capacity to resist a moment by opposing horizontal forces at the upper guide and lower guide. If the static behaviour of one leg is considered under a constant horizontal force acting at the deck, then the distribution of the leg bending moments and shear forces may be schematized as shown in fig 11. The factor μ is the ratio of the moment in the leg at the foundation and the moment in the leg at the lower guide. The factor β is the fraction of the leg bending moment reacted by the leg to clamp connection. The factor μ depends on the stiffness of the rotational spring at the bottom and the stiffness of the whole leg to deck connection, while the factor β depends on the stiffness of the rotational spring at the clamp connection.

The distributions described above can be deduced from the measurements. The measured leg bending moment is filtered in a range around the first natural frequency so that only the inertia force from the acceleration of the hull and leg masses are contributing to the measured (interpolated) bending moment profile (fig.12). From this profile it may be seen that the point of a zero bending moment (the inflection point of the leg) is located halfway from mudline to the clamps. This corresponds to a value for μ of 1,23. The percentage of the measured shear force above the clamps (Q_u) and below the lower guide (Q_0) is listed in table 6 and is estimated to be 22,1 %.

The measured bending moment profile is based on measurements of bending moments at only two different elevations (32,6 m and 87,5 m above the mudline) of one leg. Further it is assumed that the shear force is constant along the leg, which only is true if the mass and thus the inertia force of the legs is negligible compared with that of the deck and fluid load is negligible. Despite these assumptions and the limited data on the profile it will be assumed that the conclusions drawn from this profile are valid.

4.1.5 Solution method

For the solution of the dynamic equation of motion "modal dynamic with static correction" (see chapter 3) has been chosen since it is the most accurate one:. To ensure no loss of any important mode shape, 16 eigenvectors or modes have been generated and 8 modes associated with the lowest frequencies have been used in the solution.

4.1.6 Calibration of the structural model

The model should satisfy certain constraints which values are deduced from the measurements. These values vary slightly from storm to storm. The present analysis has been performed for the first storm only thus the values of the constraints corresponding to that storm have to be satisfied here. The constraints and their values are listed in table 6.

1. natural period

The first three natural periods of the structure, corresponding to the first two bending modes and the first torsion mode, have been compared to the natural periods deduced from the measurements. In the report on the

measurements (ref. 1), the natural period of the first two modes is estimated to be 4,21 (±0,025) seconds while that of the first torsion mode is 3,45 (± 0,025) seconds.

2. leg/soil stiffness equal to leg/hull stiffness

To verify the accuracy of the simplified model it has been tested in the DYNAL program using regular waves. In order to make a comparison with the results from the measurements, the model has been tested in DYNAL in two ways:

1) a static analysis to determine the bending moment profile and shear force profile in one of the legs under a static horizontal force of $1,33*10^4$ kN ($=3.10^3$ kips) applied at the deck.
2) a dynamic analysis to determine the first three natural periods of the model (two bending modes in the global x-z and y-z plane, and one torsion mode in the global x-y plane)

Several parameters influence the natural period of the structure and the distribution of forces and moments along the leg. The parameters which have been adjusted are:

- foundation spring stiffness, influencing natural bending period, and moment distribution on the leg
- clamp rotational spring stiffness, influencing natural bending period, and moment distribution
- horizontal stiffness of the upper guide and the clamp, influencing the ratio between clamp stiffness and total leg/hull stiffness, the shear force distribution and moment distribution.
- distribution of the lumped mass at the deck, in a vertical sense influencing slightly the bending period and not the torsion period, in a horizontal sense only influencing the torsion period.

Since the parameters are interactive, the calibration has been an iterative process, which converged to a model which satisfies the constraints. The result of this process is shown in fig. 13 for the leg bending moment distribution and in table 6 for the natural periods and the values associated with the leg/hull and leg/soil stiffness.

The rotational spring stiffness at the foundation obtained from the iterative process described above has been estimated as $1,02*10^8$ (kNm/rad) ($=0,9*10^9$ kips-in/rad). A complete survey of the stiffnesses and lengths of the pseudo-members used is given in table 7.

4.2. DESCRIPTION OF THE SEA STATE MODEL

4.2.1. Introduction

The description of the sea is the second major input for the DYNAL program. The constraints of this description depend on the required output from the simulations. If only response frequency spectra or peak values are required then it is sufficient to have as input a measured surface elevation spectrum and a directional spreading function. The response spectra may be obtained from the time-domain simulation based on wave kinematics generated from this spectrum.

The generated time histories of the wave kinematics and wave surface are random and likely to differ from the measured wave kinematics. To make a time-domain description which fits the measured wave kinematics and surface elevation it is necessary to make use of the 'conditioned simulation' option of the GENERATE program.

4.2.1. Description of the input

grid

The number of grid points used at each level is given in table 8. Because of the decreasing importance of the wave kinematics with increasing distance below the sea surface, the grid point density will decrease from sea surface to mudline.

wave spectrum

The measured wave kinematics contain information on surface elevation at two different locations and velocities at two different levels in two directions. Therefore it is possible in principle to estimate from these measurements a directional wave spectrum. Because of the relatively large distance from the sea surface at which the measurements of the velocities were taken and the uncertainties of the interaction of the current and the wave kinematics no directional spectrum has been estimated as input but an assumed directional spreading function has been used in combination with the measured frequency spectrum. This spectrum is measured in a fixed reference frame, thus the Doppler-shift switch will be on.

directional spreading function

If $S(f)$ is the measured one dimensional frequency spectrum and $G(f,\theta)$ an suitable directional spreading function, then the two dimensional spectrum $S(f,\theta)$ calculated by GENERATE will be:

$$S(f,\theta) = S(f)\ G(f,\theta)$$

For wind-driven waves the use of the cosine power spreading function is proposed in Sarpkaya (ref. 2). This function has the form:

$$G(f,\theta) = C(f) \left[\cos \left(\frac{\theta - \theta_0(f)}{2} \right) \right]^{2s(f)}$$

$G(f,\theta)$ = directional spreading function

$\theta_0(f)$ = central direction of the waves with frequency f, with respect to an arbitrary reference direction

θ = direction with respect to the reference direction

$s(f)$ = degree of spreading exponent

$C(f)$ = normalization function such that $\int_0^{\infty} \int_0^{2\pi} G(f,\theta)\, d\theta\, df = 1$

Larger values of s(f) give narrower directional spectrum (see fig. 19). From here on the function G will be considered independent on the frequency (central angle and degree of spreading are constants for each sea state).

The spreading value 's' may be estimated in two different ways.

The first is based on the measured direction of the water particle velocities. From the measured wave velocities in both x and y directions one can estimate at each time step the angle of the resulting wave velocity with respect to a certain reference. The spreading value 's' may be estimated if the relation between these measured angles and the spreading function is known (see ref. 12 and 19)

The second is based on measured particle velocities and surface elevations in combination with conditioned simulation (see chapter 4.2.3). It will be used here because of the availability of combined information on wave height and direction and because of its simplicity.

The central direction of the spectrum has been set equal to the measured wave propagation direction (ref. 1) and the value of the spreading exponent (s) obtained from the conditioned simulations (see chapter 4.2.3); s has been estimated to be 4. This is in agreement with other data for similar storms on the North Sea.

current profile

The current profile as well as the direction of the current has been estimated from the mean values of the measured horizontal velocities. Fig. 20 and table 9 show the calculated mean values and the directions of the current. The current profile has been represented as linearly varying between four points: two points corresponding to the elevation of the meters, one point at mean water level assuming this to have the same current velocity as current meter # 1 and one point at the mudline assuming zero current velocity here.

4.2.3. Conditioned simulation

conditioning variables

In principle it is possible to condition elevations and slope of sea surface, wave induced water particle velocities,and pressure at any location of the three-dimensional grid. The water particle velocities however were measured only at one location in the x,y plane (two different levels) and surface elevations at two locations.

By simply comparing the measured surface elevation with the simulated one at the same location it was possible to test the working of the conditioning.

First the conditioning has been tested using the input wave spectrum of wave meter #1, and a spreading corresponding to a value of s=20 in the cosine power spreading function.

When the surface elevation at the location of wave meter #1 is conditioned in combination with the x components of velocity from current meter #1, the reproduced surface elevation is in excellent agreement with the measured one (see fig. 21).

Subsequently, the y as well as the x component velocity was used for conditioning. This leads to a large difference between the measured surface elevation and the simulated one (see fig. 22). In the latter case the measured velocities contain information on the direction of the wavelets and hence, on the spreading of the waves. Apparently the initial choice of spreading of s=20 was not a good one.

After increasing the directional spreading by changing from s=20 to s=4, the conditioning with the same variables (surface elevation and velocities in x and y directions) shows very good agreement with measurements (see fig. 23).

The addition of the surface elevation at the location of wave meter #2 did not improve the simulation but led to somewhat larger errors in the simulated surface elevation at location #1 and very large errors at the location of wave meter #2. This might be explained by the disturbing effects from the legs; the measured central direction of the waves indicates that wave meter #2 is located in the wake of the bow leg.

condition the simulations ?

The question is whether the conditioned sea state as found above is suitable for use in the simulations. Assuming that the measured frequency spectra at the locations of the wave meters are representative of the spectra at other locations, then the spectra of the simulated surface elevation at the various gridpoints should be equal to the measured frequency spectra.

A comparison has been made between a measured surface elevation spectrum of wave meter #1 and the simulated spectra with, respectively, conditioning on the surface measured at wave meter #1, and conditioning on the surface at wave meter #1 in combination with the velocities from current meter #1. For both cases the surface elevation spectrum was generated at location x=0 and y=0 (see fig. 24). The spectrum from the first conditioned simulation is in good agreement with the measured one. However, the spectrum in the second case (conditioned surface and velocities) has been dramatically blown up (peak is twice the measured peak). The reason for this may be that if the conditioning is accurate in the small area of the location of the conditioned variables, a price has to be paid in the accuracy of the simulated sea state at locations "far" away.

As the dynamic behaviour of the jack-up is excited by wave forces acting simultaneously at every leg, a rational conditioned simulation (involving the conditioning of directionally dependent variables such as velocities) could be made if these variables had been measured at locations close to all three legs.

In the present simulation only the conditioned surface of wave meter #1 will be used, since this produces spectra that are in good agreement with the measurements.

4.3. SENSITIVITY ANALYSIS

4.3.1. Structural sensitivity

In order to obtain some insight into the sensitivity of the natural period to the various parameters, the DYNAL model has been executed several times, changing each time one parameter and determining the proportional change of the longest three natural periods. Table 10 (I and II) shows the results of this analysis.

For purposes of interpretation the structure may be approximated by a one degree of freedom system or flagpole model. In that case the natural period is simply:

$$T_n = 2\,\pi\,\sqrt{\left(\frac{M^*}{K^*}\right)}$$

M^* = effective mass

K^* = effective stiffness

This simple expression for the natural period provides insight into the nature of the sensitivities found above. An extensive calculation and formulations which may be used for M^* and K^* is given in appendix A8.

The hull contains roughly 75% of the total mass and is therefore the major contributor to the effective mass, M^*.

The mass of the legs is about 25% of the total mass and does not contribute very much to the mass term. Moreover this mass like that of the hull is not subject to great uncertainty.

The foundation stiffness is one of the parameters which influences the stiffness of the structure (K^*). For a relative change of 10% in the foundation stiffness, the relative change in T_n is only 1.5 percent, but there is a lot of uncertainty in this parameter. Thus, it is still very significant for the modelling. This holds also for the stiffness of the leg hull connection, that is the combination of leg clamp stiffness and stiffness of the guides.

The approximation for the equivalent shear area as well as the equivalent moments of inertia seems to be validated well enough in practice and is not open to too much doubt. At least this approximation has also been used for the calculations of forces from the measured stresses.

Young's modulus of elasticity (E) influences the stiffness term as well and should be well known, but the measurements report (ref. 1) suggest that the modulus of elasticity (E) may be 10 percent larger than assumed.
The torsion constant or polar moment of inertia (J) influences only the torsion natural period.

4.3.2. Sensitivity of fluid loading members

The previous chapter showed the sensitivity of the natural periods to changes in the structural parameters. In order to obtain some insight into whether the fluid-forces on the structure are dominated by the 'drag' term or the 'inertia' term of the Morison equation, an analysis is also made of the sensitivity of dynamic responses to changes in the features of the fluid loading members,

The peak displacements of the centre of the deck (x=0, y=0) are analyzed as a result of fluid loading from regular Stokes waves. The response of the first 40 cycles has been ignored to ensure that the structural response has reached a steady state.

Considering a linear wave theory, the drag term becomes relatively more important with increasing amplitude of the water particles motion, that is with increasing wave height. This behaviour has been analyzed for waves with a period close to the dominant wave period of the measured wave spectrum of storm #1 and for waves with a period close to the natural period of the first bending modes of the structure. The results of this analysis are listed in table 11. This table shows the peak displacement of the deck (U) for two cases. In the first case, the displacement is simulated using

'realistic' Morison's coefficients, while in the second case the inertia coefficient Cm has been doubled. The ratio of the displacement U in the second case and the first case (δ) shows the relative importance of the inertia coefficient for the dynamic response. It is likely that if both the inertia and drag coefficient are doubled that this ratio (δ) will be equal to 2.

Table 11 shows that for waves with a period of 7,7 seconds and wave heights of 10 feet and lower, the dynamic response is dominated by the inertia part of the Morison equation. For waves with a period of 7,7 seconds and a waveheight close to 20 feet both terms are equally important.

For waves with a period of 4,0 seconds the wave force is even more inertia dominated than in case of a period of 7,7 seconds.

For very high waves with a period of 10 seconds and a wave height of 60 feet, close to the design wave, the wave force is drag dominated.

The maximum individual wave height in the storm analyzed does not exceed 20 feet, thus the force of the structure will be dominated by the inertia term in case of waves with frequencies close to the natural period (tail of wave spectrum), whereas the inertia and drag term are equally important for waves with frequencies around the dominant wave period.

When the direction of propagation of the wave is changed from 90° (waves propagating into the positive y-direction) to 0° (waves propagating into positive x-direction), the excitation is an order of magnitude lower for waves with a period T=7,7 s and height H=20,0 ft. This may be caused by the phase difference between the wave forces on each leg, which results in cancellation of the individual forces at each leg. This effect will also be present for waves in an irregular sea and may lead to differences in results when changing the central direction of the frequency spectrum.

4.3.3. Discussion of 'pinned spudcan' model

The measurements showed that the stiffness of the foundation should not be ignored. Modelling practice, however, often assumes a pinned spudcan, in other words a hinge connection at foundation level, without additional springs, in combination with infinite stiffness at the leg/deck connection.

Using a "pinned spudcan" in the model described above will lead to an increase in natural periods from 4,2 to 5,4 seconds for the bending mode and from 3,45 to 4,3 seconds for the torsion mode. This means that the natural frequency of the model will be lower than the real period. This natural frequency corresponds to a more energetic part of the tail of the surface elevation spectrum, and causes a severe overestimation of the dynamic forces in the structure.

Brekke (ref. 3) showed, for a clay soil that the assumption of a "pinned spudcan" leads to a 25 percent overestimation of the natural period and a 20 percent increase in the maximum static moment in the leg, due to the shift in the bending moment profile.

Should the assumption of an infinitely stiff leg to deck connection still be valid, then a foundation rotational spring stiffness of $K = 0,5\ 10^9$ is necessary to satisfy the measured natural frequencies. This value of K does not, however, lie in the range of stiffnesses found from the simple foundation stiffness model in appendix A7 ($K = 0,6*10^8 - 1,8*10^8$). This supports the assumption that foundation stiffness might be close to leg to hull stiffness and hence, that conventional modelling may not be accurate.

5. COMPARISON OF MEASUREMENTS WITH DYNAL RESULTS

5.1. INTRODUCTION

In principle data for four storms is available for use in comparison. Some characteristics of these storms or corresponding data segments are listed in table 1. This shows that the measured maximum wave height and mean wind velocity were the largest for data segment #1. Therefore data segment #1 has been chosen for comparisons in the present report. Some characteristics of this data segment will be discussed first.

5.1.1. Characteristics of storm #1

In order to obtain insight in the measured met-ocean quantities some spectral analyses and time domain analyses have been carried out for three different parts of data segment #1. Data segment #1 contains information for 5900 time steps or 2950 seconds. The analyses have been carried out for both wave meters for the first 1024 time steps, the next 1024 time steps and the following 2048. Table 12 shows the calculated zero-order moment or area under the spectrum; while table 13 shows the mean wave amplitudes of the largest 10% of all peaks.

The tables show that, the energy decreases slightly in time and that the measured significant wave amplitudes are somewhat lower for wave meter #2 compared to wave meter #1. Notable is the difference between wave meter #1 and #2 for the first 512 seconds. Wave meter #2 is located at the port side of the deck (see fig. 6), and might be situated in the wake of the bow leg considering the central angle of wave propagation (table 1).

The data from wave meter #1 has been used to generate the input surface elevation spectrum to avoid misleading data from wave meter #2 particularly for the first 512 seconds.

5.1.2. Overview of the comparison

The present comparison between measured and calculated results has been carried out for deck acceleration and for forces in the legs such as axial forces and bending moments. These responses are studied in the frequency-domain by comparing characteristic peaks of the measured and simulated response spectra, and in the time-domain by comparing measured and simulated significant peak values. The peaks from the spectra are estimated from the figures while the peaks from the time histories are calculated by the program which generates the spectra and time histories.

For all practical purposes, the motion of a jack-up platform under wave action is fully determined by its lowest three modes which correspond to the two global bending modes and the torsional mode. Natural frequencies of the individual legs are 10 to 7 times higher and can be disregarded in calculating dynamic responses (ref. 4).

In the comparison of the peak values of the various spectra three important peaks, corresponding to the following frequencies, will be distinguished:

1) the frequency corresponding to the dominant frequency of the surface elevation spectrum (around 1,0 rad/sec)

2) the frequency corresponding to the first two bending modes (around 1,5 rad/sec)

3) the frequency corresponding to the lowest torsional mode (around 1,8 rad/sec)

The peaks listed in the tables correspond to this numbering.

The mean of the calculated time histories has been removed because the mean of the measured data is artificial and had to be removed in order to obtain realistic values.

In the comparison of the time histories the following significant peaks have been analysed (A = quantity analyzed: acceleration, force,...):

A1/3 : mean of largest one third off all peaks/troughs

A1/10: mean of largest one tenth off all peaks/troughs

Amax : maximum or minimum value of A in the record

No distinction has been made between peaks and troughs, the absolute highest value is always listed.

The comparisons are made for the following two different intervals:

1. from the 1st to the 1024th data point (512 seconds)
2. from the 1025th to the 2048th data point (512 seconds)

This means that for these intervals the corresponding surface elevation spectrum has been used as input for GENERATE in combination with the appropriate conditioned time series of wave meter #1.

For the first interval comparisons have been made of the acceleration of the bow in x-direction and y-direction (frequency domain as well as time domain), and a comparison in the frequency domain of the shear force in x-direction of the bow leg. A comparison has been made also for damping ratios of both 3 percent and 2 percent of critical damping.

The analysis of the second interval is more extensive. The accelerations of the bow and stern have been compared as well as axial forces and bending moments in all three legs.

5.2. COMPARISON INTERVAL #1

5.2.1. Deck acceleration comparison

introduction

The measured acceleration of the bow has been compared to the simulated acceleration of joint #1021.

Figure 25 and 26 show the measured and the simulated acceleration spectra in x and y directions and table 14 gives their peak values.

acceleration spectra

From the spectra of the acceleration in x direction, it can be seen that most of the energy of the motion is caused by dynamic vibration in the torsion mode. Since, at the bow, the y direction is normal to motion generated by rotation, the torsional mode does not influence significantly the acceleration of the deck in the y direction and is therefore omitted in the table.

The shape of the spectra from DYNAL is similar to that of the measurements. The densities at peak #1 and peak #2 are underestimated by DYNAL, whereas the density of peak #3 shows an overestimation by DYNAL.

If influences of over- or underestimation of Morison coefficients is ignored, then these differences may be caused by assuming too low damping value in the torsion mode and too much damping in the bending modes or an error due to an realistic central direction of the frequency spectrum. This central direction is assumed to be constant during the entire storm and to be constant for all frequencies. Neither is likely to be the case.

time histories

From the ratio of the significant peaks of DYNAL and the peaks from the measurements (table 15) it can be seen that DYNAL overestimates the acceleration in the x direction and underestimates in the y direction. This is compatible with the findings from the spectra.

5.2.2. Shear force comparison

The shear force in the bow leg has been measured at an elevation of 87,5 meter above the mudline. This corresponds to the shear force in joint 119 of the present mode for the DYNAL simulation.

Figure 27 and table 16 show the spectra and the spectral peaks. This figure and table shows that DYNAL underestimates the peaks at frequencies #1 and #2 and overestimates the peak at frequency #3. This is also in agreement with the findings from the acceleration comparison. The measured spectrum further shows a peak at very low frequencies. This peak probably corresponds to the peak in the wind velocity spectrum see fig. 28.

5.2.3. Overturning moment comparison and influence of damping

introduction

The measured overturning moment (OTM) is calculated on a level 30 meters above mudline, whereas the DYNAL results are calculated at the mudline. The contribution of the individul leg moments to the overturning moment is relatively larger at the mudline. However, the axial forces contribute about 90 percent to the total overturning moment so it may be expected that DYNAL results are slightly 'overestimating' the OTM for spectral densities. The results will still be discussed here to show the influence of a change in damping from 3 percent to 2 percent of critical.

The overturning moment is calculated as:

$$OTMx = Mx1 + Mx2 + Mx3 + (Dy/3)\,Fz1 + (Dy/3)\,Fz2 - (2Dy/3)\,Fz3$$

$$OTMy = My1 + My2 + My3 - (Dx/2)\,Fz1 + (Dx/2)\,Fz2$$

Mxi = bending moment in leg #i
Fzi = axial force in leg #i
Dx = distance between leg #1 and leg #2
Dy = distance between leg #3 and horizontal line intersecting leg #1 and #2

Figure 29 and figure 30 show the x-overturning moment related to the quasi-static overturning moment and the wave spectrum as simulated for 3 percent and 2 percent damping. The dashed line shows the measured quantity whereas the solid line shows the DYNAL simulation. There is no measured data available for the quasi-static overturning moment, thus only the DYNAL simulation is shown.

comparison of spectra

It is obvious that the change in damping from 3% to 2% has a great influence on the peak of the spectrum at the natural frequency: the peak drops by a factor of two.

The torsional mode at a frequency around 1.82 rad/sec has no influence on the dynamic overturning moments since the individual moments in each leg cancel.

Comparing the quasi-static part with the dynamic part of the response near the dominant frequency of the surface elevation spectrum reveals that there is a large dynamic effect, though it is hardly influenced by changed

damping. This is in agreement with the dynamic amplification factor for a single degree of freedom system:

$$DAF(\omega) = \frac{1}{\sqrt{((1 - \omega^2/\omega n^2)^2 + (2\ \beta\ \omega/\omega n)^2)}}$$

ω = angular frequency

ωn = natural frequency

β = damping as ratio of critical

If $\omega = \omega n$ then $DAF(\omega n) = 1/2\beta$

If damping is 2 percent, then $DAF(\omega_n) = 25$. However if it is 3 percent, the single degree of freedom $DAF(\omega_n)$ drops to 17. The DAF at the dominant frequency of the surface elevation spectrum: $\omega \simeq 1$ rad/sec is for both cases equal to 1,8 and thus almost independent of the damping ratio β.

5.3. COMPARISON INTERVAL #2

5.3.1. Deck acceleration comparison

introduction

The measured accelerations of the bow (joint 1021) and the stern (joint 1023) have been compared with the DYNAL simulations.

Figure 31 and 32, show the measured and simulated acceleration spectrum of the bow in x and y direction. The peak values are listed in table 17, while table 18 shows the significant peaks of the time histories.
Figure 33 and 34 and table 19 and 20 show similar quantities for the acceleration of the stern.

acceleration spectra

The spectra of the bow acceleration show that the 2nd density peak is overestimated by DYNAL (in contrast to the findings from the 1st interval) while the 3rd peak is slightly overestimated by DYNAL.

The 2nd peak of the acceleration in y direction shows agreement between the measured and the simulated peak. The peak of the measurements is broader, however, thus it contains more energy than the DYNAL peak.

Both the x and y directions have an angle with respect to the rotation axis of the stern, hence the spectra of the stern acceleration in x direction as well as y direction show dynamic response at the torsion frequency (peak #3)

The 2nd and the 3rd peak are slightly underestimated by DYNAL for both the x and the y direction.

time histories

The significant peak values of the time histories show that DYNAL results slightly underestimate for the y direction, but, in general, are close to the measured values.

5.3.2. Axial force comparison

influence of vertical fluid loading

Axial forces in the three individual legs are the result of gravity forces on the deck and the leg, vertical forces due to vertical fluid loading components on the inclined and horizontal members of the bay, vertical forces due to the global loading and motion of the jack up (contributions to the overturning moment), and vertical (lift) forces due to the interaction of wind and deck. The gravity loads will be assumed to be static and constant and are omitted in the comparison.

To illuminate the importance of the vertical forces due to wave loading, the spectra of the axial force in leg #3 have been compared on two levels. Fig. 35 shows the spectrum of the axial force in leg #3 at surface level ($\simeq$ 80 m above mudline) and at subsea level ($\simeq$ 30 m above mudline). Table 23 and 24 show the density peaks of the spectra and the peak values of the time histories.

The dynamic behaviour of the jack up in the bending mode is excited by horizontal components of the wave forces, whereas the influence of the vertical wave forces on the dynamic behaviour is assumed to be insignificant in the analysis.

From the spectra shown in fig. 35, it can be seen that at the natural frequency the peaks are identical, and that there is a difference only at the 1st peak (dominant frequency of the surface elevation spectrum). The

significant peaks of the time histories show a difference of less than 2 percent. Thus the influence of the quasi-static vertical components of the wave loading on the vertical forces in the leg are negligible in comparison to the vertical forces due to the global motion of the jack-up. This leads to the conclusion that omission of the vertical wave forces in the present model is acceptable.

For the present comparison the measured time histories and spectra of the axial forces at all three legs at subsea level (bay #7) have been compared to the forces at joint 207 (leg #1), joint 307 (leg #2) and joint 107 (leg #3).

axial force spectra

From the spectra of the axial force (table 21 and 23) in leg #1 (fig. 36), leg #2 (fig. 37) and leg #3 (fig. 38), it can be seen that the agreement between measurements and simulations for leg #1 and #2 is less good than for leg #3. DYNAL overestimates the second peaks. The measured spectra of leg #2 and #1 have a very crapulent shape especially in the low frequency range. This might be caused by response to the wind. Fig. 28 shows the spectrum of the wind velocity with significant energy at very low frequencies. The wind force has been omitted in the present model and thus the response to its excitation at these low frequencies is lacking in the DYNAL results. The wind passes freely under the deck, but is disturbed on the upper side which might generate a lift force as on a wing.
The relative importance of this amount of energy is least for leg #3, which indeed shows best agreement between the measured and simulated time history.

axial force time histories

The spectral distribution of the energy for leg #1 and leg #2 shows significant energy at very low frequencies and thus is very different from that of the DYNAL results, this makes a comparison of peak values questionable (table 22).

The distribution of energy for leg #3 is in better agreement which makes a comparison of the time history peaks sensible. DYNAL underestimates the peaks, but is within ten percent (table 24).

5.3.3. Leg moments comparison

introduction

The measured bending moments in x direction and y direction have been compared with the bending moments of joint #207 (leg #1) , joint #307 (leg #2) and joint #107 (leg #3).

leg moment spectra

Fig. 39 and 40 show the spectra of the bending moment in x and y direction of leg #1, fig 41 and 42 of leg #2 and fig. 43 and 44 of leg #3.

In all cases the bending moment about the x axis is larger than about the y axis. The bending moment for the two stern legs (#1 and #2) is mainly determined by the motion at the first natural frequency, whereas the bending moment about the x axis for leg #3 is determined by the lowest bending modes as well as the third natural frequency or torsion mode. These results are in agreement with the findings from the acceleration comparison.

The response to the wind is also noticeable in the bending moments. Especially for the leg bending moment about the y axis this low frequency response is relative important, and makes a comparison questionable.

Table 25 shows the peak values of the spectra of leg #1, table 27 of leg #2 and table 29 of leg #3. The tendency is an overestimation of the peaks for y-moments and an underestimation for x-moments. This is also in agreement with findings from the acceleration comparison. The response at the third frequency is in general too high compared to the bending natural frequency response, this may mean that damping is different for bending and torsion modes, and should be somewhat higher for the torsion mode.

leg moment time histories

The significant peaks of the time histories of leg #1, #2 and #3 are listed respectively tables 26, 28 and 30. From these tables it can be seen that the agreement of DYNAL with the measurements is good for y-moments and that DYNAL underestimates the leg moments by roughly 20 percent for x-moments. This is in agreement with findings from the spectra.

6. CONCLUSIONS AND RECOMMENDATIONS

conclusions

It must be emphasized that conclusions from the present study are related to the present simplified model and may not be valid in general. Moreover, the present study has been carried out for data from only one storm, and some of the model features, like foundation stiffness, leg to hull stiffness, and Morison coefficients have not been specified exactly. Moreover, the damping influences the results significantly and has been chosen (within limits known from literature), so that rational results have been obtained.

From the present study it may be concluded that:

1) The dynamic behaviour of a jack-up can be estimated reasonably well by means of a simplified model in DYNAL.

2) The agreement of DYNAL resuts with measurements is best for global responses such as deck accelerations, and less good for computations of individual leg forces and moments. Peak values are typically accurate within 20 percent.

3) Wind loads may be omitted for the estimation of global responses (deck acceleration and overturning moment), but may be significant for the axial force spectra.

4) Conditioning of the simulations will improve the accuracy of the simulation of the seastate, but conditioning of too many variables in a too small area may cause unrealistic simulations of the sea surface at locations outside this area.

- modeling very good
- interpr. measurements
  - wind
  - bending moments

5) If the input spectrum is a one-dimensional one combined with an assumed directional spreading function, then the accuracy of the conditioning strongly depends on the amount of spreading. If directionally dependent variables such as fluid velocities or accelerations are conditioned, then the conditioned simulation may be used for an estimation of the amount of spreading.

6) Damping values in the lowest torsion mode may be different from those in the lowest bending mode. Damping should be more for the torsion mode.

recommendations

1) The present model has been used for comparisons with data from storm #1 and may be used for comparisons with data obtained from the other three storms.

2) The influence of the central direction of the frequency spectrum on the global responses of the model may be investigated.

3) Considering the uncertainties of some variables used in the present model more research is desirable on the following subjects:
   - foundation stiffness of spudcans;
   - stiffness of the leg to deck connection;
   - Morison coefficients.
   - damping ratios.

4) Practical use of the model for predictions under extreme wave conditions may be valuable if non-linearities in the behaviour of the foundation and the leg to deck connection are quantified.

APPENDICES

APPENDIX A1

wave forces on circular cylinders

Sarpkaya (ref. 2) mentions four methods of calculating wave forces on circular cylinders. The one recommended by him and used for the calculations here is as follows.

The resultant velocity and acceleration may be decomposed into components normal and tangential to the cylinder axis. The tangential kinematics may be ignored.

The three-dimensional Morison equation then is, see fig. 14

$$\vec{F} = \begin{Bmatrix} Fx \\ Fy \\ Fz \end{Bmatrix} = 0.5\,\rho\,Cd\,D \begin{Bmatrix} u_{nx} \\ u_{ny} \\ u_{nz} \end{Bmatrix} \sqrt{(u_{nx}^2+u_{ny}^2+u_{nz}^2)} + 0.25\,\rho\,\pi\,D^2\,Cm \begin{Bmatrix} \dot{u}_{nx} \\ \dot{u}_{ny} \\ \dot{u}_{nz} \end{Bmatrix}$$

$$e_x = \sin\phi\,\cos\psi$$

$$e_y = \cos\phi$$

$$e_z = \sin\phi\,\sin\psi$$

$$\underline{e} = e_x\underline{i} + e_y\underline{j} + e_z\underline{k}$$

$\underline{e}$ = unit vector along cylinder axis

The velocity vector normal to the cylinder axis is:

$$\vec{W}n = \underline{i}u_{nx} + \underline{j}u_{ny} + \underline{k}u_{nz}$$

If the waves propagate in the x-direction and U is the horizontal velocity and V is the vertical velocity then the resultant velocity $\vec{U}$ will be:

$$\vec{U} = \underline{i}U + \underline{j}V$$

The component normal to the cylinder axis will then be:

$$\vec{W}n = \underline{e} \times (\vec{U} \times \underline{e})$$

or written in components

$$u_{nx} = U - e_x(e_xU + e_yV)$$

$$u_{ny} = V - e_y(e_xU + e_yV)$$

$$u_{nz} = - e_z(e_xU + e_yV)$$

The derivation for the acceleration vector is analogous:

$$\dot{u}_{nx} = \dot{U} - e_x(e_x\dot{U} + e_y\dot{V})$$

$$\dot{u}_{ny} = \dot{V} - e_y(e_x\dot{U} + e_y\dot{V})$$

$$\dot{u}_{nz} = - e_z(e_x\dot{U} + e_y\dot{V})$$

It is obvious that if the member is not oriented normal to the wave direction, the vertical velocities and accelerations also contribute to a drag and inertia force acting in a horizontal plane. This will be the case for the force acting on a jack-up bay because of the diagonal members. Due to the simplification of the three-dimensional bay into a single (vertical) beam this effect is ignored.

The most important contribution to the peak horizontal forces arises from the horizontal kinematics. Neglecting horizontal forces due to the vertical wave motion may be an acceptable approximation.

The equivalent beam in the present model is vertically oriented, which has the consequence that vertical forces due to wave loading are not accounted for. However, since the vertical forces due to the dynamic excitation of the structure and dead load may be expected to be an order of magnitude higher, the vertical wave loading may be neglected.

In this case only the wave forces acting in a horizontal plane will be considered. Because of the different orientation of each member in a bay a formula will be derived which lumps all the forces acting in the direction of the fluid velocity (x direction).

This force is the x-component of the Morison equation:

$$Fx = 0.5\ \rho\ Cd\ D\ \{u_{nx}\}\ \sqrt{(u^2_{nx}+u^2_{ny}+u^2_{nz})} + 0.25\ \rho\ \pi\ D^2\ Cm\ \{\dot{u}_{nx}\}$$

Ignoring the vertical velocity V gives:

$$u_{nx} = U - e_x(e_x\ U)$$

Using equations (x.x, x.x)

$$u_{nx} = U(1 - \sin^2\phi\ \cos^2\psi)$$

$$\sqrt{(u^2_{nx}+u^2_{ny}+u^2_{nz})} = |Wn| = (U^2 - (e_x U)^2)^{1/2}$$

using equations (x.x, x.x) again:

$$|Wn| = U(1 - \sin^2\phi\ \cos^2\psi)^{1/2}$$

For the acceleration part holds:

$$\dot{u}_{nx} = \dot{U}(1 - \sin^2\phi\ \cos^2\psi)$$

The force per unit length in x-direction acting on a member i with length Li and diameter Di will be:

$$Fx = 0.5\ \rho\ Cd\ Di\ U|U|(1 - \sin^2\phi\ \cos^2\psi)^{3/2} + 0.25\ \pi\ \rho\ Cm\ Di^2\ \dot{U}(1 - \sin^2\phi\ \cos^2\psi)$$

According to Sarpkaya two vertical cylinders, situated along the axis of flow attack, behave as if they are mutually independent for spacing ratios L/D (D is diameter and L is distance between centrelines) larger than 2,5. The influence of spacing for a three-dimensional bay is more obscure. It may be expected that at the several joints of such a bay, where several members come together, the fluid motion is influenced. However, the spacing between individual brace members is in general larger than 2,5 times the diameter. Hence the total force acting on one bay may be calculated by a simple summation of all single contributions of the several members (index i).

The force per unit length acting on (brace members of) one bay with bay height Lb will then be:

$$Fx = \frac{1}{Lb} \sum_{i=1}^{12} \{0.5\ \rho\ Cd\ Di\ U|U|(1 - \sin^2\phi_i\cos^2\psi_i)^{3/2} Li\} +$$

$$+ \frac{1}{Lb} \sum_{i=1}^{12} \{0.25\ \pi\ \rho\ Cm\ Di^2\ \dot{U}(1 - \sin^2\phi_i\cos^2\psi_i)\ Li\}$$

APPENDIX A2

lumped mass calculations

added mass

The added or virtual mass is directly related to the volume in the inertia part of the Morison equation. This can be seen if the equation of motion for one bay is considered (ref. 2)

$$(M + \rho\ Ca\ V)\ \ddot{x} + C\ \dot{x} + K\ x = \rho\ V\ Cm\ \dot{u} + 0.5\ \rho\ Cd\ A\ |u|u$$

Cm = Ca + 1
Ca = added mass coefficient
ρ = density of water
M = mass of the steel in the bay
V = equivalent volume of one bay
C = damping value
K = stiffness value
Cm = inertia coëfficient
Cd = drag coëfficient
A = equivalent area of bay (see appendix A1)
x = displacement of bay
u = velocity of fluid

The term 'ρCaV' represents the added mass. This added mass is related to the acceleration of the fluid relative to the acceleration of the bay. Experiments showed that the added mass coefficient Ca may be equal to one (ref. 4).

The motion of the bay will be assumed to be horizontal. This means that the equivalent volume V of the bay may be taken as the summation of the horizontal cross sectional areas times the projected lengths (on vertical plane) of the individual bay members.

This calculation method for the equivalent volume V differs from the suggested method in appendix A1 of decomposing the fluid accelerations into one perpendicular to the member axis and one along the axis.

Both calculation methods are described in appendix A5. The first method is chosen for use in the present model.

APPENDIX A3

<u>equivalent stiffnees calculations</u>

equivalent shear area (Ash)

The calculation of the equivalent shear area will be made first for the two dimensional case, followed by the extension to the three dimensional case.

As an approximation of the behaviour of one bay (see fig. 15) under a shear force Q, the following deformation mechanism will be considered:

1) the deformation due to the elongation and shortening of the diagonal brace members,leading to a displacement δ_1 and a stiffness k_1.

2) the deformation due to the elongation of the horizontal brace member, leading to a displacement δ_2 and a stiffness k_2.

3) the deformation due to the rotation and local bending of the chord members and horizontal members, leading to a displacement δ_3 and a stiffness k_3.

If it is assumed that the stiffnesses of the three mechanisms are independent on each other, the connection of the horizontal member and chord member is infinitely stiff, and the connection of the diagonal members does not transmit moments, then the total stiffness will be the series stiffness of k^1 and k^2 parallel to k^3:

$$k_{eq} = k_3 + \frac{1}{\frac{1}{k_1} + \frac{1}{k_2}}$$

calculation k_1:

elongation of the diagonal: $$e_d = \frac{Q\ d}{2\ E\ Ad\ \cos\phi}$$,

displacement: $\delta_1 = \frac{e_d}{\cos\phi}$, using: $\cos\phi = \frac{h}{2\ d}$, and:

$k_1 = \frac{Q\ s}{\delta_1}$, leads to: $$k_1 = \frac{E\ Ad\ h^2\ s}{2\ d^3}$$

calculation of k_2:

elongation of horizontal brace member: $e_d = \frac{Q\ h}{4\ E\ Av}$, leading to:

$$k_2 = \frac{4\ E\ Av\ s}{h}$$

calculation of k_3:

From ref. 13, follows:

$$k_3 = \frac{24\ s}{\frac{s^3}{E\ Icp} + \frac{2\ h\ s^2}{E\ Ihb}}$$

For the stiffness due to a shear force Q in the case of the equivalent beam holds:

$k_{eq} = G\ Aeq = \frac{E\ Aeq}{2\ (1 + \nu)}$, using $k_{eq} = k_3 + \frac{1}{\frac{1}{k_1} + \frac{1}{k_2}}$ leads to:

$$Aeq = \frac{48\ (1 + \nu)}{\frac{s^2}{Icp} + \frac{2\ h\ s}{Ihb}} + \frac{(1 + \nu)}{\frac{d^3}{Ad\ b^2\ s} + \frac{h}{4\ Av\ s}}$$

Due to the relatively low bending stiffness of the horizontal brace members the contribution of the first term is less than 1 percent. Thus this term can be neglected.

$$Aeq = \frac{(1 + \nu)}{\frac{d^3}{Ad\ b^2\ s} + \frac{h}{4\ Av\ s}}$$

This simplification also makes the extension to three dimensions less complicated.

extension to three dimensions

All contributions to the stiffness due to bending of the members will be ignored.

The deformation of the bay will be a combination of a translation of AC and BC in its own plane (ACDF and BCEF) leading to B'C' and A'C' and a rotation about DF and EF leading to A''C'' and B''C''. (fig. 16)

The ultimate deformation due to the shear force will then be $\delta_{CC''}$.

On one bay the shear force Q^* leads to deflection $\delta_{CC'}$

Aeq = equivalent shear area of a two dimensional bay.
Ash = equivalent shear area of the three dimensional bay.

$$\delta_{CC''} = \frac{\delta_{CC'}}{\cos\phi}$$

$$Q = G\ Ash\ \frac{\delta_{CC''}}{s}\ , \qquad Q^* = \frac{Q}{2\ \cos\phi}$$

$\delta_{CC'} = \frac{Q \ s}{2 \cos\phi \ G \ Aeq}$, using these formulations leads to:

$Ash = 2 \cos^2\phi \ Aeq = 1,5 \ Aeq$

equivalent moment of inertia Iy, Iz and torsion moment of inertia It.

The moments of inertia are directly related to the cross-sectional area of the corner post, if the axial forces in the corner posts determine most of the bending stiffness. The torsion moment of inertia is directly related to the shear area of the leg.

The formulations are (ref. 17):

cross section area: $A = 3 \ Aci$

Aci = cross sectional area of cornerpost

shear area: $Ash = 1.5 \ Aeq$

Aeq = equivalent shear area for two-dimensional bay

$Iy = Iz = \frac{1}{2} \ Aci \ W^2$

$J = \frac{1}{4} \ Aeq \ W^2$

APPENDIX A4

conditioned simulation (theoretical background)

Only the main principle of the conditioned simulation will be explained here, for further details see ref. 6.

The objective of conditioned simulations is to minimize the error in amplitude and phase between generated random wave kinematics and measured kinematics.

Any variable (wave amplitude, wave velocities, free surface slope and pressure) on which the simulation is to be conditioned may be represented as

$$Vcond = \sum_{m} \sum_{j} T(f_{mj},\theta_{j},z)\ A_{mj}\ \cos(\Phi_{mj} + \tau(f_{mj},\theta_{j},z))$$

$T(f_{mj},\theta_{j},z)$ = amplitude transfer function

$\tau(f_{mj},\theta_{j},z)$ = phase transfer function

A_{mj} = free surface wave amplitude

Φ_{mj} = free surface wave phase

m = frequency subscript

j = directional subscript

As long as the conditioned variable is a linear function of the free surface displacement it will be possible to condition a simulation with it.

The minimization routine roughly follows the following steps. First it generates from the given wave amplitude spectrum a random realization of each conditioned variable. At any frequency each variable is a sum of wavelets. Via Fast Fourier Transformation of the measured variable an amplitude and phase are obtained at each frequency. The amplitude and phase at each frequency initially simulated will be compared to that of the measured one. By manipulating the phases, amplitudes and directions of the

simulated wavelets in the following way it tries to minimize the error:

1) Shift the phases of all the wavelets the same amount
2) Shift the phase of each wavelet individually
3) Change the direction of each wavelet, then repeat step 2)
4) Multiply all of the wavelet amplitudes by the same number
5) Multiply each wavelet amplitude individually

these five steps are repeated until no reduction in the error occurs or an acceptable error level is reached.

APPENDIX A5

<u>calculations</u>

lumped Morison coefficients, corner post

The Morison equation with lumped coefficients is

$$Bcp = \sum_{i=1}^{3} AREAcp_i Cd\ \rho,$$

$$Acp = \sum_{i=1}^{3} VOLUMEcp_i Cm\ \rho,$$

$AREAcp_i$ = projected area per unit length of corner post i

$VOLUMEcp_i$ = volume per unit length of corner post i

For a circular corner post without racks, the projected area would be equivalent to the diameter D and the volume equivalent to $0.25\ \pi\ D^2$.

When racks are attached to the corner post, the problem is more complex. The racks make the coefficients dependent on the direction of flow attack and reduce the distinction between rough coefficients and smooth coefficients for Cd and Cm.

No useful experimental values are available, investigation of these will be carried out by KSEPL in the near future.

The projected area will be assumed to be equal to the diameter of the circular part and all the influence of the racks will be lumped into the drag coefficient Cd. The cornerpost will assumed to be smooth.

The Cd value follows from the corner post calculations of the Maersk Giant. The used formulation is based on a combination of drag coefficients for a circular cylinder and for a flat plate.

$$Cd = 0.7 + (2\ (D/d) - 0.7)\ \sin^2 a$$

D = "diameter" rack to rack

d = diameter circular part

a = flow attack angle

The directional influence of the racks has been accounted for by averaging the angle dependent Cd values over a range from $a=0$ to $a=\pi$. This lead to a Cd value equal to 2.05.

The influence of the racks on the volume will be calculated directly in the volume and is simply the sum of the volume of the circular part and the rack part, ignoring directional influences. The Cm value now is 2.0 and is the same for all members: circular and cornerposts.

$$VOLUMEcp_i = Ac + Ar \qquad [m^3/m^1]$$

Ac = area circular part

Ar = area rack part

$$Ac = 0.25\ \pi\ d^2$$

$$Ar = \left(\frac{D1 + D2}{2} - d\right)\ t$$

D1 = largest "diameter" of rack (tooth to tooth)

D2 = smallest "diameter" of rack

numerical results

D = 1.7 m; d = 1.0 m; ρ = 1025 kg/m^3; D1 = 1.26 m; D2 = 1.7 m; t = 0.1778 m

is giving:

Acp = 5355.1 kg/m^1
Bcp = 3151.9 kg/m^2

lumped Morison coefficients, brace members

The Morison equation with lumped coefficients for the brace members is:

$$Bbm = \frac{1}{Lb} \sum_{i=1}^{12} \{0.5\ \rho\ Cd\ Di\ (1 - \sin^2\phi_i \cos^2\psi_i)^{3/2} Li\}$$

$$Abm = \frac{1}{Lb} \sum_{i=1}^{12} \{0.25\ \pi\ \rho\ Cm\ Di^2\ (1 - \sin^2\phi_i \cos^2\psi_i)^{1} Li\}$$

i = member number i
Di = diameter of member i [m]
Li = length of member i [m]
ϕi = orientation of member i
ψi = orientation of flow direction
Lb = bay height

The Cd and Cm values used by KSEPL are:

Cd_rough = 1.20 Cm_rough = 2.0
Cd-smooth = 0.63 Cm_smooth = 2.0

The differences due to different flow attack angles (β=0° to β=30°) are about 1,5 %. The calculations are made for β = 15°, giving an intermediate value.

The calculations have been made for two different types of bays. The lower bays (#1 to #5) and the upper bays (#6 to #19). Bays with higher numbers are always above the sea surface. Bays lying above mean sea level are assumed to be smooth, while those below are assumed to be rough.

numerical results

(see fig. 14) for definitions

L1 = L2 = L4 = L5 = L7 = L8

L3 = L6 = L9

L10 = L11 =L12

(analogue for Di)

bay #1 - #5:

L1 = 6,273 m; L3 = 11,000 m; L10 = 5,595 m; Lb = 4,000 m

D1 = 0,356 m; D3 = 0,406 m; D10 = 0,169 m

ϕ' = 56°; ψ' = 60°

Bbm = 2211,0 kg/m²

Abm = 2498,9 kg/m¹

bay #6 - #19

L1 = 6,273 m; L3 = 11,000 m; L10 = 5,595 m; Lb = 4,000 m

D1 = 0,356 m; D3 = 0,406 m; D10 = 0,169 m

ϕ' = 56°; ψ' = 60°

Bbm = 2211,0 kg/m² (rough, #6 - #16)

Bbm = 1161,0 kg/m² (smooth, #17 - #19

Abm = 2233,0 kg/m¹

calculations of Abm from DYNAL added mass calculations

These calculations have been carried out by running the DYNAL program for a single bay. DYNAL calculates the added mass in three directions. Only the horizontal directions are in case of the equivalent beam important.

$$Abm = \frac{Cm\ Madded}{Lb} \quad [kg/m^1]$$

bay #1 - #5:

Abm_x-direction = 3291,7 kg/m¹
Abm_y_direction = 3538,3 kg/m¹

bay #6 - #19

Abm_x-direction = 2985,1 kg/m¹
Abm_y_direction = 3196,7 kg/m¹

APPENDIX A6

damping estimation

The dynamic response of a structure at the natural frequency is largely specified by its damping ratio, defined as percentage of critical damping:

$$\beta = \frac{c}{c_{cr}}$$

Damping is caused by energy losses due to friction in the structure, energy dissipation at the foundation and velocity differences between the motion of the structure and the fluid (hydrodynamic damping).

There is great uncertainty on the magnitude of each contribution to the total damping ratio. For this reason the damping has been estimated here by using the measured responses of the jack-up. This estimation is based on several simplifications and should therefore be considered as only an indication of the damping ratio.

an estimation of the damping ratio

The principle is as follows:

From the measured surface elevation spectrum $S_{\eta\eta}(\omega)$ one can derive the spectrum $S_{FF}(\omega)$ of the applied force on the structure by using the Morison equation. The corresponding response spectrum $S_{rr}(\omega)$ (for example the overturning moment spectrum) follows from this force spectrum via a transfer function. This response spectrum can be derived from the measurements as well.

If the drag part of the Morison equation is neglected and the inertia coefficient is assumed to be independent of the frequency (at least in the frequency range considered in this analysis), the transfer function $H_{F\eta}(\omega)$ from surface elevation η to applied wave force F may be estimated by: $H_{F\eta}(\omega)$ = A.

The transfer function from the applied forces to the dynamic response is estimated as a constant B (quasi static part), multiplied by the dynamic amplification factor of a 'single degree of freedom' system:

$$DAF(\omega) = \frac{1}{\sqrt{((1 - \omega^2/\omega_n{}^2)^2 + (2\ \beta\ \omega/\omega_n)^2)}} \quad ,$$

thus,

$$H_{rF}(\omega) = B\ DAF(\omega)$$

Now the damping ratio can be estimated from the ratio of the response and surface elevation spectral values at the dominant wave frequency and the natural frequency of the structure:

$$S_{rr}(\omega) = A^2\ B^2\ DAF^2(\omega)\ S_{\eta\eta}(\omega)$$

The damping may be neglected at the dominant wave frequency ω_0 thus follows:

$$DAF^2(\omega_0) = 1/(1 - \omega_0{}^2/\omega_n{}^2)^2$$

The DAF at the natural frequency is only dependent on the damping ratio:

$$DAF^2(\omega_n) = 1/(2\ \beta)^2.$$

After some algebra it follows that:

$$\beta = \frac{1}{2\ DAF(\omega_0)} \sqrt{\left(\frac{S_{\eta\eta}(\omega_n)\ S_{rr}(\omega_0)}{S_{\eta\eta}(\omega_0)\ S_{rr}(\omega_n)}\right)}$$

The right-hand side can be estimated from the spectra derived from the measurements. The first bending modes are associated with the over turning moment, and the bow y-acceleration. The bow acceleration in x-direction shows heavy response at the first torsion mode and so is used to estimate the damping of the torsion mode.

The ratio $\frac{S_{\eta\eta}(\omega_n)}{S_{\eta\eta}(\omega_0)}$ follows from the wave amplitude spectrum of wave meter #1 (see fig. 22) and is about 0,042.

The results are listed in table 31.

One may conclude from this table that the damping ratio falls in a range from 1 percent to 3 percent and may be dependent on the mode. The bending mode seems to have more damping than the torsion. The y-direction in which the responses are the largest (OTM-x) seems to be more damped than the less important x-direction.

APPENDIX A7

foundation stiffness calculation

The rotational stiffness follows from the following equation which is derived for circular, infinitely stiff plates on top of a perfectly elastic half space (ref. 18):

$$K_\theta = \frac{M}{\theta} = \frac{8\ G\ R^3}{3\ (1 - \nu)}$$

K_θ = rotational spring stiffness

θ = angle of rotation

M = moment over spudcan

G = shear modulus

ν = Poisson's ratio

R = footing radius

The horizontal projection of the spudcan is a polygon (fig. 17), but has been modelled as a circular plate with an equivalent radius R of 9 meter. Poisson's ratio will be around 0,25 for the firm sand considered. The shear modulus G has been estimated as 30 MPa given the firm sand and the expected stress level under preload. The inaccuracy of this value is around 20% due to the lack of any soil data, whereas the inaccuracy of the model itself is negligible for elastically behaving materials.

Two phenomena which are not included in the model affect the stiffness and will be accounted for by multiplying the stiffness with correction factors. The first is the reduction in stiffness when more bearing capacity is mobilised. For instance this may be a factor of 2 if the soil strength has been mobilised for 50%. The second effect is the increase by at least the same factor of stiffness due to "setting" of the spudcan and consolidation of the ground.

Since the loads which have been calculated in this report indicate that the sea states analysed are low (the strength will not be mobilised by more than 5%) the rotational stiffness is expected to have a value around:

$K_\theta = 0,6*10^8-1,8*10^8$ [kNm/rad]

APPENDIX A8

<u>estimation of the natural period by hand</u>

The natural period of a jack-up may be estimated by:

$$T_n = 2\,\pi\,\sqrt{\left(\frac{M^*}{K^*}\right)}$$ where

M^* = effective mass related to one leg

K^* = effective stiffness of one leg

If the expressions, which are suggested by Odland (ref. 17), are used the following calculation of the estimation of the natural period may be made.

$$M^* = (1/3)\,M_H + c_1\,M_L$$

M_H = total mass of hull and mass of

part of the legs located above the lower guide

M_L = mass of one leg located between top of spudcan and lower guide

$c_1 = 0{,}5 - 0{,}125\,\mu$

μ = coefficient which determines stiffness of foundation (fig. 11)

$$K^* = (1 - \frac{P}{P_E})\ k$$

$$k = \frac{1}{f_B + f_Q} = \text{transverse stiffness}$$

f_B = bending flexibility

f_Q = shear flexibility

P = axial force in one leg due to functional loads

$$P_E = \frac{\pi^2\ E\ I}{K^2\ l^2} = \text{Euler load}$$

E = Young's modulus of elasticity

I = average moment of inertia of the part of the leg below the lower guides

K = effective length factor = $2\sqrt{c}$

$$c = \frac{3\ E\ I}{l^3\ k}$$

$$k = \frac{1}{f_B + f_Q} \quad \text{where}$$

$$f_B = \frac{l^3}{3\ E\ I}\ (1 - \frac{3}{2}\ \frac{\mu}{1 + \mu} + \frac{i}{1 + \mu}\ \frac{d}{l})$$

$$f_Q = \frac{1}{G\ A_Q}\ (1 + \frac{a}{1 + \mu}\ \frac{l}{d}) \quad \text{where}$$

$$a = \frac{A_Q}{A_{Q0}}\ (1 - \beta)$$

$$i = \frac{I}{I_0}\ (1 - \beta\ (1 - 3\ \frac{b}{d}\ + \frac{3}{2}\ (\frac{b}{d})^2)$$

A_{Q0} = average shear area of one leg between upper and lower guides

I_0 = average moment of inertia of one leg between upper and lower guide

A_Q = average shear area of one leg below lower guide

I = average moment of inertia of one leg below lower guide

β = fraction of leg bending moment reacted by leg to clamp connection

calculations

The following numerical values belong to the model used.

$M_H = 1{,}8*10^7$ Kg; $M_L = 1{,}3*10^6$ Kg

l = 95,9 m; $E = 2{,}1*10^{11}$ N/m²; $G = E/2{,}6 = 3{,}5*10^{10}$;

d = 18,4 m; b = 4,6 m; $\beta = 0{,}92$; $\mu = 1{,}07$; I = 34 m²; $I_0 = 20{,}8$ m²;

$A_Q = 0{,}085$ m²; $A_{Q0} = 0{,}086$ m²;

Using these values in the various equations holds:

$M^* = 7{,}7*10^6$ Kg

$f_Q = 3{,}87*10^{-8}$

$f_B = 1{,}33*10^{-8}$

$K^* = 1{,}86*10^7$

$$T_n = 2\,\pi\,\sqrt{\left(\frac{M^*}{K^*}\right)} = 4{,}0 \text{ s}$$

This is close to the natural period of $T_n = 4{,}2$ s calculated by DYNAL, which supports the calculation method suggested by Odland.

TABLES

Data Segment	Maximum Individ. Wave Hgt [meter]	Dominant Wave Period [seconds]	Mean Current Velocity [m/s]	Mean Wind Speed [m/s]	Direction of Wave Propagation (see note)
#1 Feb.4 21:00 h	6,2	7,7	0,015	28,8	30,1° 47,0°
#2 Feb.6 01:40 h	5,6	7,7	0,772	23,1	- 54,3°
#3 Feb.8 22:00 h	1,7	4,3	0,411	10,3	285,1° 290,4°
#4 Feb.6 03:10 h	5,6	7,5	0,576	25,2	43,7° 56,5°

Note: the direction of wave propagation is the predominant wave direction and is measured clockwise from true North. Waves are propagating toward this direction. The first angle of each pair is the estimation from the data of current meter #1, the second is the estimation from c.m. #2.

Table 1, summary of met-ocean quantities, ref 1.

JOINT NB	MASS OF STEEL (metric-tons)	ADDED MASS (metric-tons)	BUOYANCY (kNewton)
100	81.79922		
101	59.27097	16.45960	-182.1780
102	59.27097	16.45960	-182.1780
103	59.27097	16.45960	-182.1780
104	59.27097	16.45960	-182.1780
105	59.27097	16.45960	-182.1780
106	47.63794	18.18264	-198.8258
107	47.63794	18.18264	-198.8258
108	47.63794	18.18264	-198.8258
109	41.82162	18.18264	-198.8258
110	41.82162	18.18264	-198.8258
111	41.82162	18.18264	-198.8258
112	41.82162	18.18264	-198.8258
113	41.82162	18.18264	-198.8258
114	41.82162	18.18264	-198.8258
115	41.82162	18.18264	-198.8258
116	41.82162		
117	41.82162		
118	42.13387		
119	42.74464		
120	44.23721		
121	49.01889		
122	50.46001		
123	51.87969		
124	53.27517		
125	52.43000		
126	53.53989		
127	50.80570		
128	46.57230		
129	43.29298		
130	41.82162		
131	41.82162		
132	60.41840		

Table 2 ,Mass distribution of one leg, others similar.

MEMBER NB	CROSS SECT. AREA (m**2)	SHEAR AREA (m**2)	MOMENT OF INERTIA (Ix=Iy) (m**4)	TORSION CONST. (J) (m**4)
100	3.22579980	0.64515996	70.75910187	2.08115005
101	2.88653612	0.05442123	69.23529816	1.95798898
102	2.88653612	0.05442123	69.23529816	1.95798898
103	2.88653612	0.05442123	69.23529816	1.95798898
104	2.88653612	0.05442123	69.23529816	1.95798898
105	2.88653612	0.05442123	69.23529816	1.95798898
106	0.94583035	0.05715494	22.68630791	2.05634332
107	0.94583035	0.05715494	22.68630791	2.05634332
108	0.94583035	0.05715494	22.68630791	2.05634332
109	0.78470165	0.05714158	18.82153893	2.05586243
110	0.78470165	0.05714158	18.82153893	2.05586243
111	0.78470165	0.05714158	18.82153893	2.05586243
112	0.78470165	0.05714158	18.82153893	2.05586243
113	0.78470165	0.05714158	18.82153893	2.05586243
114	0.78470165	0.05714158	18.82153893	2.05586243
115	0.78470165	0.05714158	18.82153893	2.05586243
116	0.78470165	0.05714158	18.82153893	2.05586243
117	0.78470165	0.05714158	18.82153893	2.05586243
118	0.78470165	0.05875819	18.82153893	2.11402559
119	0.78470165	0.06175366	18.82153893	2.22179794
120	0.78470165	0.06847971	18.82153893	2.46379018
121	0.86850792	0.07632747	20.83168221	2.74614024
122	0.86850792	0.08281776	20.83168221	2.97965074
123	0.86850792	0.08905876	20.83168221	3.20419168
124	0.86850792	0.09535674	20.83168221	3.43078303
125	0.86850792	0.09023971	20.83168221	3.24668026
126	0.86850792	0.09517298	20.83168221	3.42417145
127	0.78470165	0.09756332	18.82153893	3.51017213
128	0.78470165	0.07863963	18.82153893	2.82932806
129	0.78470165	0.06175335	18.82153893	2.22178674
130	0.78470165	0.05714158	18.82153893	2.05586243
131	0.78470165	0.05714158	18.82153893	2.05586243

Table 3, Member properties of one leg, others similar.

	Data Segment	Total Hull Mass [tons]	Hull Mass on Each Leg [tons] Leg #100 Bow	Leg #200 Stern Prt.	Leg #300 Stern Stbd.
#1	Feb.4 21:00 h	15922	4800	5590	5530
#2	Feb.6 01:40 h	15794	4760	5550	5480
#3	Feb.8 22:00 h	15555	4729	5460	5366
#4	Feb.6 03:10 h	15794	4760	5550	5480

Table 4, mass of hull distribution, ref 1.

JOINT NB	LUMPED MASS (metric-tons)
1014	3789.0269
1024	947.2567
1091	3188.1745
1092	3895.9826
1093	3967.1715

CROSS SECTIONAL AREA:	3.2258	m**2
MOMENT OF INERTIA	:	374.61	m**4
TORSION CONSTANT	:	4.1623	m**4
SHEAR AREA	:	3.2258	m**2

TOTAL MASS OF DECK	:	15787.6	tons
TOTAL MASS OF LEGS (steel)	:	4865.7	tons
TOTAL ADDED MASS	:	792.4	tons
TOTAL BUOYANCY	:	8697.6	kN

Table 5 ,Lumped deck masses, deckmember properties and mass totals.

Data Segment	Natural Period (sec)		Leg/Hull, Leg/Soil fixity	
	1st,2nd Bending	1st Torsion	Ru/P (%)	μ (-)
#1 Feb.4 21:00 h	4,21	3,45	22,1	1,23
#2 Feb.6 01:40 h	4,18	3,45	22,2	1,23
#3 Feb.8 22:00 h	4,12	3,45	21,4	1,23
#4 Feb.6 03:10 h	4,18	3,44	20,9	1,23
DYNAL-Model	4,22	3,45	20,0	1,07

Table 6, constraints of the structural model and DYNAL results, ref 1.

MEMBER NB.	STIFFNESS OF PSEUDO MEMBER K(1)	K(2)	K(3)	K(4)	K(5)	K(6)
		[kips/in]			[kips-inch/rad]	
1051	0.3E+04	0.3E+04	0,0	0,0	0,0	0,0
1052	0.3E+04	0.3E+04	0,0	0,0	0,0	0,0
1053	0.3E+04	0.3E+04	0,0	0,0	0,0	0,0
1061	0.3E+04	0.3E+04	0,0	0,0	0,0	0,0
1062	0.3E+04	0.3E+04	0,0	0,0	0,0	0,0
1063	0.3E+04	0.3E+04	0,0	0,0	0,0	0,0
1064	0.1E+02	0.1E+02	0.1E+16	0.2E+10	0.2E+10	0.7E+19
1065	0.1E+02	0.1E+02	0.1E+16	0.2E+10	0.2E+10	0.7E+19
1066	0.1E+02	0.1E+02	0.1E+16	0.2E+10	0.2E+10	0.7E+19

The member numbers listed in this table correspond to those in fig. 18. All the pseudo members have a small artificial length of 4,31 mm (= 0,17 inch), but are not physical beams. The stiffnesses listed above have the following meaning:

K(1) = stiffness along member x axis

K(2) = stiffness along member y axis

K(3) = stiffness along member z axis

K(4) = stiffness about member x axis

K(5) = stiffness about member y axis

K(6) = stiffness about member z axis

Members number 1051 to 1053 and 1061 to 1063 correspond to the lower and upper guide connection, while that members number 1064 to 1066 correspond to the leg/clamp connection.

Table 7, stiffnesses of pseudomembers

THE MINIMIZED GRID HAS A RECTANGLE OF GRIDPOINTS AT EACH LEVEL

LEVEL (ft)	MINIMUM X (ft)	MAXIMUM X (ft)	MINIMUM Y (ft)	MAXIMUM Y (ft)	NUMBER OF GRID POINTS AT THIS LEVEL
0.000	-108.800	108.800	-64.844	124.700	460
-10.000	-108.800	108.800	-66.018	124.700	224
-20.000	-108.800	108.800	-62.350	124.700	120
-30.000	-108.800	108.800	-62.350	124.700	120
-50.000	-108.800	108.800	-62.350	124.700	56
-80.000	-108.800	108.800	-62.350	124.700	56
-120.000	-108.800	108.800	-83.133	124.700	36
-160.000	-108.800	108.800	-74.820	124.700	25
-200.000	-108.800	108.800	-62.350	124.700	20
-230.000	-108.800	108.800	-62.350	124.700	20
			TOTAL NON-SURFACE GRID POINTS		1137

SURFACE GRID DESCRIPTION

0.000	-108.800	108.800	-64.844	124.700	460
			TOTAL NUMBER OF GRID POINTS		1597

Table 8, number of grid points and spacing per level.

# ref. to fig. 20	numb. of points	Vnorth [1] (knots)	Veast [1] (knots)	|V| (knots)	direct.[2] of |V|
1	256	2,45E-2	7,20E-2	7,60E-2	189°
2	256	3,10E-2	5,65E-2	6,44E-2	204°
3	2048	5,00E-2	5,24E-2	7,24E-2	214°
4	2048	2,35E-2	6,45E-2	6,87E-2	195°
5	4000	2,09E-2	1,95E-2	2,86E-2	217°
6	4000	1,27E-2	3,44E-2	3,67E-2	197°

Note 1) North and East of currentmeter. North of c.m. #1 = 261° anti-clockwise to positive x-axis. North of c.m. #2 = 267°

Note 2) Direction with respect to positive x-axis. Wind acting towards this direction.

Table 9, current velocities and angles.

The relative change in percentages of the 'real' or unchanged period is:

$$\epsilon(x) = \frac{T(Y=Yx\%) - T(Y=Yo)}{T(Y=Yo)} * 100\%$$

T(.) = natural period

Yo = value of the parameter to be changed

$\epsilon(x)$ = relative change of natural period

x = percentage of change

Yx = (1 + x/100)*Yo

Y.	x=+10%	x=-10%	x=+20%	x=-20%	Yo
mass of the deck					
T(bending)	+4.1	-4.3	+8.1	-8.7	$1,6*10^7$
T(torsion)	+3.9	-4.0	+7.6	-8.2	(kg)
foundation stiffness					
T(b.)	-1.6	+1.8	-3.0	+3.9	$1,0*10^8$
T(t.)	-1.5	+1.7	-2.8	+3.9	kNm/rad
shear area					See
T(b.)	-1.0	+1.2	-1.9	+2.8	Table 3
T(t.)	-0.9	+1.1	-1.7	+2.5	
leg clamps stiffness					See
T(b.)	-1.0	+1.2	-1.8	+2.4	Table 7
T(t.)	-0.9	+1.1	-1.7	+2.2	

Table 10 (I), relative change of natural period, $\epsilon(x)$ (%), (to be continued)

Y.	x=+10%	x=-10%	x=+20%	x=-20%	Yo
modul. of elast., E					
T(b.)	-0.9	+1.1	-1.7	+2.4	$2,1*10^{11}$
T(t.)	-0.8	+1.0	-1.5	+2.2	(N/m^2)
moment of inertia, I					See
T(b.)	-0.9	+1.0	-1.6	+2.3	Table 3
T(t.)	-0.9	+0.9	-1.4	+2.0	
mass of the legs					See
T(b.)	+0.8	-0.8	+1.5	-1.5	Table 2
T(t.)	+1.0	-1.1	+2.1	-2.1	
stiffness upper guide					See
T(b.)	-0.5	+0.5	-1.0	+1.1	Table 7
T(t.)	-0.5	+0.6	-1.0	+1.1	
stiffness lower guide					See
T(b.)	-0.4	+0.5	-0.8	+1.1	Table 7
T(t.)	-0.3	+0.4	-0.6	+0.9	
torsion constant J					See
T(b.)	0.0	0.0	0.0	0.0	Table 3
T(t.)	-0.5	+0.5	-0.9	+0.9	

Table 10 (II), relative change of natural period, $\epsilon(x)$ (%)

amplitude of displ. joint 1024 (in)	Cd = 0,6 Cm = 2,0	Cd = 0,6 Cm = 4,0	δ	Cd = 0,6 Cm = 2,0	Cd = 0,6 Cm = 4,0	δ
	T = 7,7 s H = 5,0 ft			T = 4,0 s H = 5,0 ft		
U-max.	0,092	0,176	1,91	1,273	2,509	1,97
	T = 7,7 s H = 10,0 ft			T = 4,0 H = 10,0 ft		
U-max	0,237	0,176	1,75	3,036	5,879	1,94
	T = 7,7 s H = 20,0 ft			T = 4,0 H = 20,0 ft		
U-max	0,756	1,150	1,55	Not a stable wave		
	T = 10,0 s H = 60,0 ft					
U-max	5,614	6,374	1,14			

The factor δ is the ratio of the excitation for the 'Cm = 4' case and the 'Cm = 2' case.

Table 11, results of changes in the Morison equation terms.

Wave Meter	number of time steps, 1 step = 0,5 seconds		
	step 1 - 1024	1025 - 2048	2049 - 4096
#1	$0,63895*10^1$	$0,63502*10^1$	$0,62714*10^1$
#2	$0,94436*10^1$	$0,63534*10^1$	$0,59753*10^1$

Table 12, zero order moments of surface elevation spectra (m^2)

Wave Meter	time interval, 1 step = 0,5 seconds		
	step 1 - 1024	1025 - 2048	2049 - 4096
#1	1,8453	1,8970	1,8049
#2	2,2008	1,7483	1,7243

Table 13, peak wave amplitude exceeded by 10 % of all peak amplitudes (m)

	BOW X-ACCELERATION (m/s²)/(rad/s)			BOW Y-ACCELERATION (m/s²)/(rad/s)		
	1	2	3	1	2	3
MEAS.	0,03E-3	0,30E-3	0,65E-3	0,03E-3	0,95E-3	-
DYNAL	0,02E-3	0,15E-3	0,78E-3	0,01E-3	0,28E-3	-
Dyn/Meas. (-)	0,67	0,50	1,20	0,33	0,29	-

Table 14, peak values of Bow acceleration spectra, 1st interval

	BOW X-ACCELERATION (m/s²)			BOW Y-ACCELERATION (m/s²)		
	X1/3	X1/10	Xmax	Y1/3	Y1/10	Ymax
MEAS.	0,023	0,030	0,037	0,020	0,026	0,031
DYNAL	0,022	0,030	0,046	0,014	0,018	0,022
Dyn/Meas. (-)	0,96	1,00	1,24	0,70	0,69	0,71

Table 15, significant peaks of Bow acceleration time histories, 1st interval

X-SHEAR FORCE LEG #3 (kN)²/(rad/s)			
	1	2	3
MEAS.	4,5 E+3	10,2E+3	9,5 E+3
DYNAL	2,0 E+3	5,5 E+3	12,2E+3
Dyn/Meas. (-)	0,44	0,54	1,28

Table 16, leg #3 (joint #119), significant peaks of x shear force spectra.

	BOW X-ACCELERATION (m/s²)²/(rad/s)			BOW Y-ACCELERATION (m/s²)²/(rad/s)		
	1	2	3	1	2	3
MEAS.	0,05E-3	0,10E-3	0,47E-3	0,03E-3	0,60E-3	-
DYNAL	0,03E-3	0,15E-3	0,54E-3	0,01E-3	0,61E-3	-
Dyn/Meas. (-)	0,60	1,50	1,15	0,33	1,02	-

Table 17, peak values of bow acceleration spectra, 2nd interval

	BOW X-ACCELERATION (m/s²)			BOW Y-ACCELERATION (m/s²)		
	X1/3	X1/10	Xmax	Y1/3	Y1/10	Ymax
MEAS.	0,0197	0,0260	0,0337	0,0196	0,0261	0,0335
DYNAL	0,0231	0,0290	0,0378	0,0158	0,0192	0,0238
Dyn/Meas. (-)	1,17	1,12	1,12	0,81	0,74	0,71

Table 18, peak values of bow acceleration time histories, 2nd interval

	STERN X-ACCELERATION DENS. (m/s²)²/(rad/s)			STERN Y-ACCELERATION DENS. (m/s²)²/(rad/s)		
	1	2	3	1	2	3
MEAS.	0,05E-4	0,25E-3	0,10E-3	0,02E-3	0,80E-3	0,40E-3
DYNAL	0,01E-3	0,20E-3	0,09E-3	0,02E-3	0,61E-3	0,35E-3
Dyn/Meas. (-)	2,00	0,80	0,90	1,00	0,76	0,88

Table 19, peak values of stern acceleration spectra, 2nd interval

	STERN X-ACCELERATION (m/s²)			STERN Y-ACCELERATION (m/s²)		
	X1/3	X1/10	Xmax	Y1/3	Y1/10	Ymax
MEAS.	0,0140	0,0189	0,0271	0,0259	0,0350	0,0451
DYNAL	0,0150	0,0193	0,0236	0,0216	0,0307	0,0444
Dyn/Meas. (-)	1,07	1,02	0,87	0,83	0,88	0,98

Table 20, significant peaks of Stern accel. time histories, 2nd interval

	AXIAL FORCE LEG #1 (kN)²/(rad/s)			AXIAL FORCE LEG #2 (kN)²/(rad/s)		
	1	2	3	1	2	3
MEAS.	1,5*E04	8,5E04	-	8,0*E03	2,2*E04	-
DYNAL	2,8*E04	1,1*E05	-	1,0*E04	5,6*E04	-
Dyn/Meas. (-)	1,87	1,29	-	1,25	2,56	-

Table 21, peak values of Axial force Leg #1 and Leg #2 frequency spectra, 2nd interval

	AXIAL FORCE LEG #1 (kN)			AXIAL FORCE LEG #2 (kN)		
	F1/3	F1/10	Fmax	F1/3	F1/10	Fmax
MEAS.	313,5	426,4	616,4	201,8	290,0	415,8
DYNAL	284,1	374,2	541,6	221,6	282,4	380,8
Meas/Dyn. (-)	0,91	0,88	0,88	1,10	0,97	0,92

Table 22, significant peaks of axial force leg #1 (joint 207) and leg #2 (joint 307), 2nd interval

AXIAL FORCE LEG #3			
$(kN)^2/(rad/s)$			
1	2	3	
MEAS.	2,5*E04	1,7*05	-
MEAS. SURFACE	1,8*E04	1,7*05	-
DYNAL	3,0*E04	1,9*05	-
Dyn/Meas. (-)	1,20	1,12	-

Table 23, peak values of axial force leg #3 frequency spectra, 2nd interval

AXIAL FORCE LEG #3 (kN)			
	F1/3	F1/10	Fmax
MEAS.	361,2	491,9	630,1
MEAS. SURFACE	360,4	487,1	617,3
DYNAL	296,8	353,9	433,1
Dyn/Meas. (-)	0,91	0,88	0,88

Table 24, significant peaks of axial force leg #3 (joint 107), 2nd interval

	X-MOMENT LEG #1 (kNm)²/(rad/s)			Y-MOMENT LEG #1 (kNm)²/(rad/s)		
	1	2	3	1	2	3
MEAS.	1,2*E06	6,8*E06	1,0*E06	0,6*E06	2,05*E06	-
DYNAL	1,2*E06	6,5*E06	1,8*E06	1,5*E06	2,2*E06	-
Dyn/Meas. (-)	1,00	0,96	1,80	2,50	1,07	-

Table 25, peak values of bending moment leg #1 spectra, 2nd interval

	X-MOMENT LEG #1 (kNm)			Y-MOMENT LEG #1 (kNm)		
	X1/3	X1/10	Xmax	Y1/3	Y1/10	Ymax
MEAS.	2425,4	3113,3	4134,0	1498,3	2110,6	3009,0
DYNAL	2030,3	2452,1	2885,0	1587,3	2089,9	3121,0
Dyn/Meas. (-)	0,84	0,79	0,70	1,06	0,99	1,04

Table 26, significant peaks of bending moment leg #1 (joint 207), 2nd interval

	X-MOMENT LEG #2 (kNm)²/(rad/s)			Y-MOMENT LEG #2 (kNm)²/(rad/s)		
	1	2	3	1	2	3
MEAS.	1,0*E06	8,5*E06	1,0*E06	0,2*E06	2,1*E06	-
DYNAL	1,3*E06	6,6*E06	1,6*E06	0,4*E06	2,3*E06	-
Dyn/Meas. (-)	1,30	0,78	1,45	2,00	1,10	-

Table 27, peak values of bending moment leg #2 frequency spectra, 2nd interval

	X-MOMENT LEG #2 (kNm)			Y-MOMENT LEG #2 (kNm)		
	X1/3	X1/10	Xmax	Y1/3	Y1/10	Ymax
MEAS.	2662,8	3600,5	4797,8	1408,7	1891,9	3117,0
DYNAL	2080,3	2875,6	3949,7	1528,1	1950,0	2305,3
Dyn/Meas. (-)	0,78	0,80	0,82	1,09	1,03	0,74

Table 28, significant peaks of bending moment leg #2 (joint 307), 2nd interval

	X-MOMENT LEG #3 (kNm)²/(rad/s)			Y-MOMENT LEG #3 (kNm)²/(rad/s)		
	1	2	3	1	2	3
MEAS.	1,0*E06	6,3*E06	-	1,5*E06	1,9*E06	1,5*E06
DYNAL	1,0*E06	6,5*E06	-	1,0*E06	1,8*E06	2,6*E06
Dyn/Meas. (-)	1,00	1,03	-	0,67	0,95	1,73

Table 29, peak values of bending moment leg #3 frequency spectra, 2nd interval

	X-MOMENT LEG #3 (kNm)			Y-MOMENT LEG #3 (kNm)		
	X1/3	X1/10	Xmax	Y1/3	Y1/10	Ymax
MEAS.	2159,6	2856,9	3889,6	1836,0	2508,4	3716,0
DYNAL	1782,2	2193,6	3167,8	1954,2	2477,0	3302,7
Dyn/Meas. (-)	0,83	0,77	0,81	1,06	0,99	0,89

Table 30, significant peaks of bending moment leg #3 (joint 107), 2nd interval

	$DAF(\omega_0)$	$S_{rr}(\omega_0)$	$S_{rr}(\omega_n)$	β (%)
Overturning Moment x-direction (OTM-x)	1,48	$0,10*10^9$	$0,78*10^9$	2,47
Overturning Moment y-direction (OTM-y)	1,52	$0,31*10^8$	$0,36*10^9$	1,96
Bow x-acceleration (Acc-x)	1,29	$0,17/10^4$	$0,51/10^3$	1,43
Bow y-acceleration (Acc-y)	1,56	$0,10/10^4$	$1,61/10^3$	1,23

Table 31, estimation of damping ratios from measured spectral values.

REFERENCES

1) Brekke,J N, North Sea Jack-Up Measurements on Maersk Guardian, July 1989, Offshore Division EPR.55PS.89B;

2) Sarpkaya, T,and Isaacson, M, 1981, Mechanics of Wave Forces on Offshore Structures, Litton Educational Publishing, Inc.;

3) Brekke ,J N et al, Calibration of Jack-Up Leg Foundation Model Using Full-Scale Structural Measurements, May 1989, OTC 6127;

4) Hattori, Y, et al, Natural Vibration of Jack-Up Oil Rig, 1982, Nav. Archit. Ocean Eng, 20;

5) Oord v d, H J M, 1987, Collapse Behaviour of Jack-Up rigs, final thesis report TU Delft dept. of Mechanical Engineering.;

6) Rodenbusch, G,and Forristall, G Z, 1986, An Empirical Model for Random Directional Wave Kinematics Near the Free Surface, OTC 5097;

7) Timoshenko, S, and Young, D H, and Weaver W, Jr, 1974,Vibration Problems in Engineering, John Wiley & Sons, IAc.;

8) Jong-Shyong Wu and Cuann-Yeu Chang, Structural Simplifications of Jack-Up Rig and Its Dynamic Responses in Regular Waves, June 1988, Journal of Ship Research, Vol 32, No.2, pp 134-153;

9) Hambly, E C, and Nicholson B A, 1989, Fatigue of Jack-Ups: simplifying calculations, Marine Structures 2, p 237;

10) Rodenbusch, G, Random Directional Wave Forces on Template Offshore Platforms, May 1986, OTC 5098;

11) Forristall, G Z, et al, Forces on the Cognac Platform in Combined Storm Waves and Currents, May 1989, OTC 6006;

12) Nagata, Y , 1964, The statistical properties of orbital wave motions and their applications for the measurement of directional spectra, J. Oceanogr. Soc. Japan, Vol. 19.

13) Timoshenko, S, 1978, Strength of Materials Part II Advanced Theory and Problems, Van Nostrand Reinhold Company;

14) Anagnostopoulos S A, and Hennegan N M, 1980, DYNAL II: A Computer System For Dynamic and Static Analysis of Offshore Structures- Theory, Verification, and Applications, BRC 57-80;

15) Liu, P, Non-linear Dynamic Simulation of Jack-Up Platform Models, 1989, Hydraulic Engineering Group, Faculty of Civil Engineering , Delft University of Technology;

16) Battjes, J A, september 1982, Windgolven Handleiding College b78, Vakgroep Vloeistofmechanica Faculteit der Civiele Techniek, Technische Universiteit Delft 3e herdruk 1987;

17) Odland, J, 1982, Response and Strength Analysis of Jack-up Platforms, Norwegian Maritime Research NO. 4./1982.

18) American Petroleum Institute, Recommended Practice for Planning, Designing and Constructing Fixed Offshore Platforms, 2A, 1989.

19) Bowden, K F, and White, R A, 1966, Measurements of Orbital Velocities of Sea Waves and Their Use in Determining the Directional Spectrum, Geophys. J. R. Astr. Soc., Vol. 12.

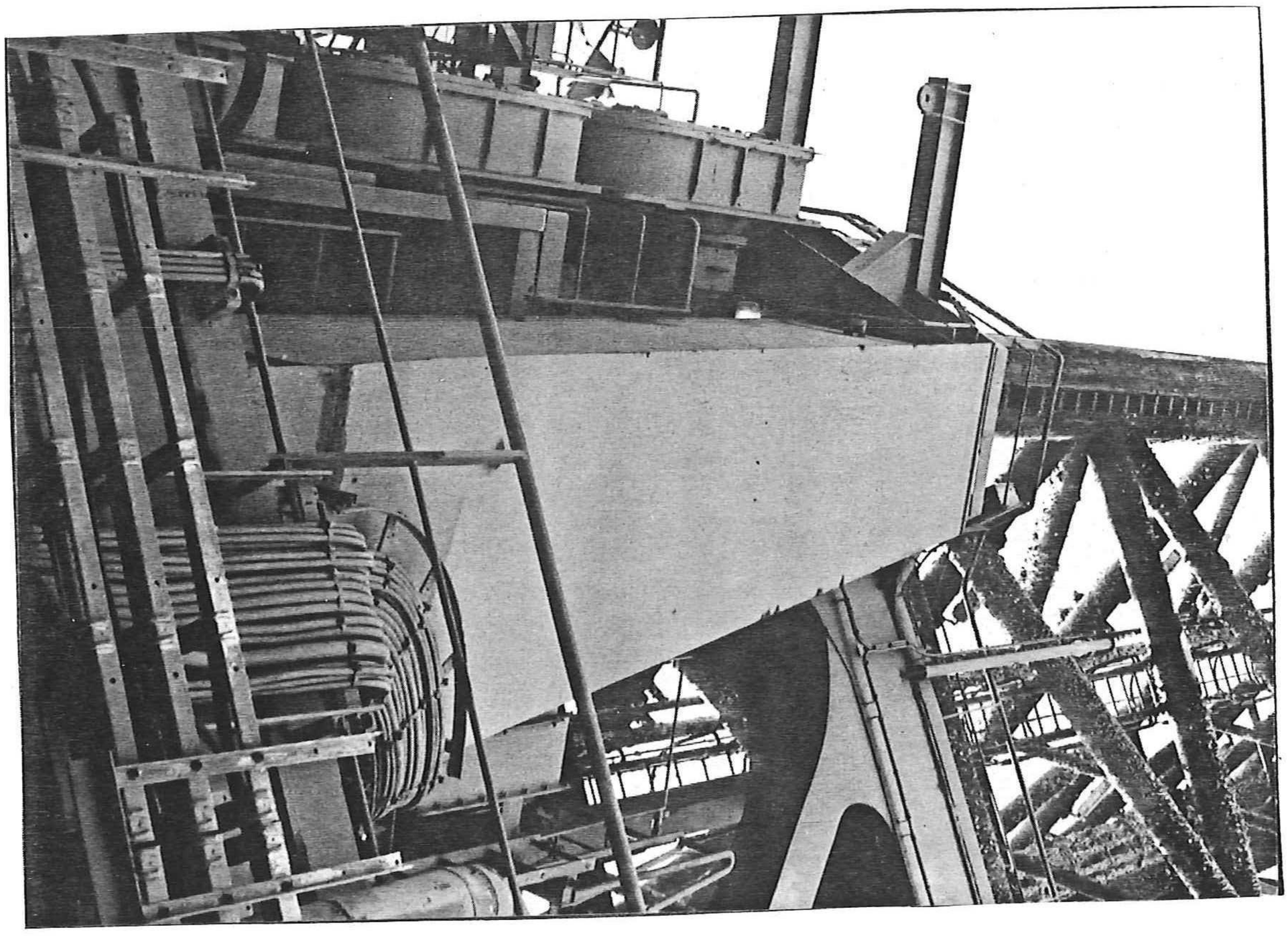

Fig. 1 ,Jacking mechanism.

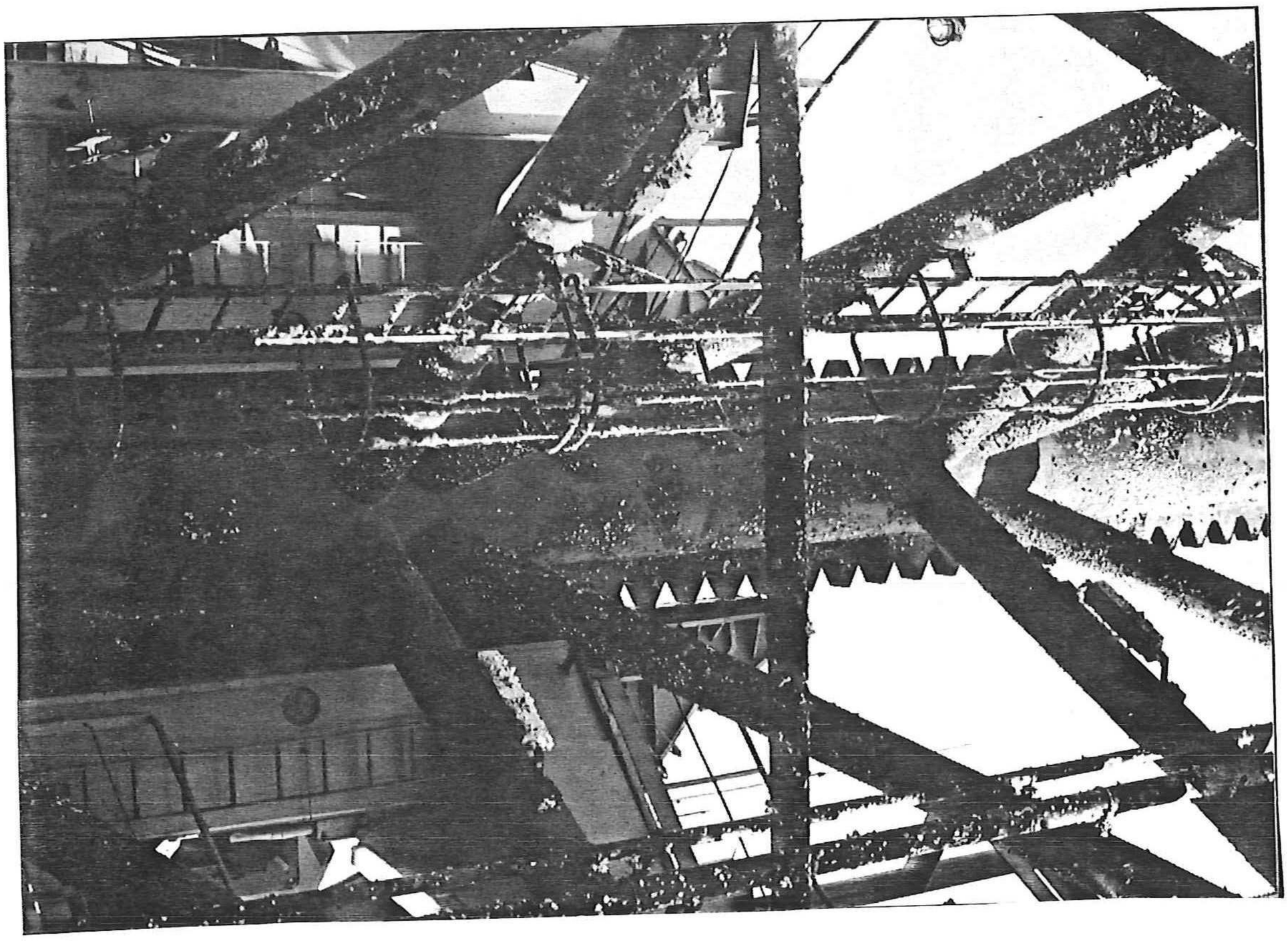

Fig. 2 ,Upper guide.

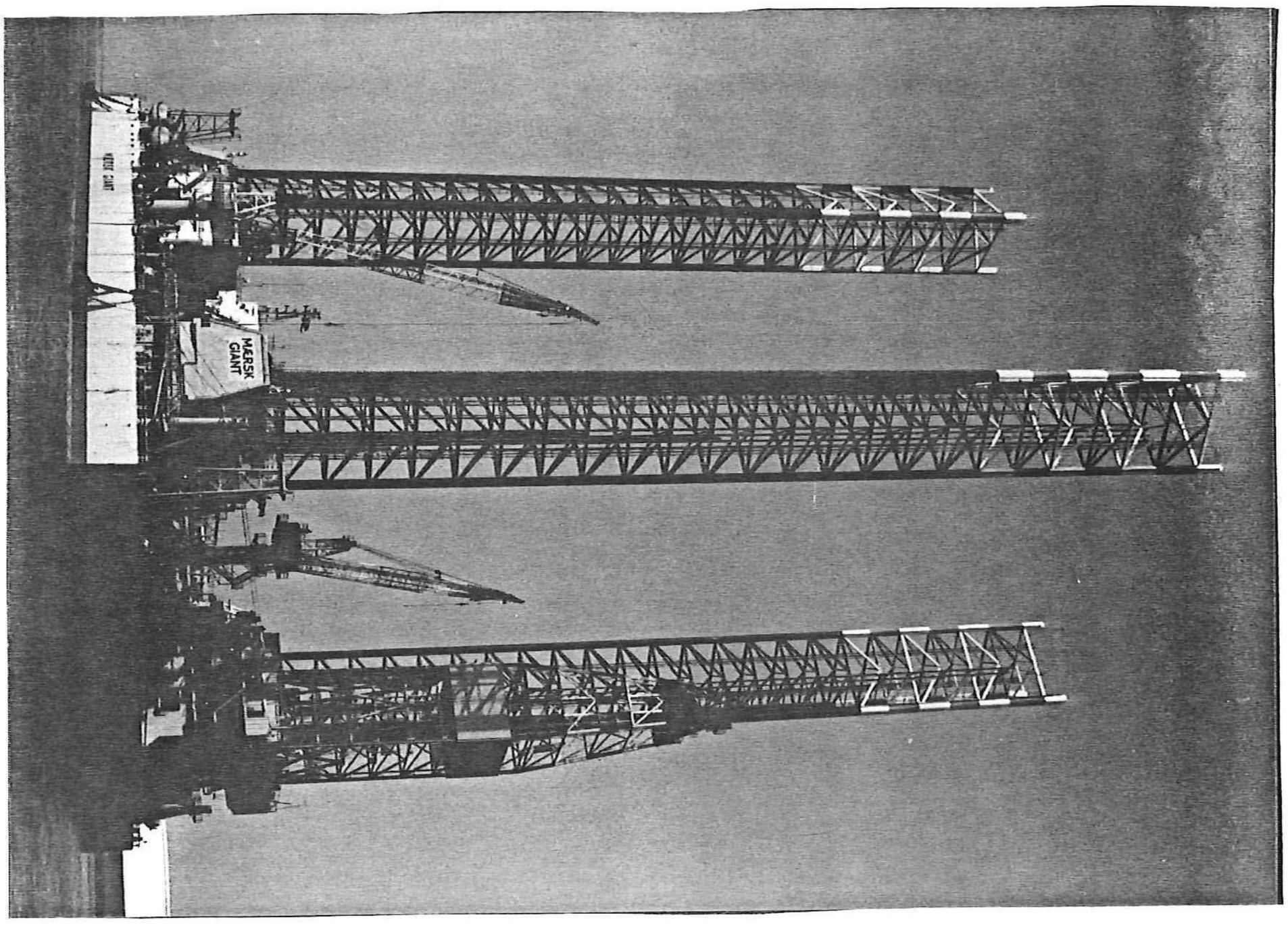

Fig. 3 ,Jack-up "Maersk Giant".

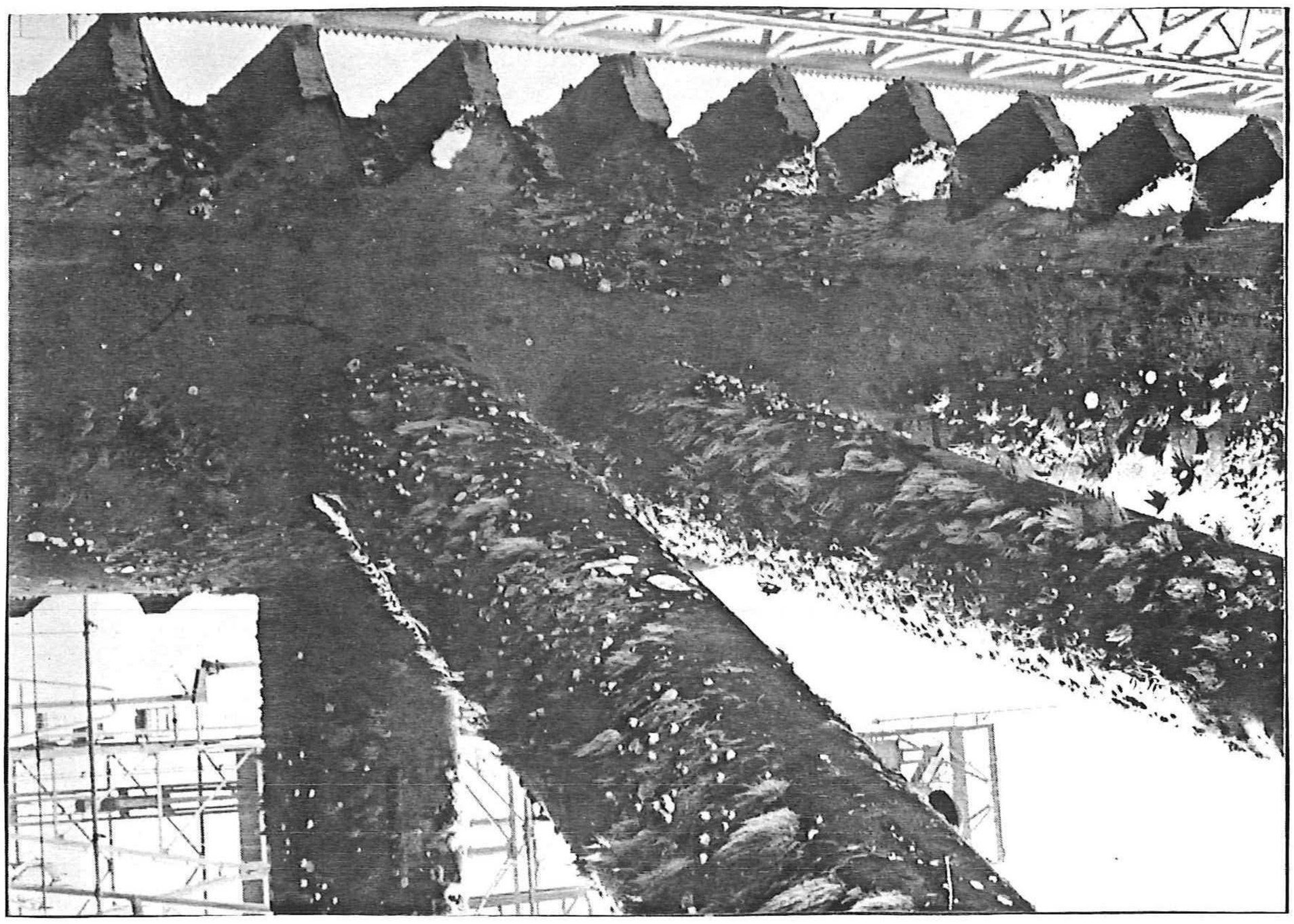

Fig. 4 ,Cornerpost and brace members.

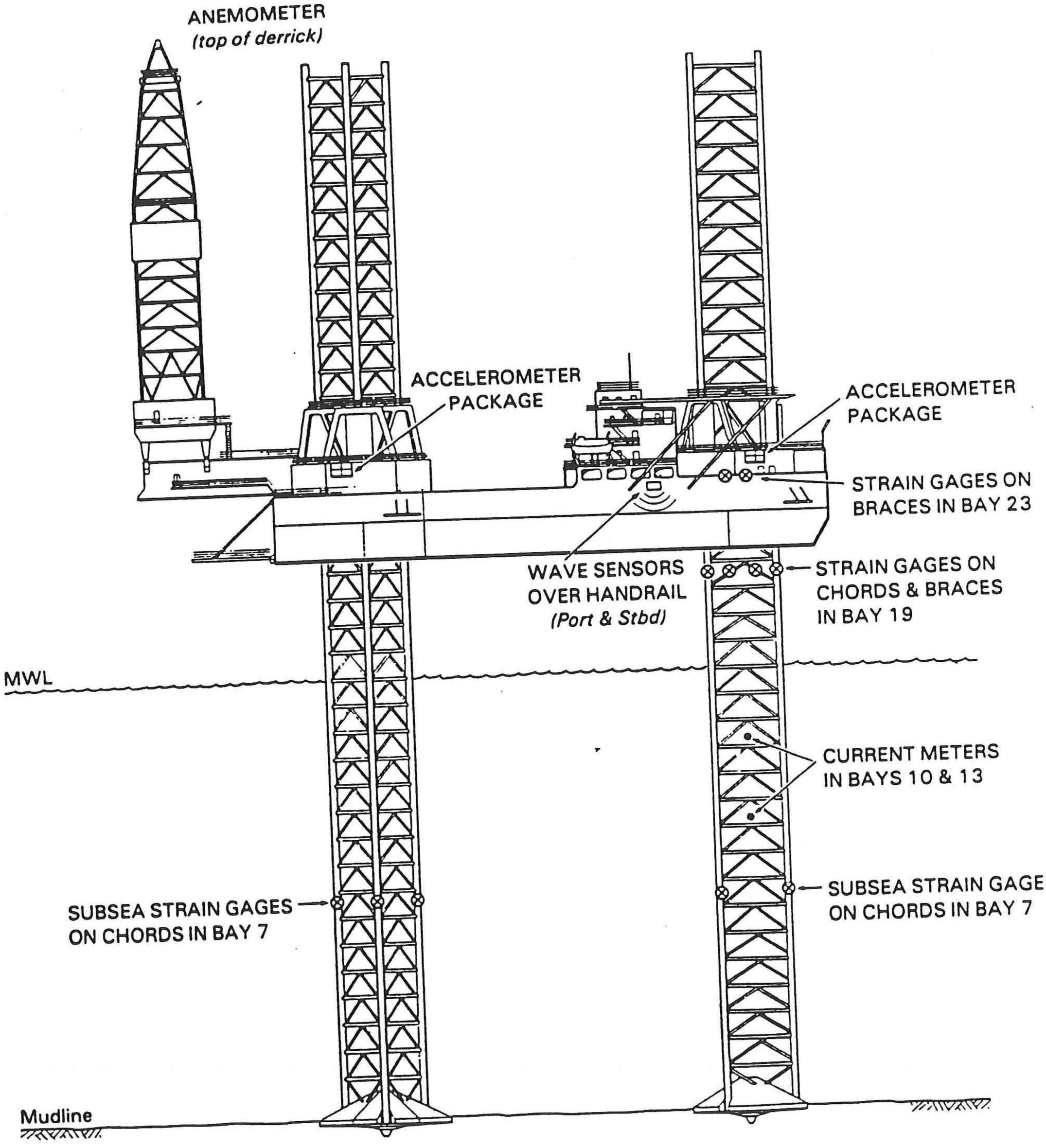

Fig. 5 ,Side view of "Maersk Guardian" and measurement system.

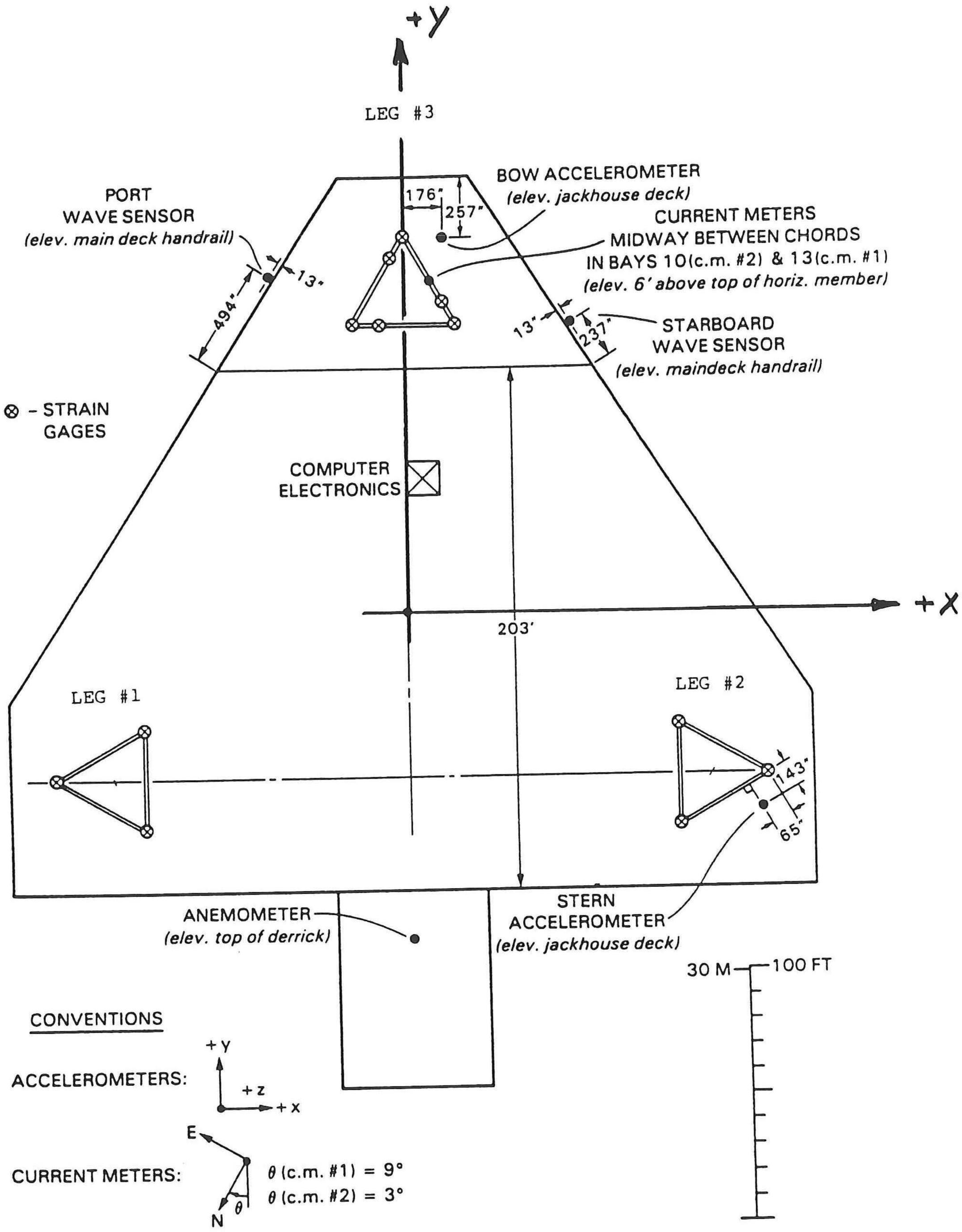

Fig. 6 ,Plan view of Measurement System, ref .

W.M. = WAVE METER

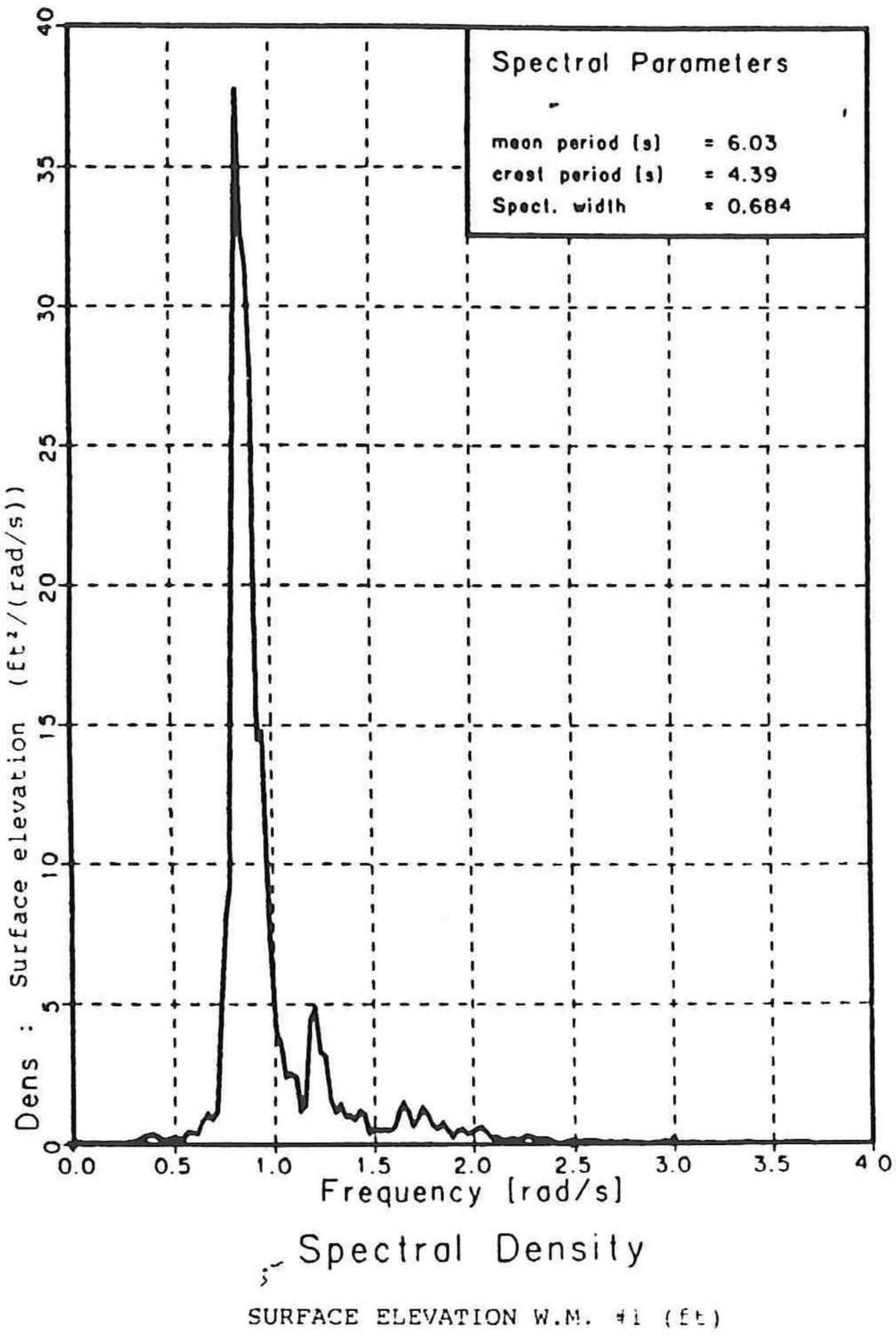

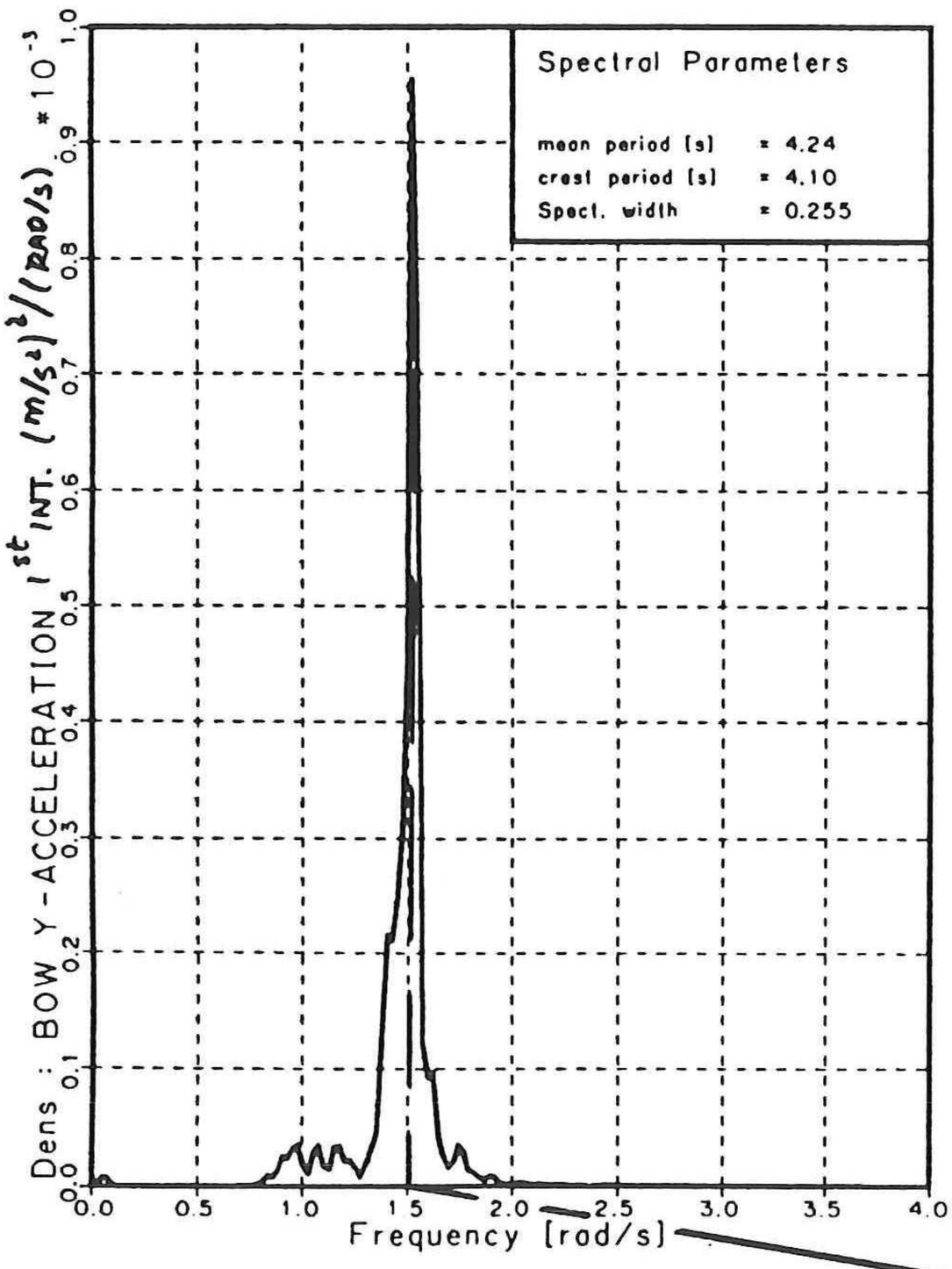

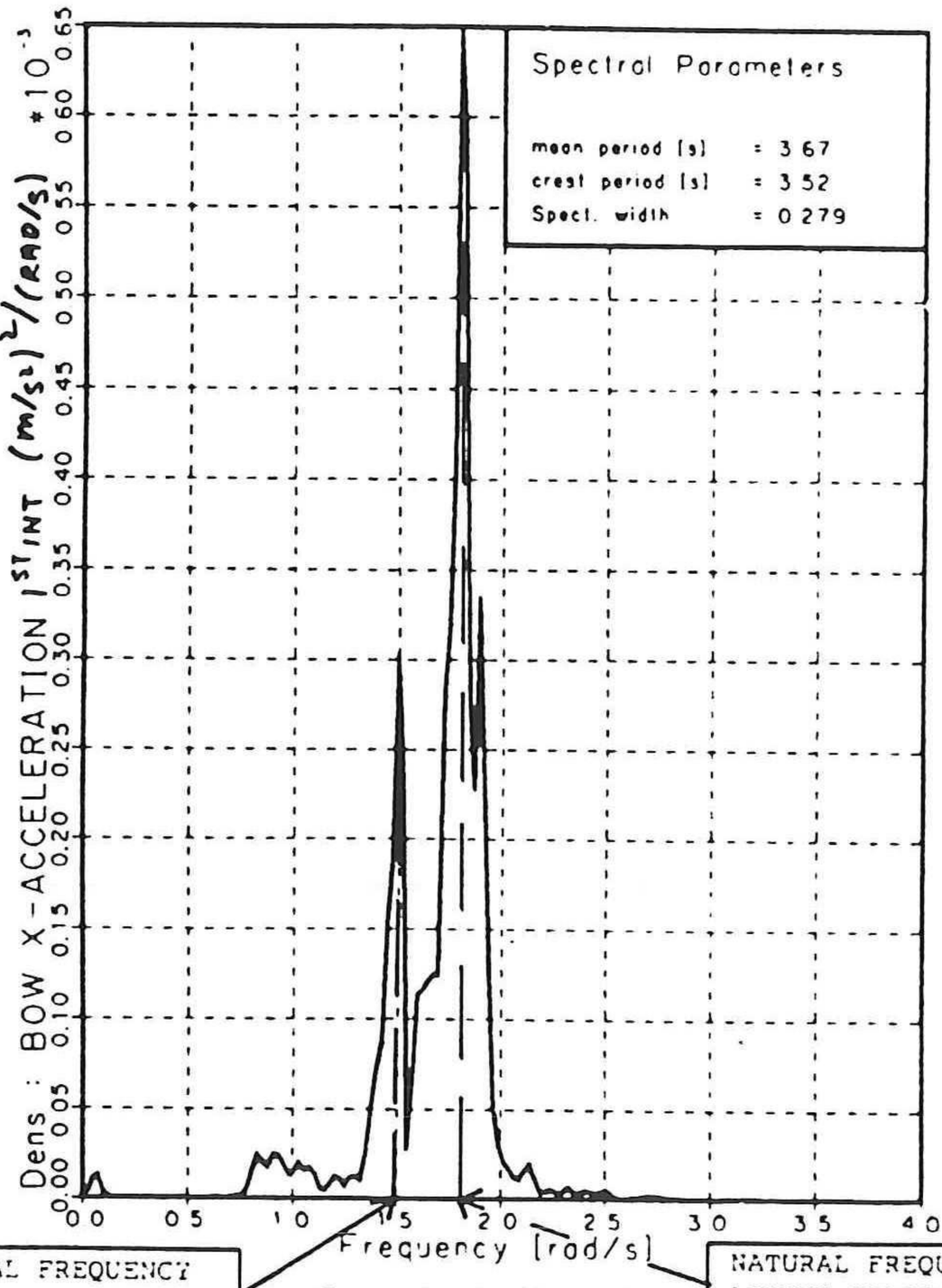

Fig. 7 ,Spectra of measured surface elevation and deck accelerations.

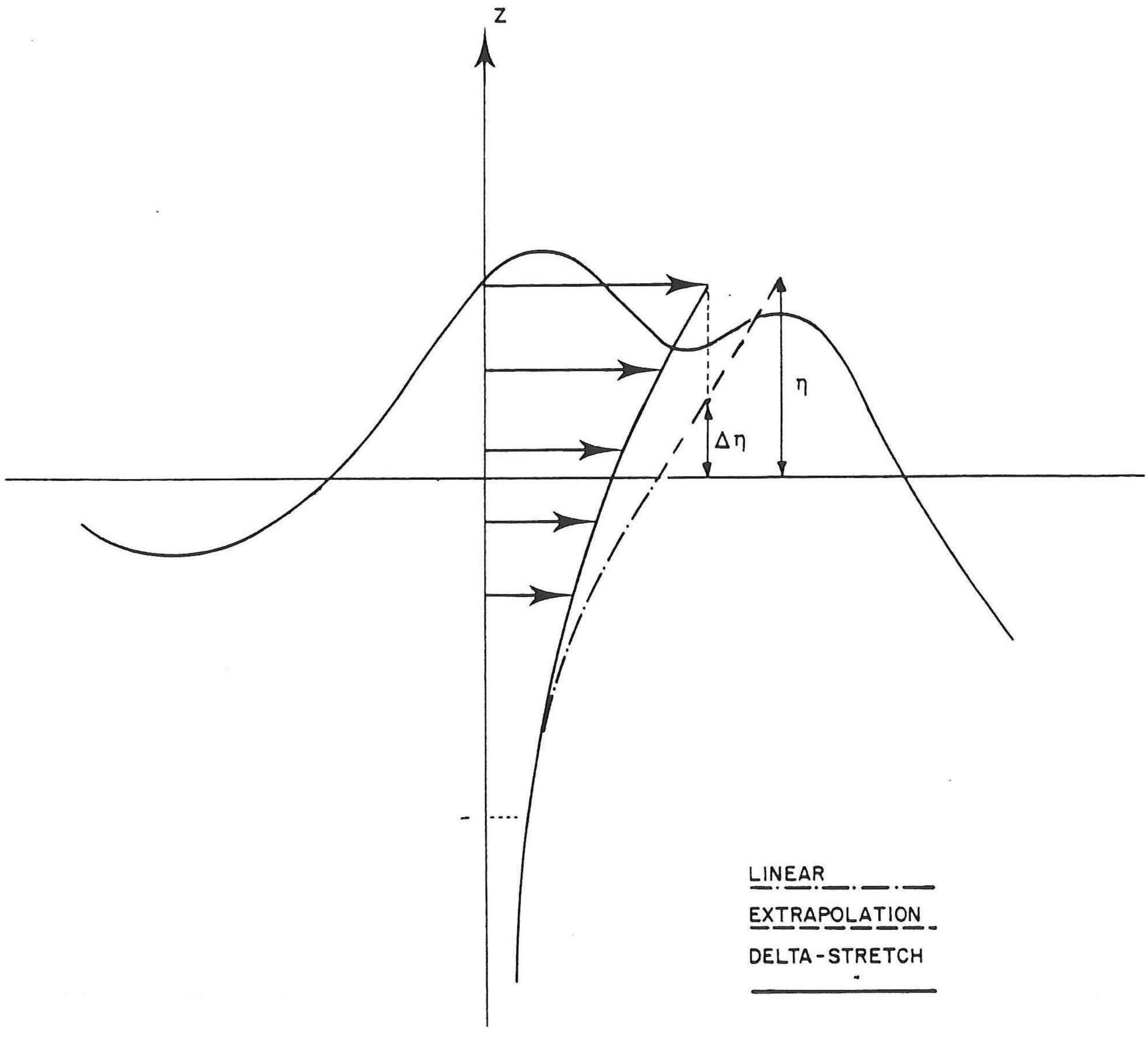

Fig. 8 ,Extrapolation and stretching of wave kinematics.

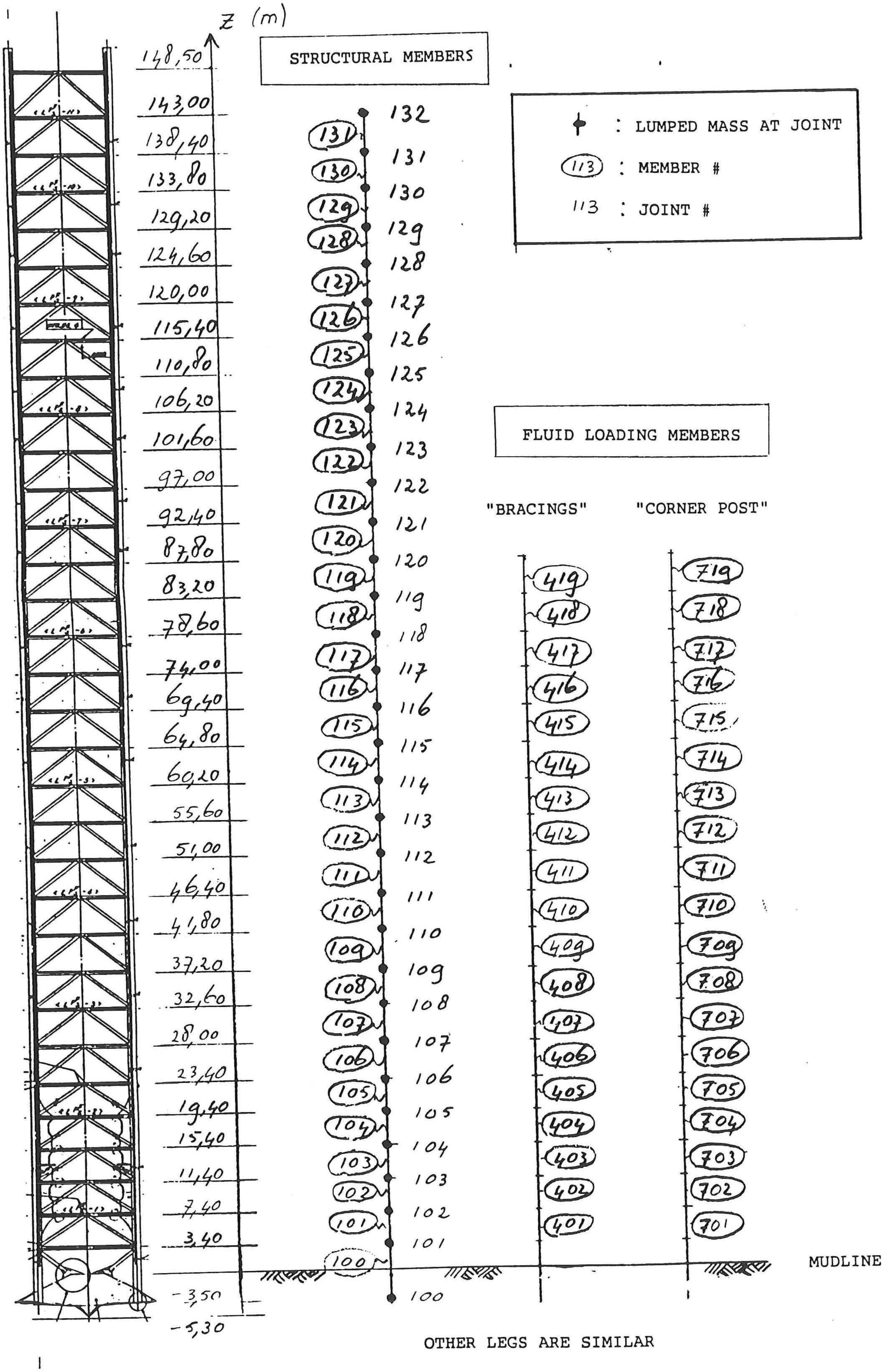

Fig. 9 ,Complete leg and modelled leg.

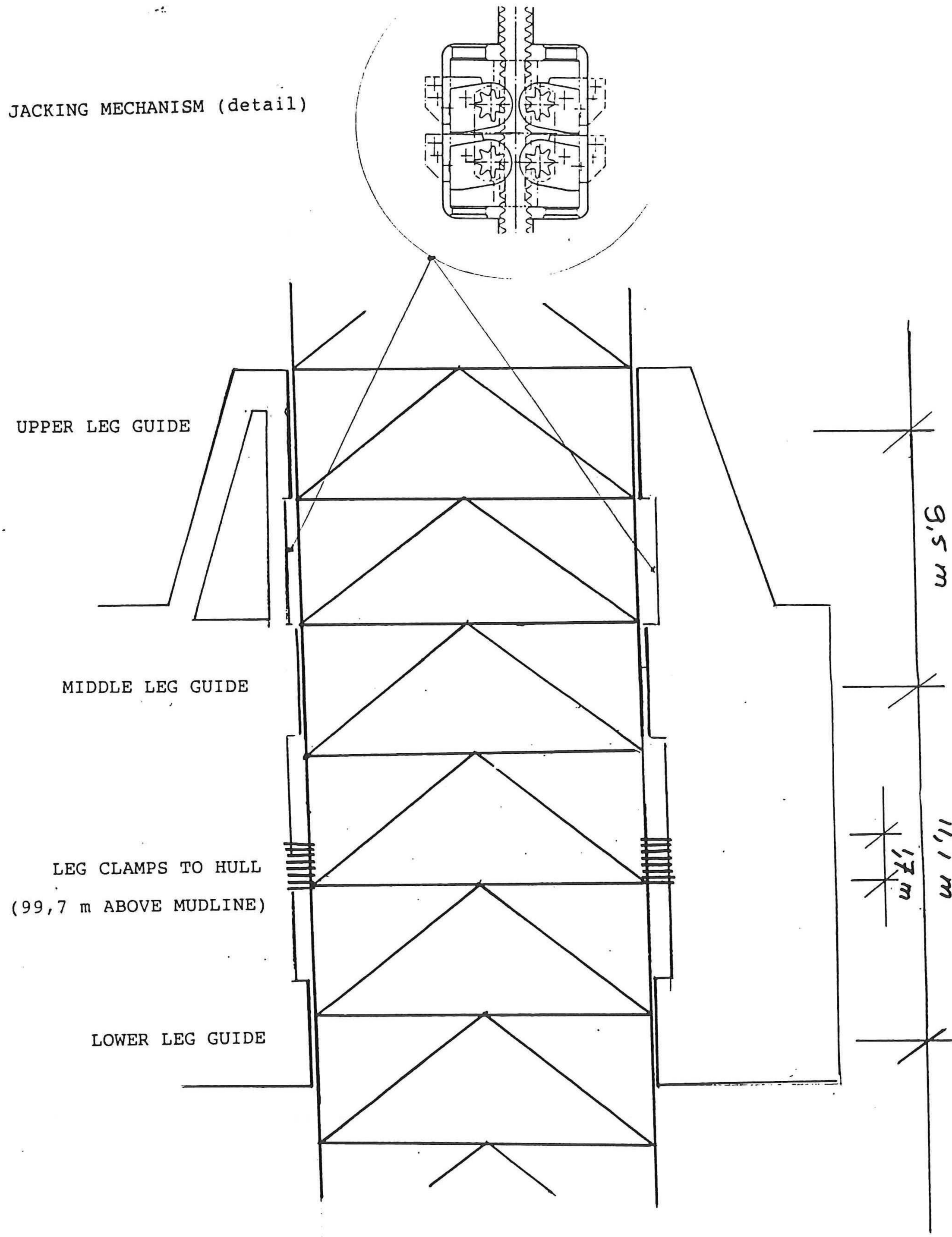

Fig. 10 ,Sketch of leg guide system.

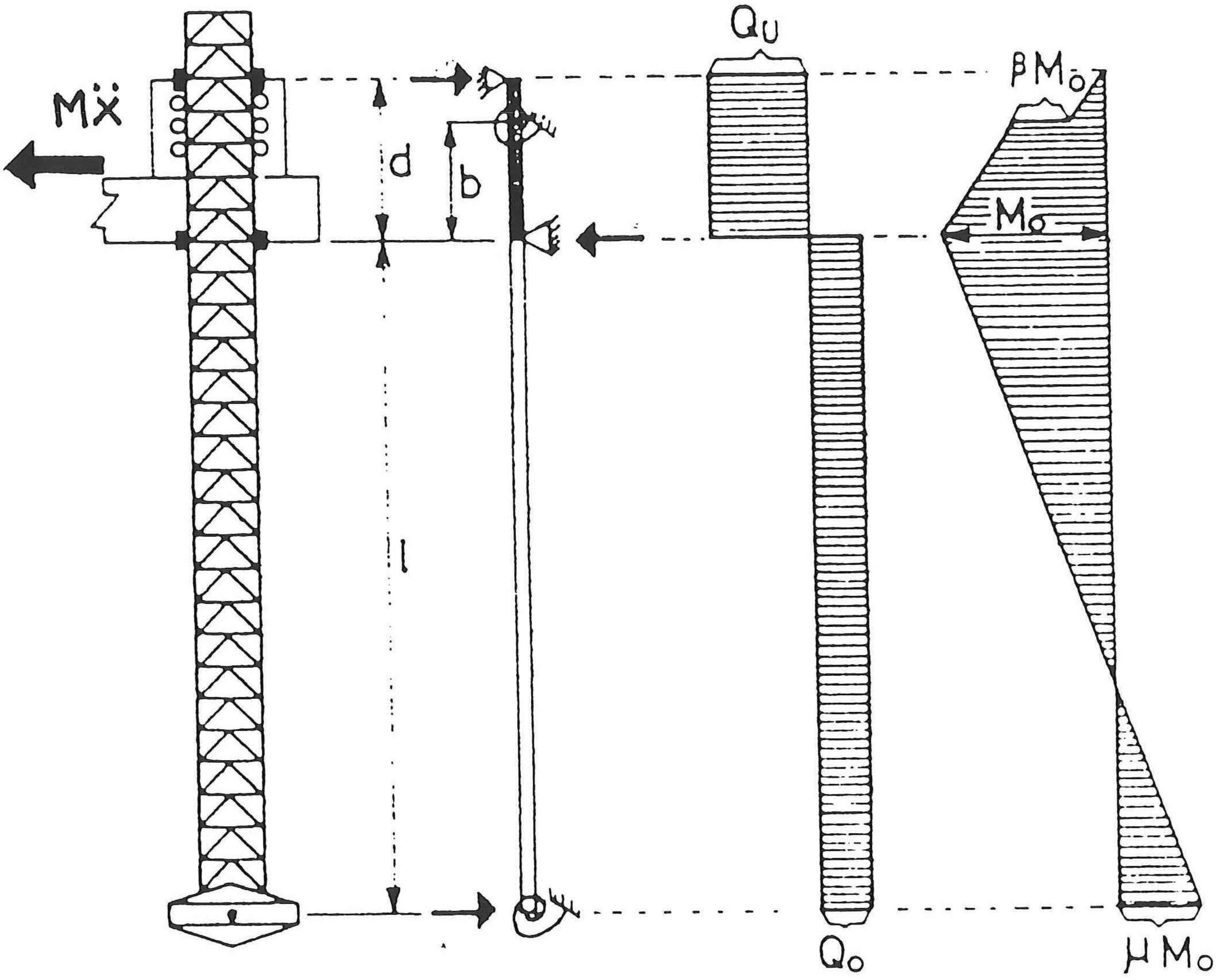

Fig. 11 ,Moment and shear force distribution under horizontal load.

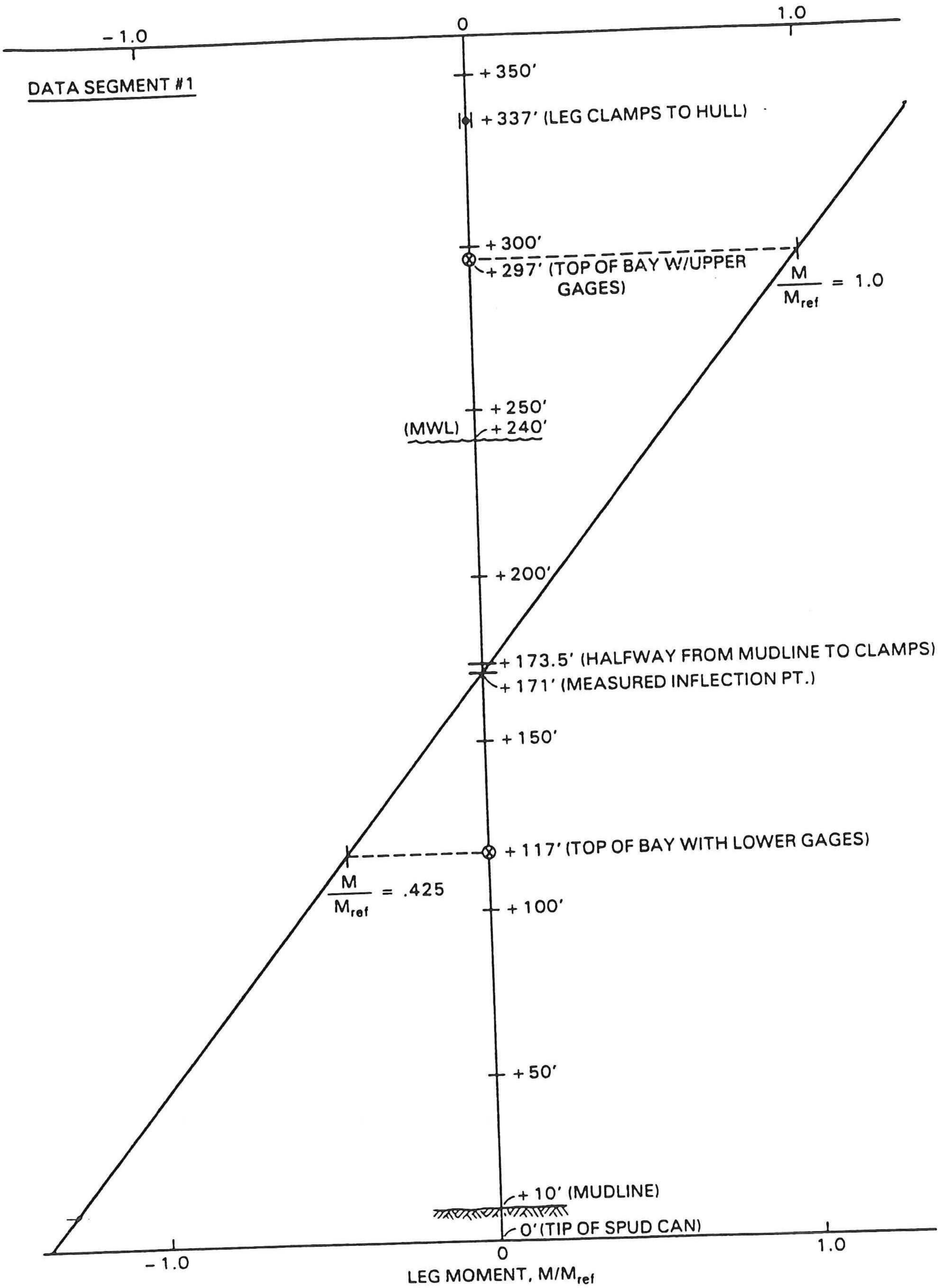

Fig. 12 ,Measured leg bending profile under inertia load, ref

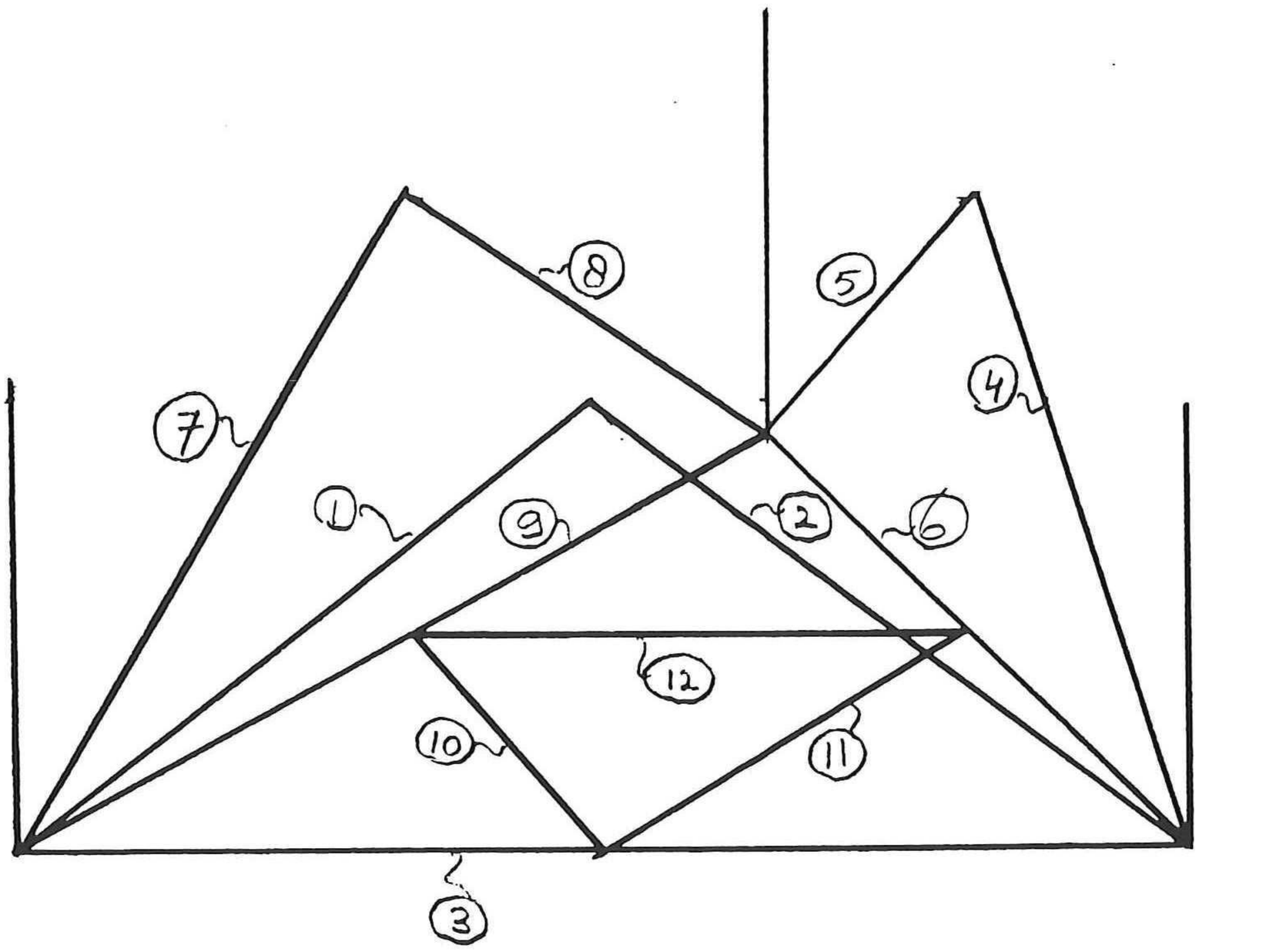

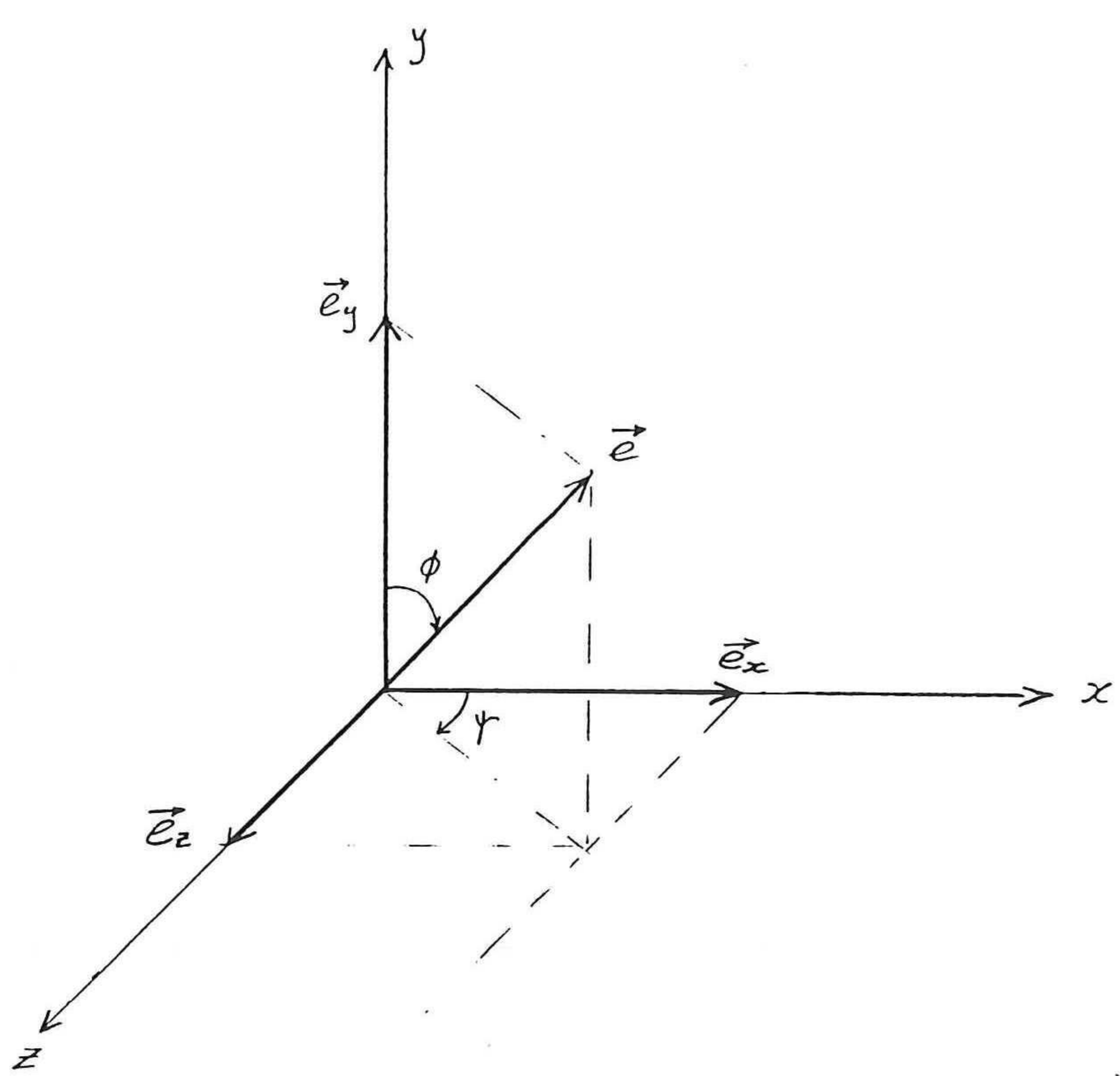

Fig. 14 ,Definition sketch.

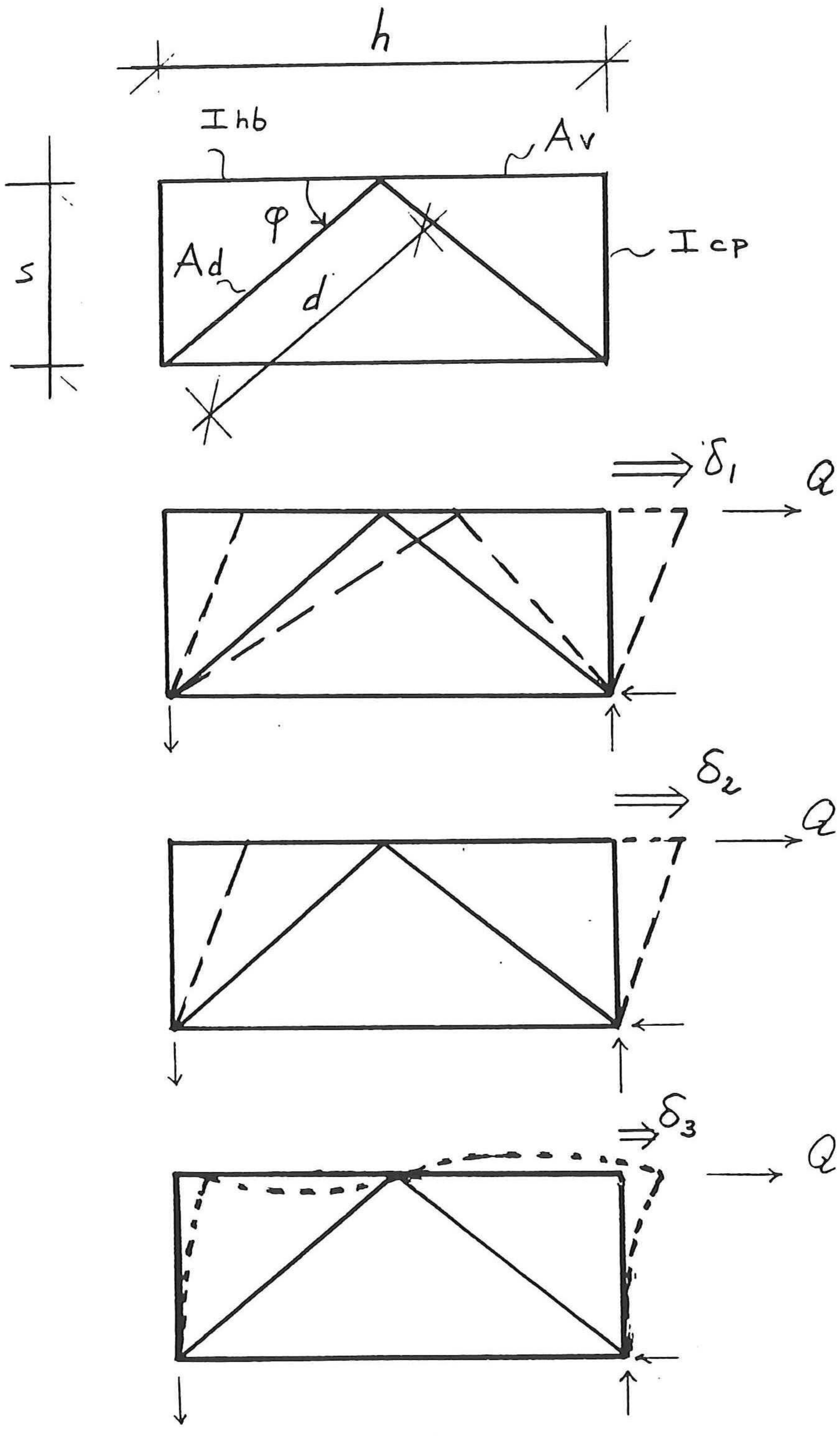

Fig. 15 ,Definition sketch.

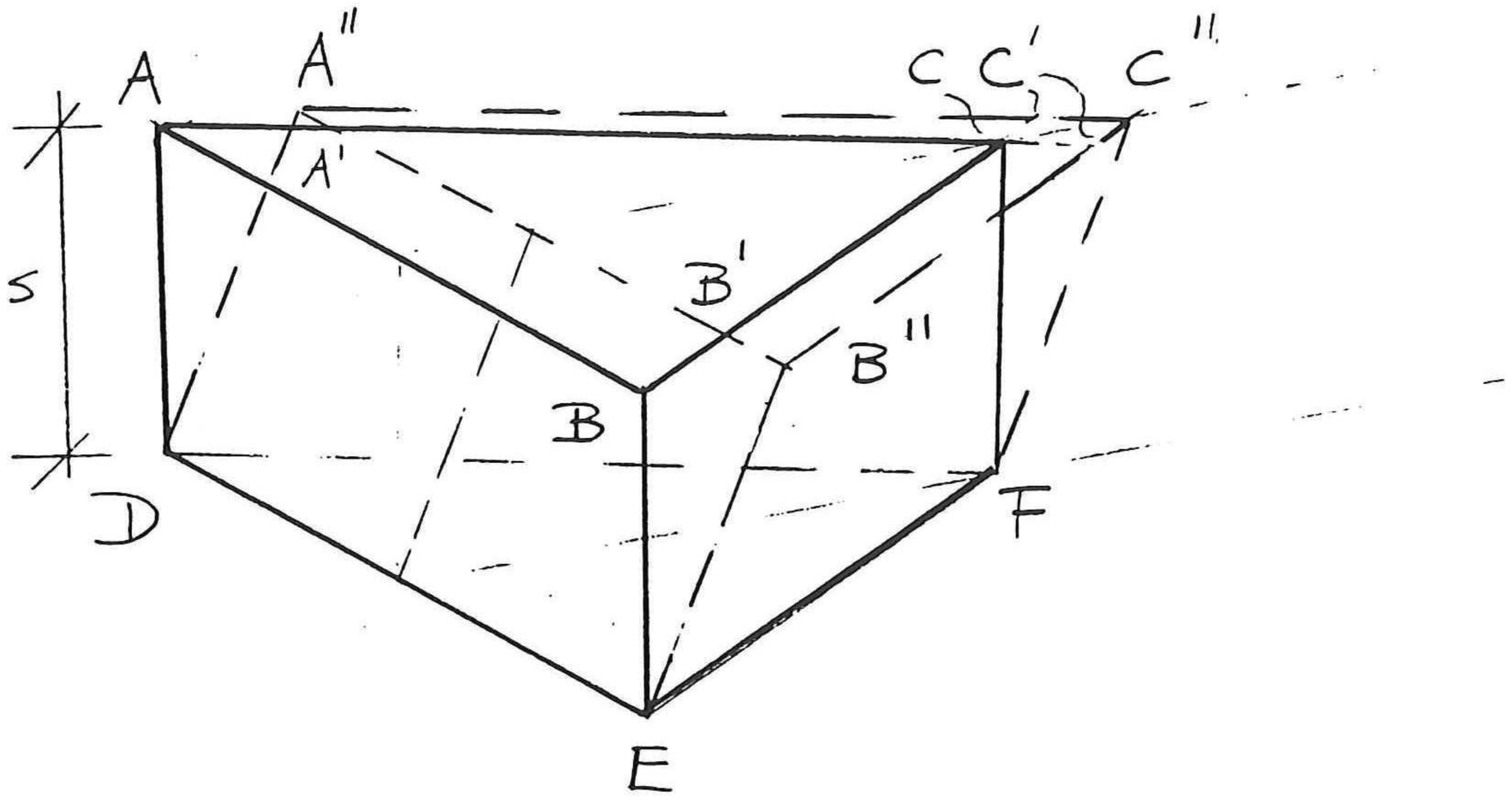

Fig. 16 ,Definition sketch, three-dimensional displacements.

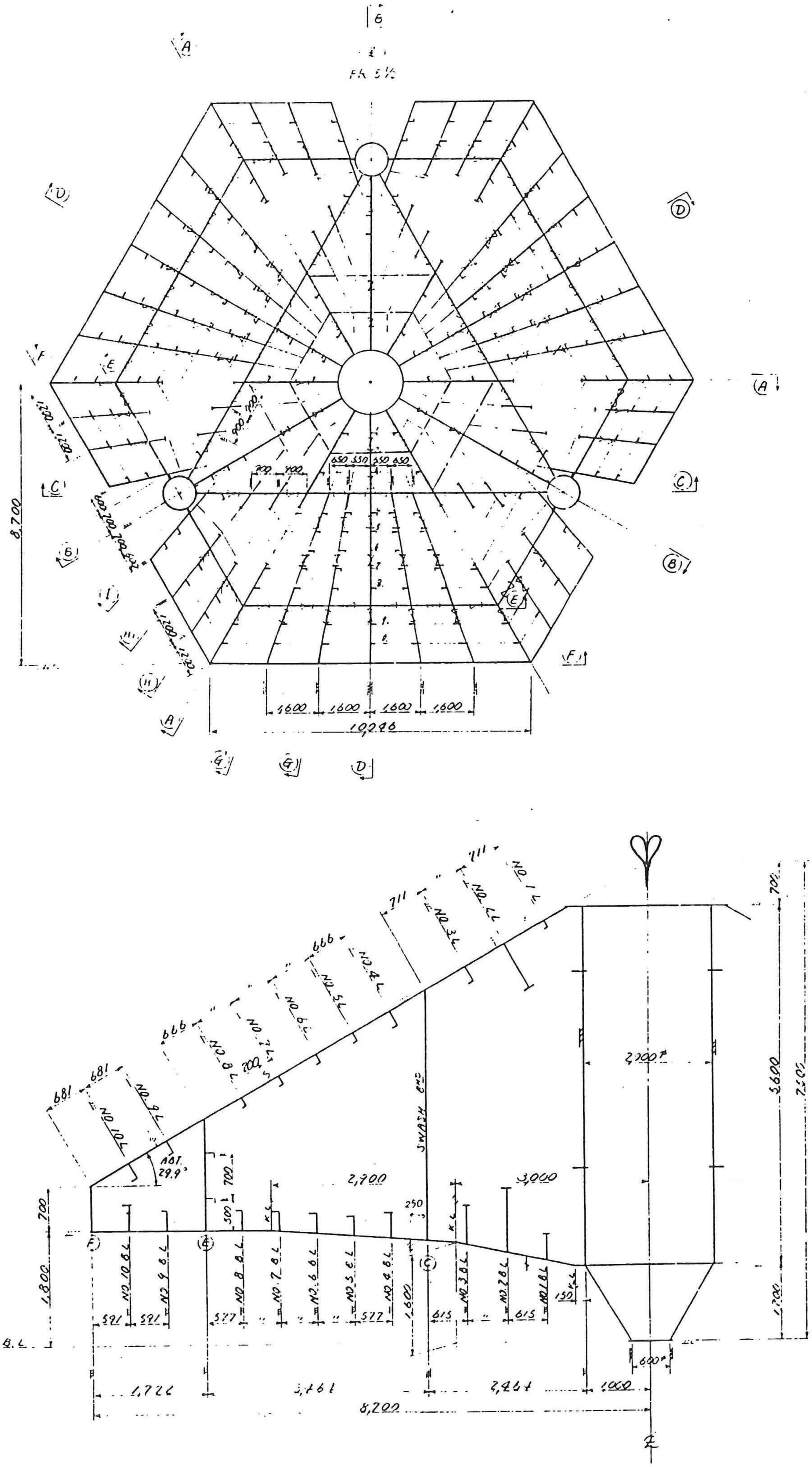

Fig. 17 ,Plan view and side view of spudcan.

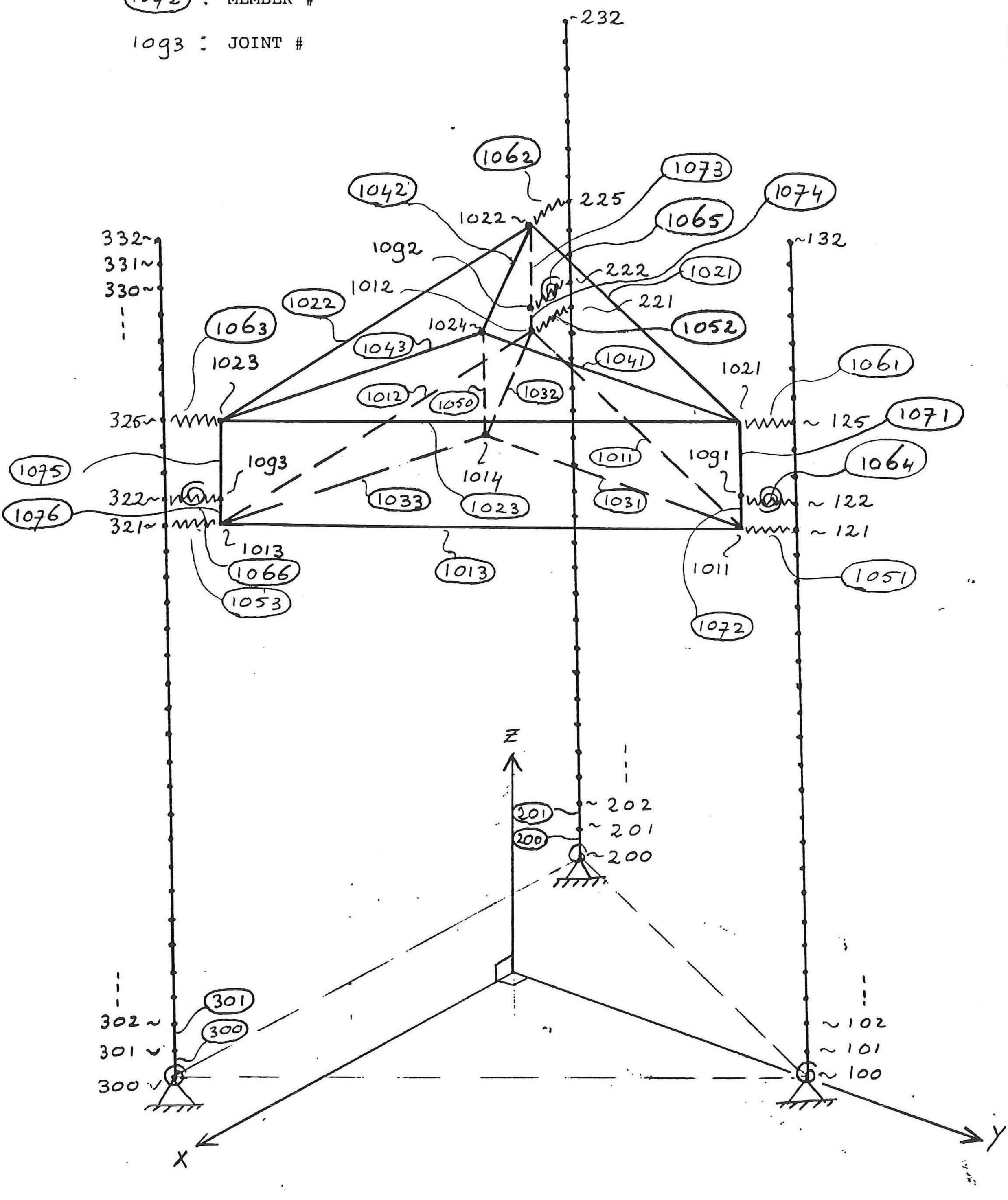

Fig. 18 ,Joint and member numbers

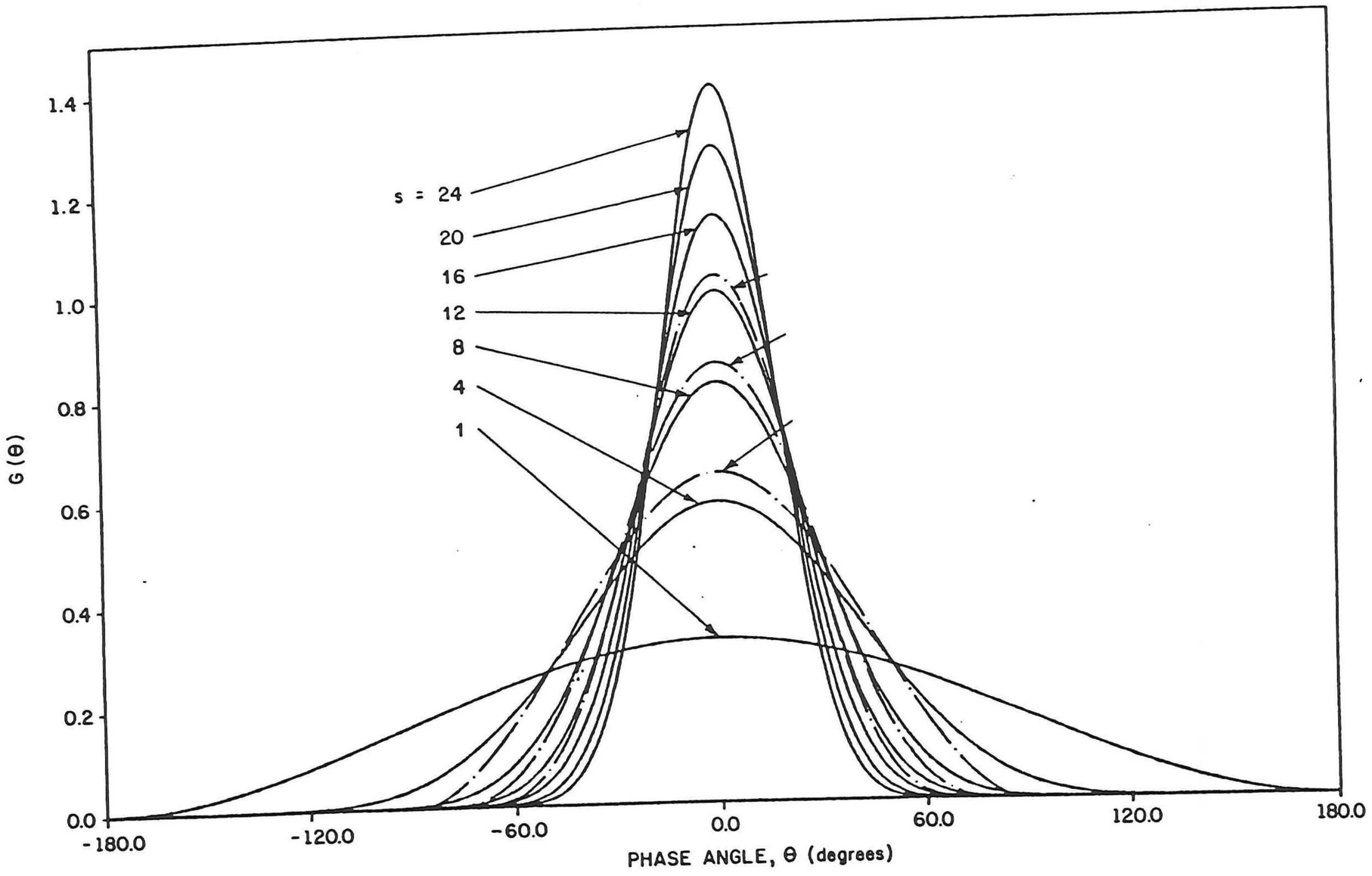

Fig. 19 ,Directional spreading function: cosine power.

$$G(\theta) = C \left[\cos \left(\frac{\theta - \theta_0}{2} \right) \right]^{2s}$$

MEAN CURRENT VELOCITIES

C.M. = CURRENT METER

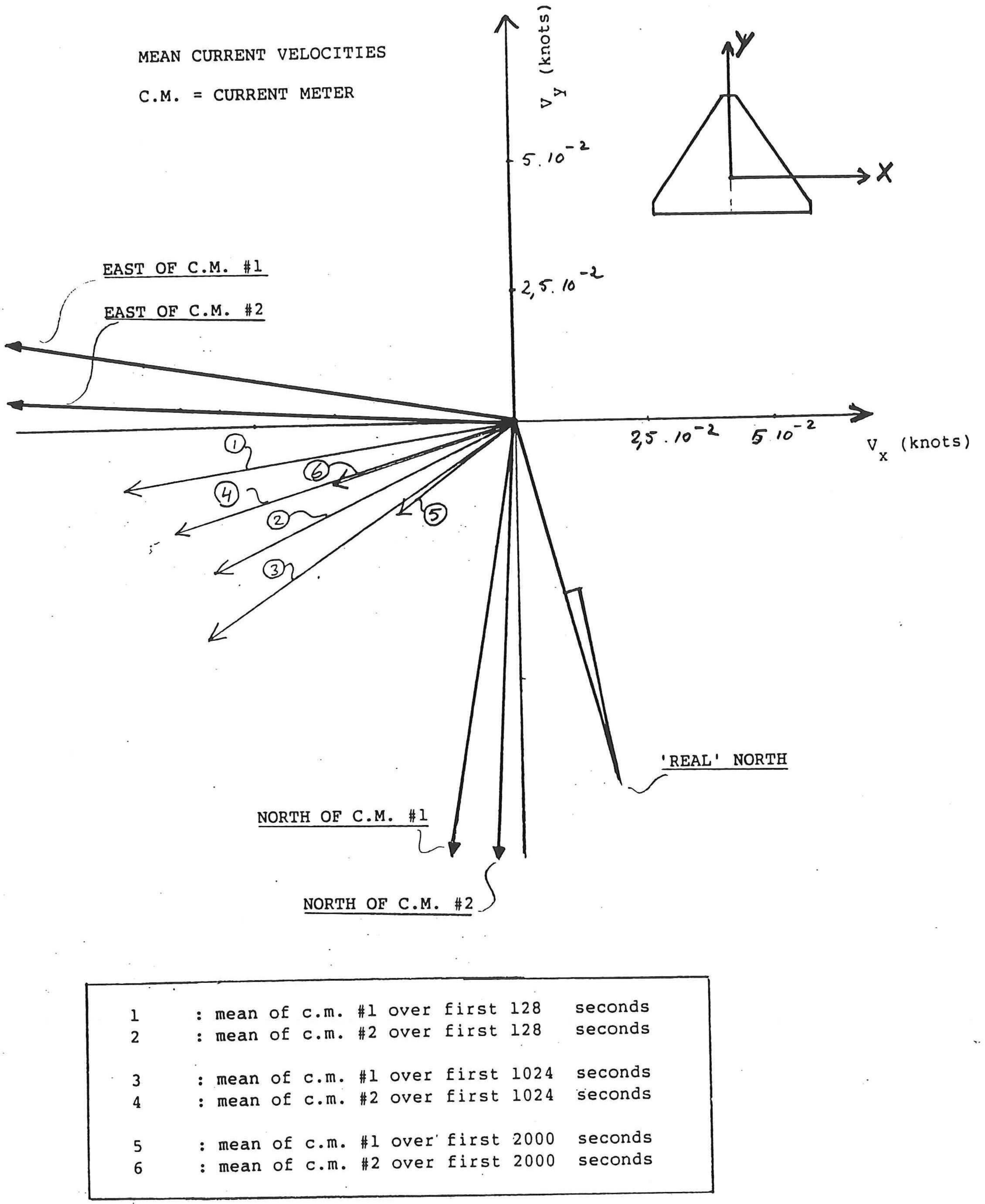

1	: mean of c.m. #1 over first 128	seconds
2	: mean of c.m. #2 over first 128	seconds
3	: mean of c.m. #1 over first 1024	seconds
4	: mean of c.m. #2 over first 1024	seconds
5	: mean of c.m. #1 over first 2000	seconds
6	: mean of c.m. #2 over first 2000	seconds

Fig. 20 ,Current velocities and directions.

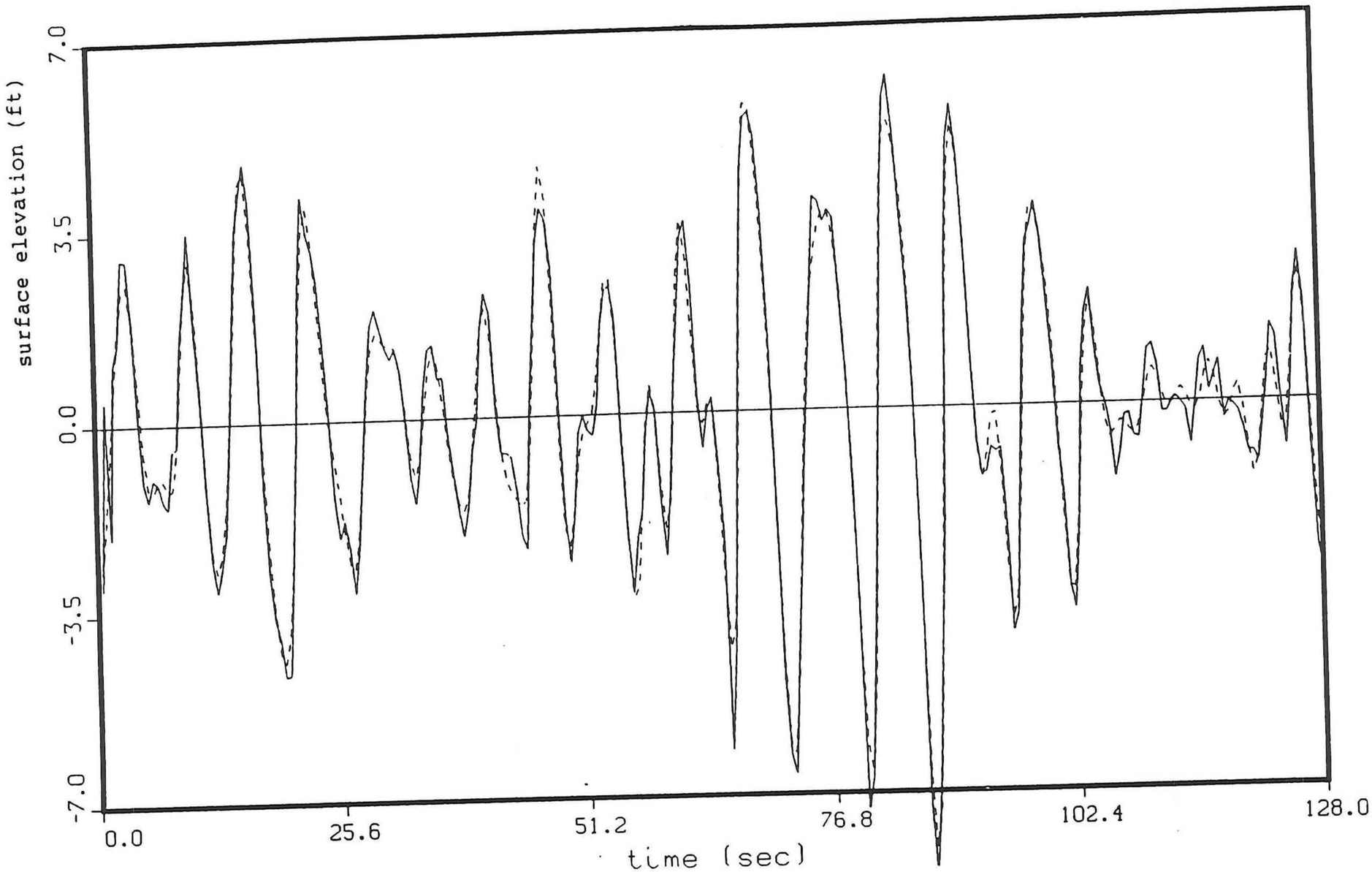

Fig. 21, Conditioned simulation.

SURFACE ELEVATION AT LOCATION OF W.M. #1

CONDITIONED: SURFACE ELEVATION W.M. #1
X VELOCITY C.M. #1
Y VELOCITY C.M. #1

SPREADING : S = 4

———— : INPUT SURFACE ELEVATION (measured)

--------- : GENERATED SURFACE (simulated)

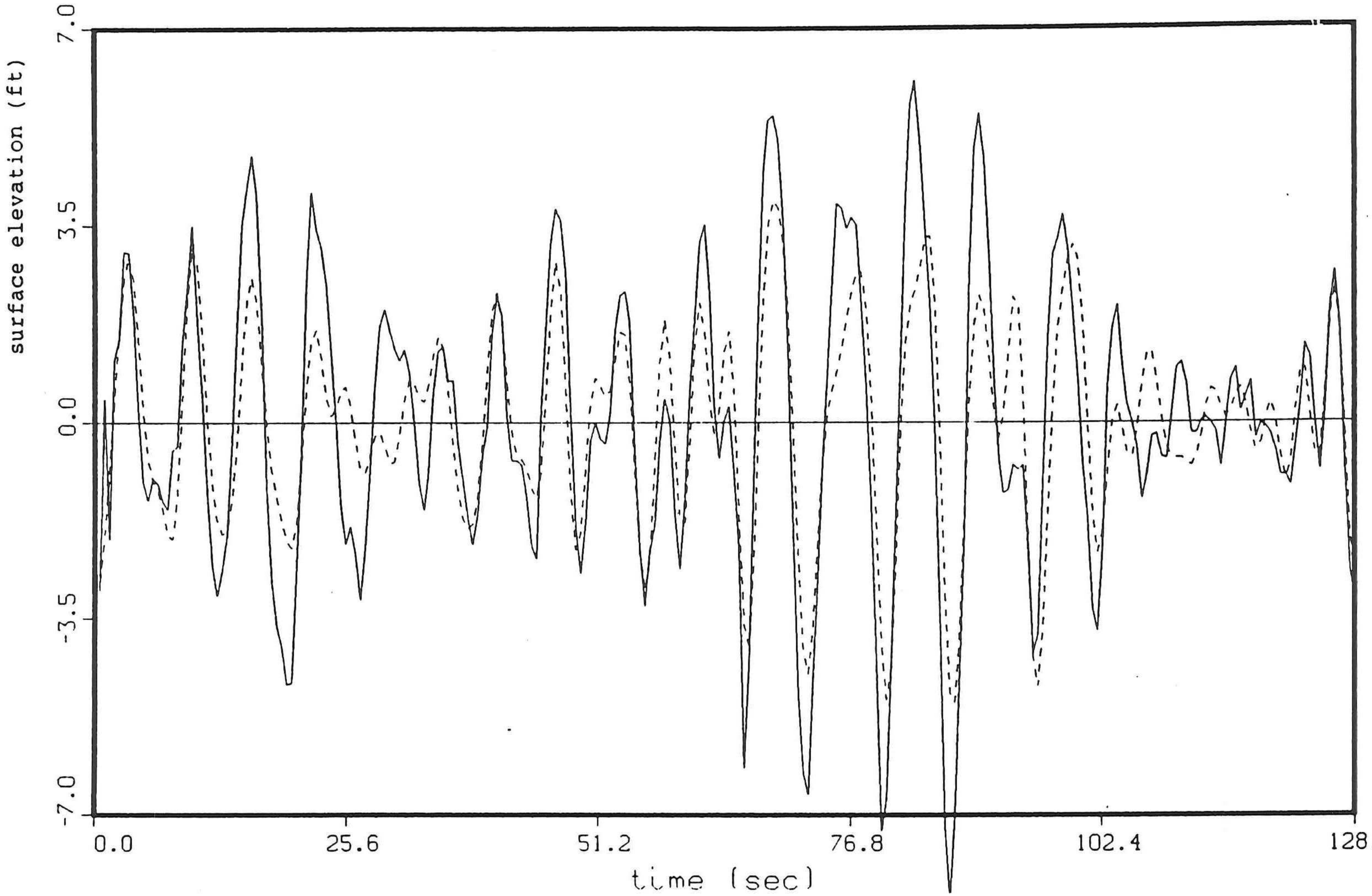

Fig. 22 ,Conditioned simulation

SURFACE ELEVATION AT LOCATION OF W.M. #1

CONDITIONED: SURFACE ELEVATION W.M. #1
X VELOCITY C.M. #1
Y VELOCITY C.M. #1

SPREADING : S = 20

———— : INPUT SURFACE ELEVATION (measured)

--------- : GENERATED SURFACE (simulated)

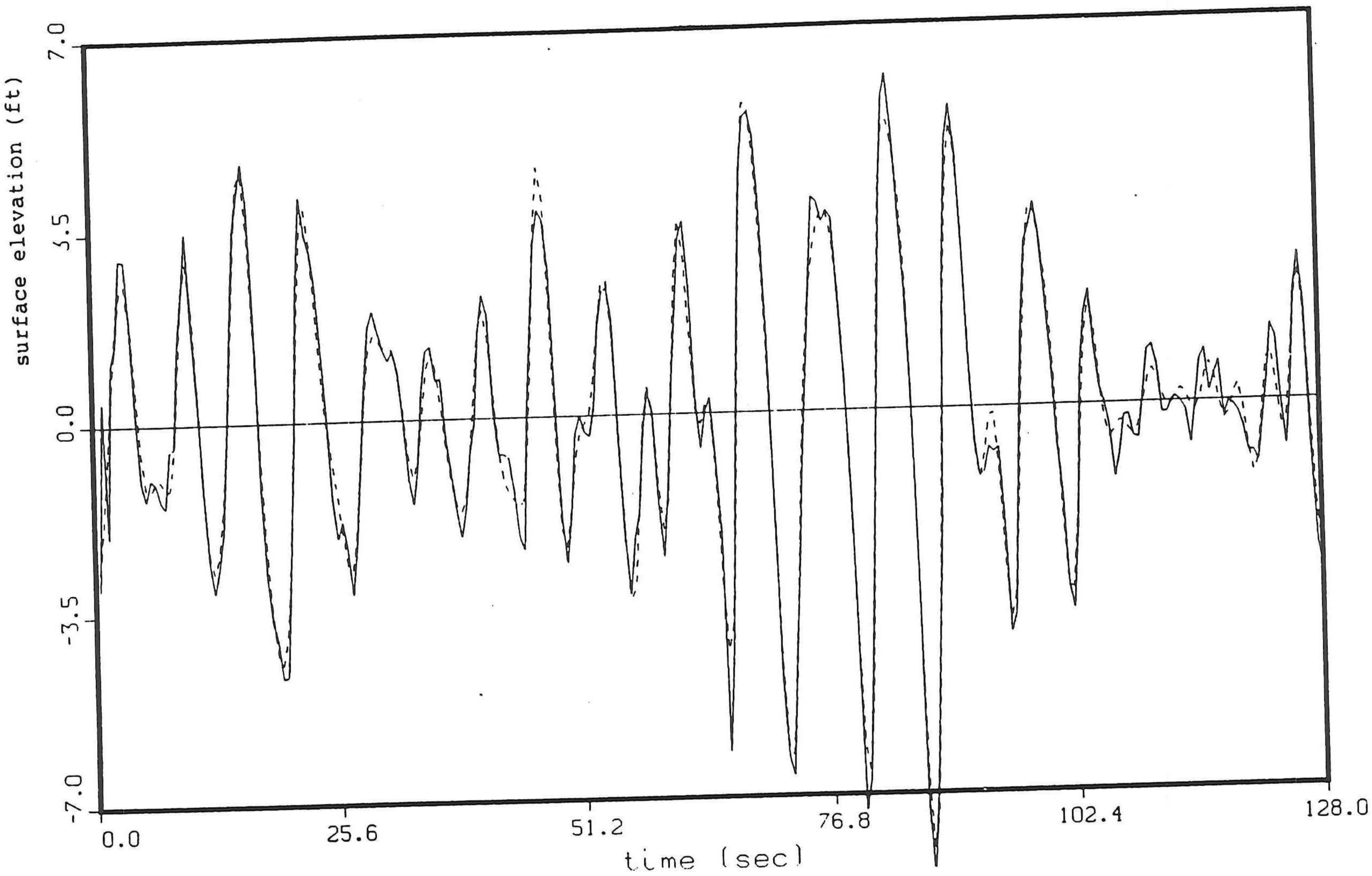

Fig. 23 ,Conditioned simulation.

SURFACE ELEVATION AT LOCATION OF W.M. #1 ———— : INPUT SURFACE ELEVATION (measured)

CONDITIONED: SURFACE ELEVATION W.M. #1
X VELOCITY C.M. #1
Y VELOCITY C.M. #1

--------- : GENERATED SURFACE (simulated)

SPREADING : S = 4

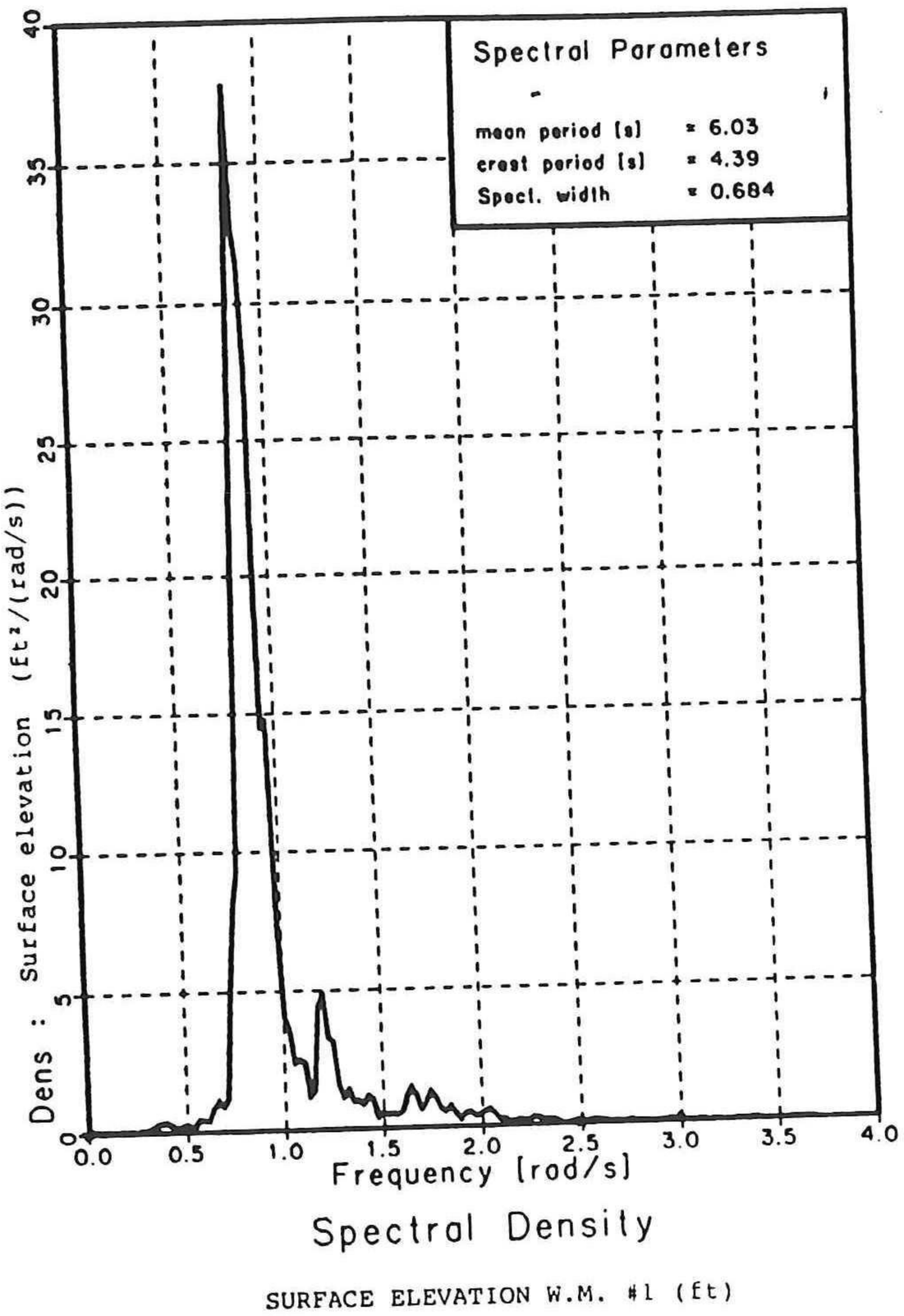

SURFACE ELEVATION W.M. #1 (ft)

W.M. = WAVE METER

C.M. = CURRENT METER

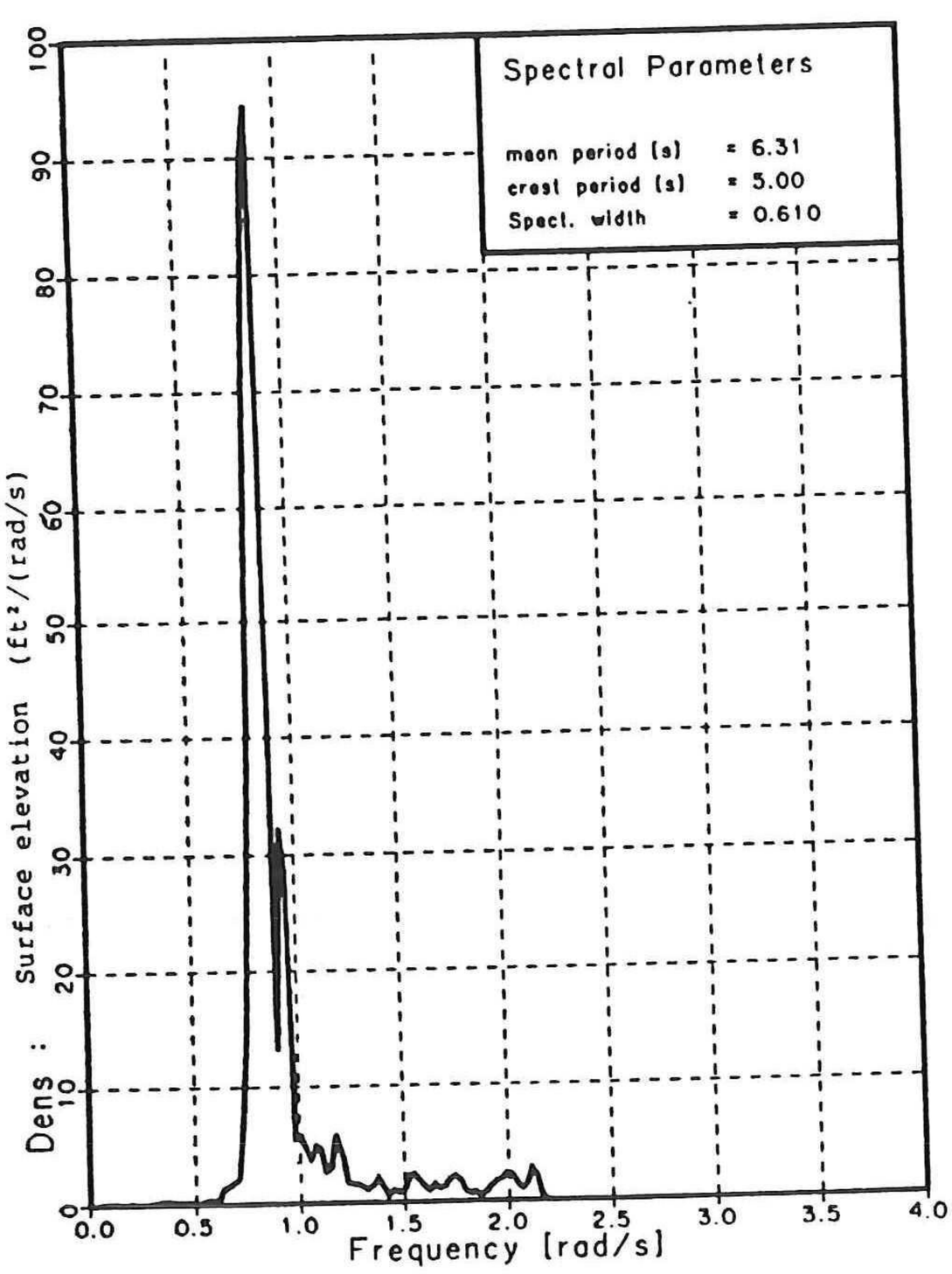

SURFACE ELEVATION (ft) AT (X=0, Y=0)

CONDITIONED SURFACE ELEVATION OF W.M. #1

CONDITIONED VELOCITIES OF C.M. #1

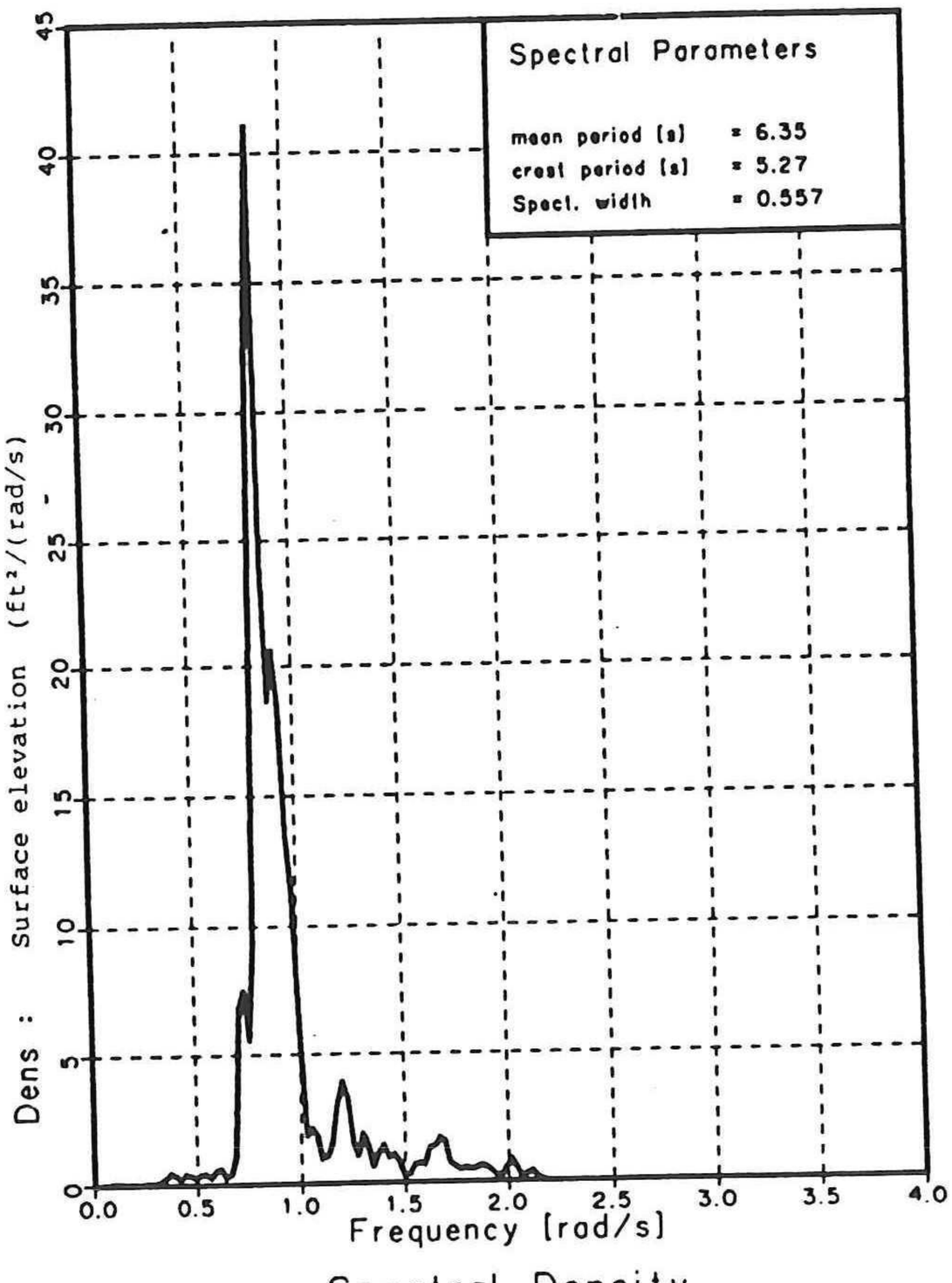

SURFACE ELEVATION (ft) AT (X=0, Y=0)

CONDITIONED SURFACE ELEVATION OF W.M. #1

Fig. 24 ,Surface elevation spectra.

MEASURED

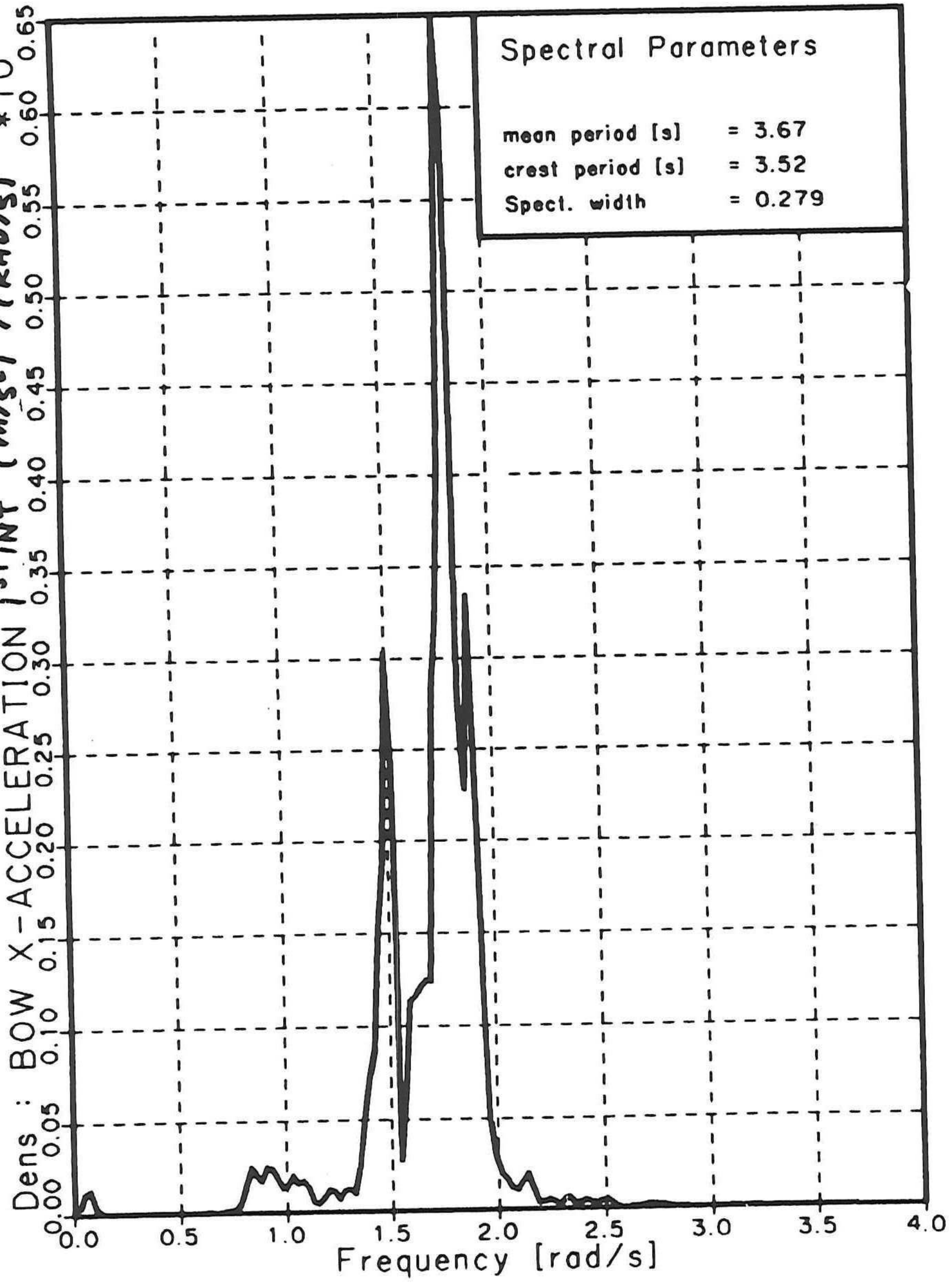

Spectral Density

BOW X-ACCELERATION (M/SEC**2)

SIMULATED

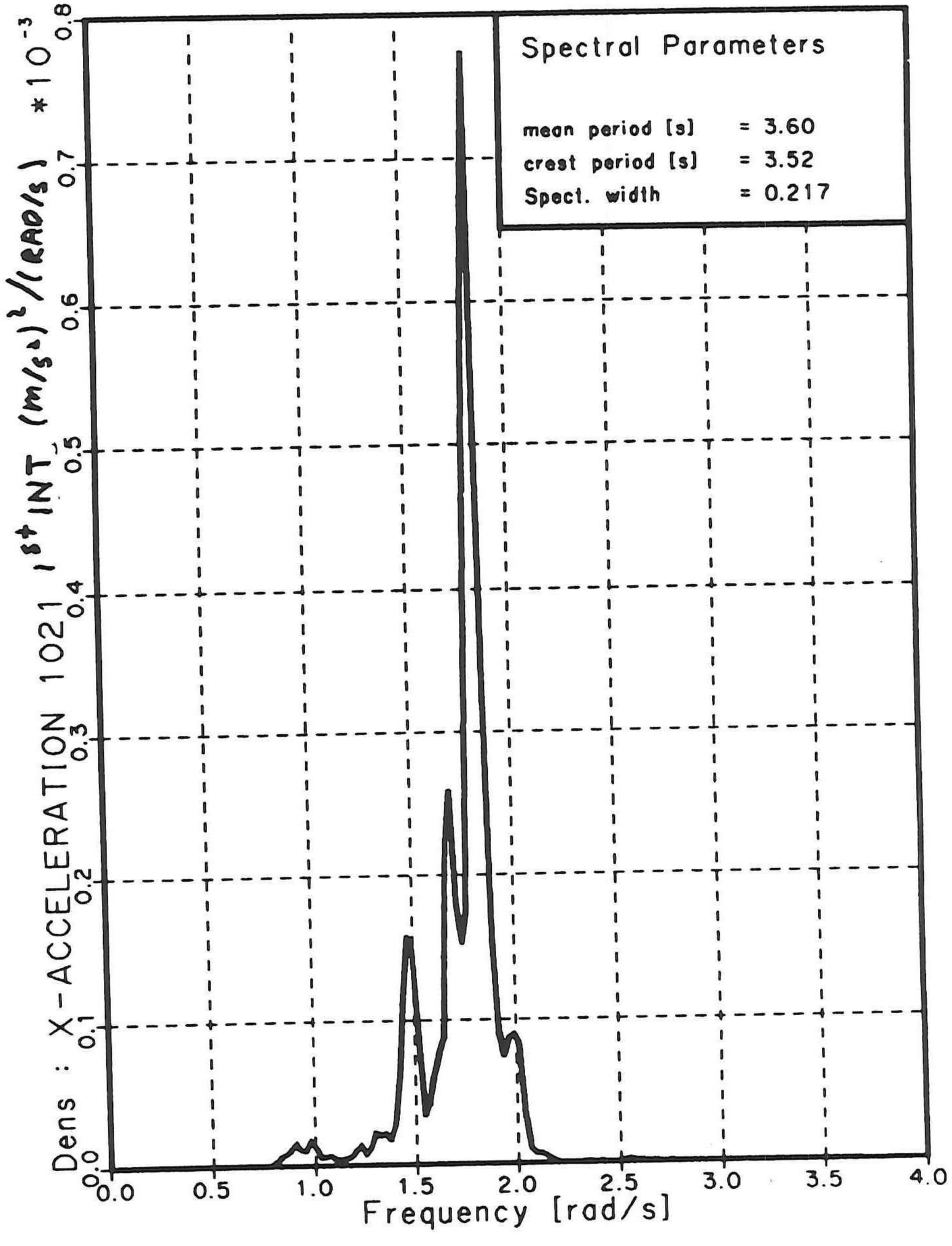

Spectral Density

X-ACCELERATION 1021 (M/SEC**2)

Fig. 25 , 1st. int., bow x acceleration spectra

MEASURED

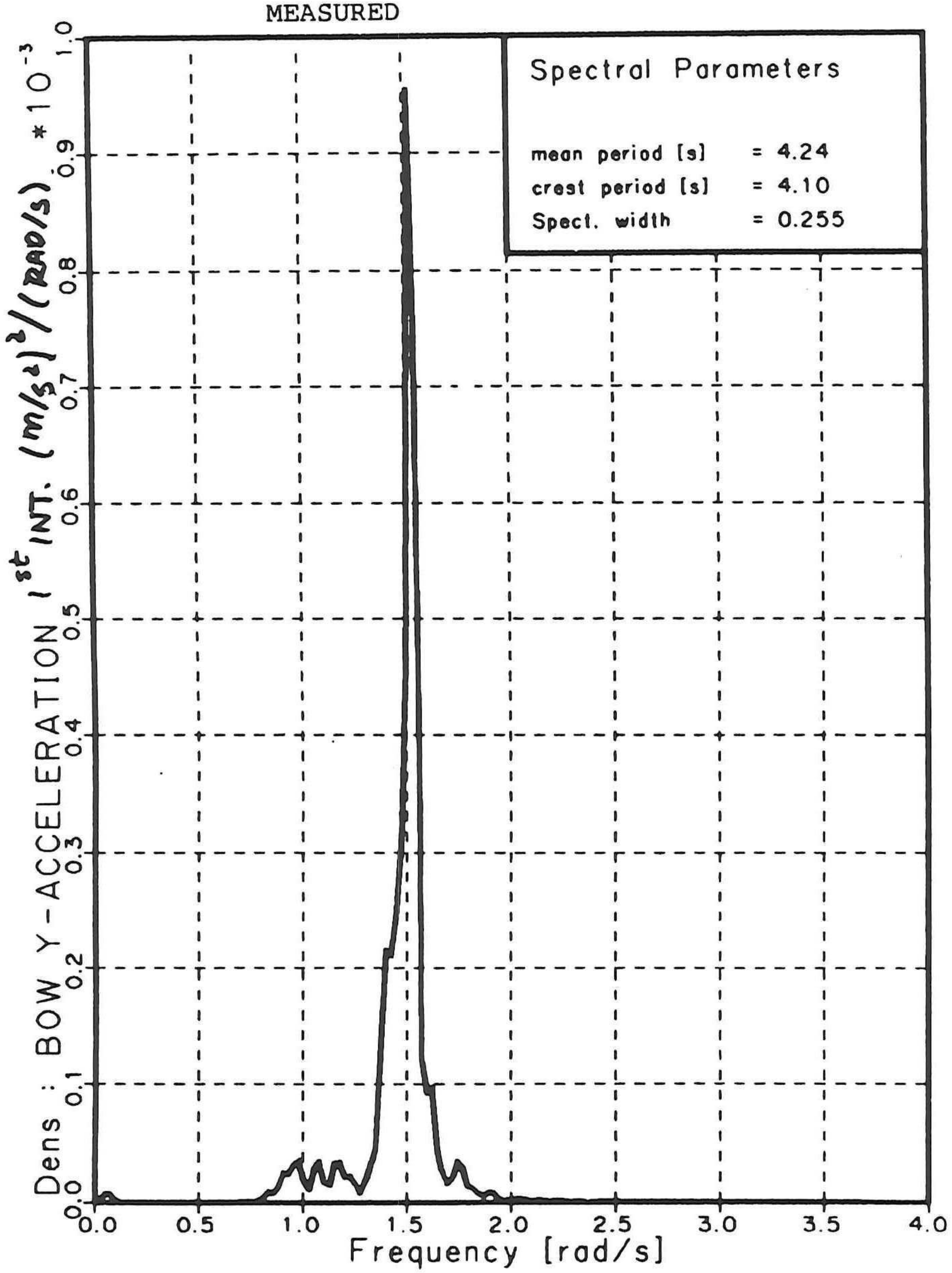

Spectral Density

BOW Y-ACCELERATION (M/SEC**2)

SIMULATED

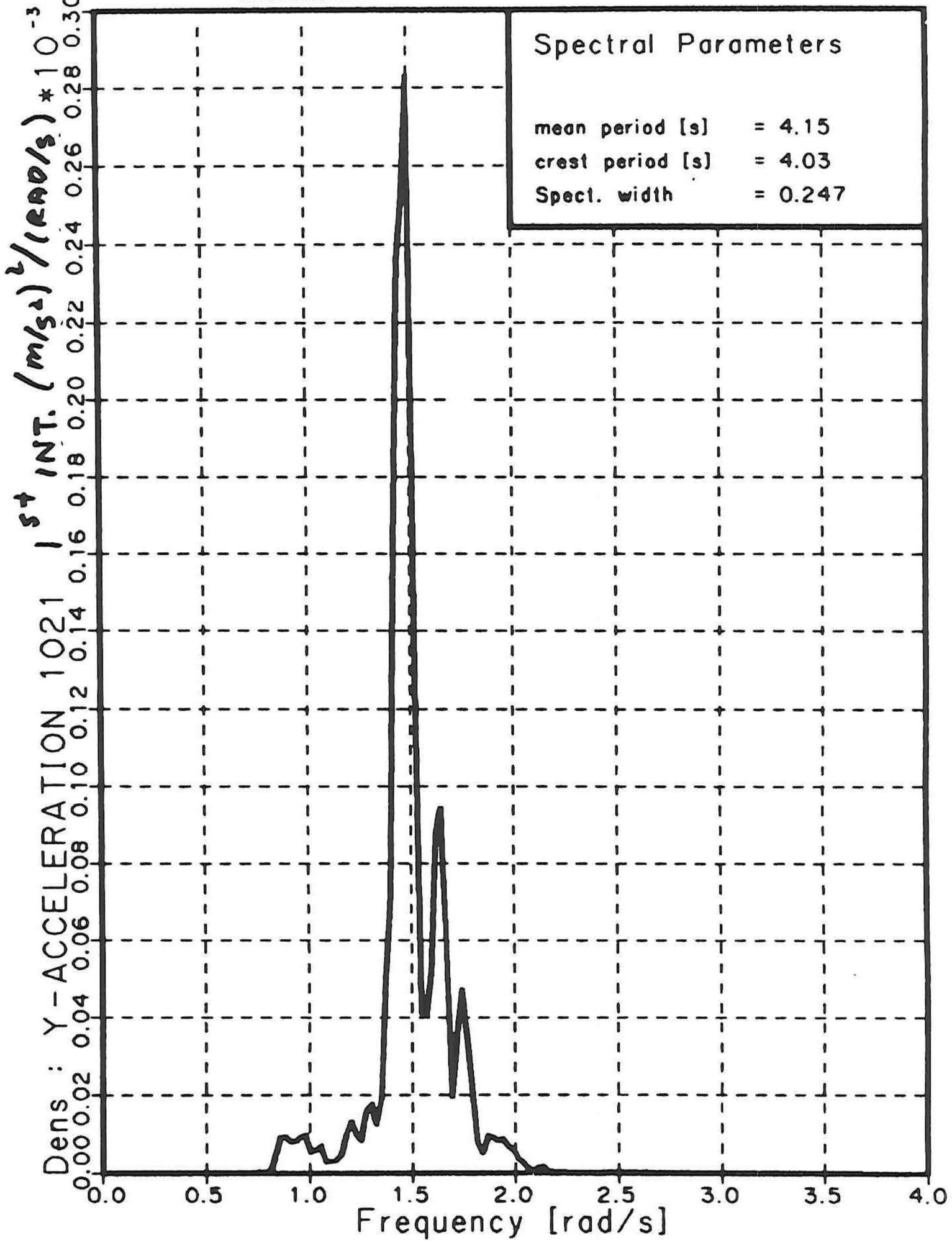

Spectral Density

Y-ACCELERATION 1021 (M/SEC**2)

Fig. 26 , 1st. int., bow y acceleration spectra

MEASURED

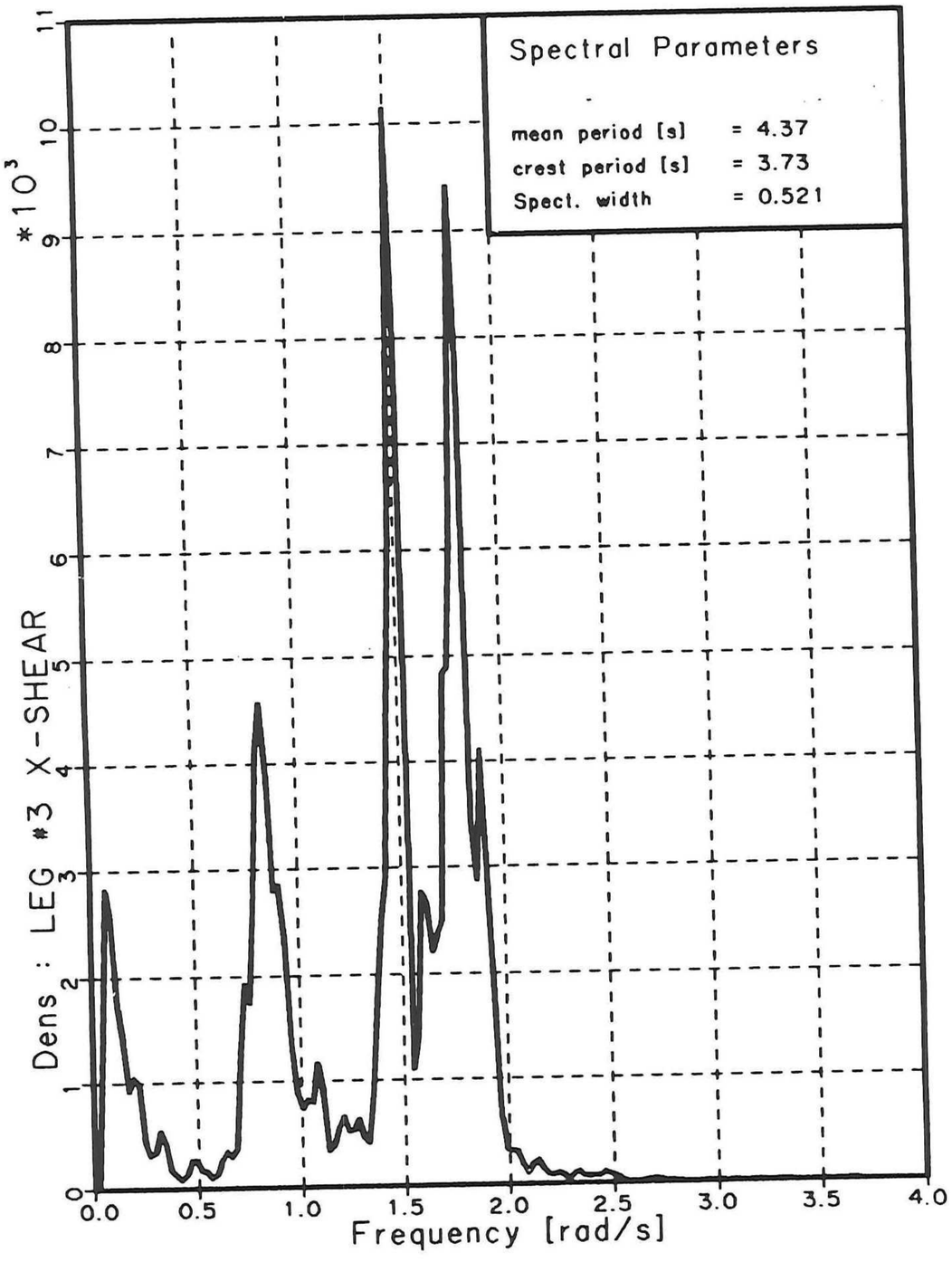

Spectral Density

LEG #3 X-SHEAR (kN)

SIMULATED

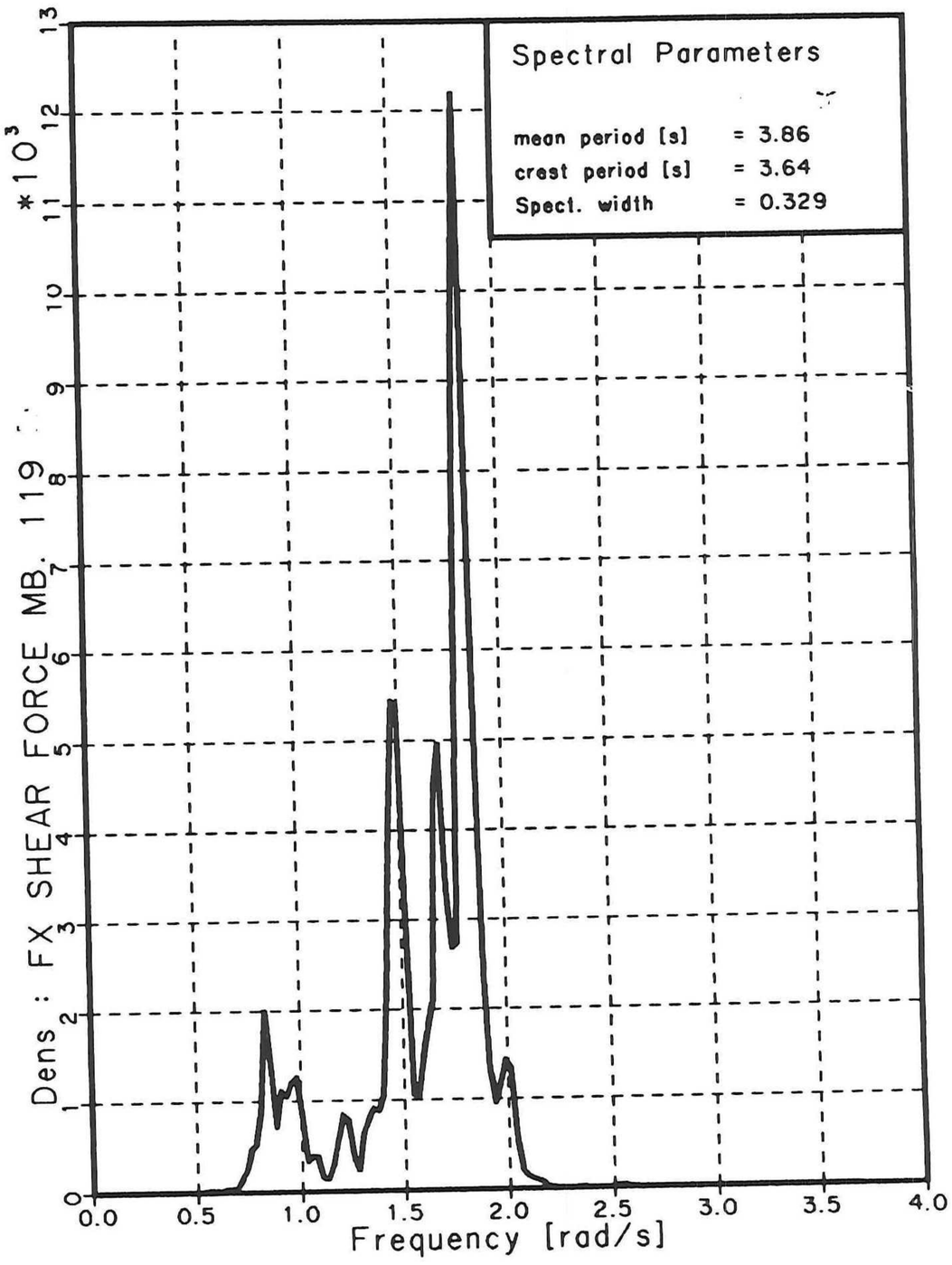

Spectral Density

FX SHEAR FORCE MB. 119

Fig. 27 , 1st. int., leg #3 x shear force spectra

MEASURED

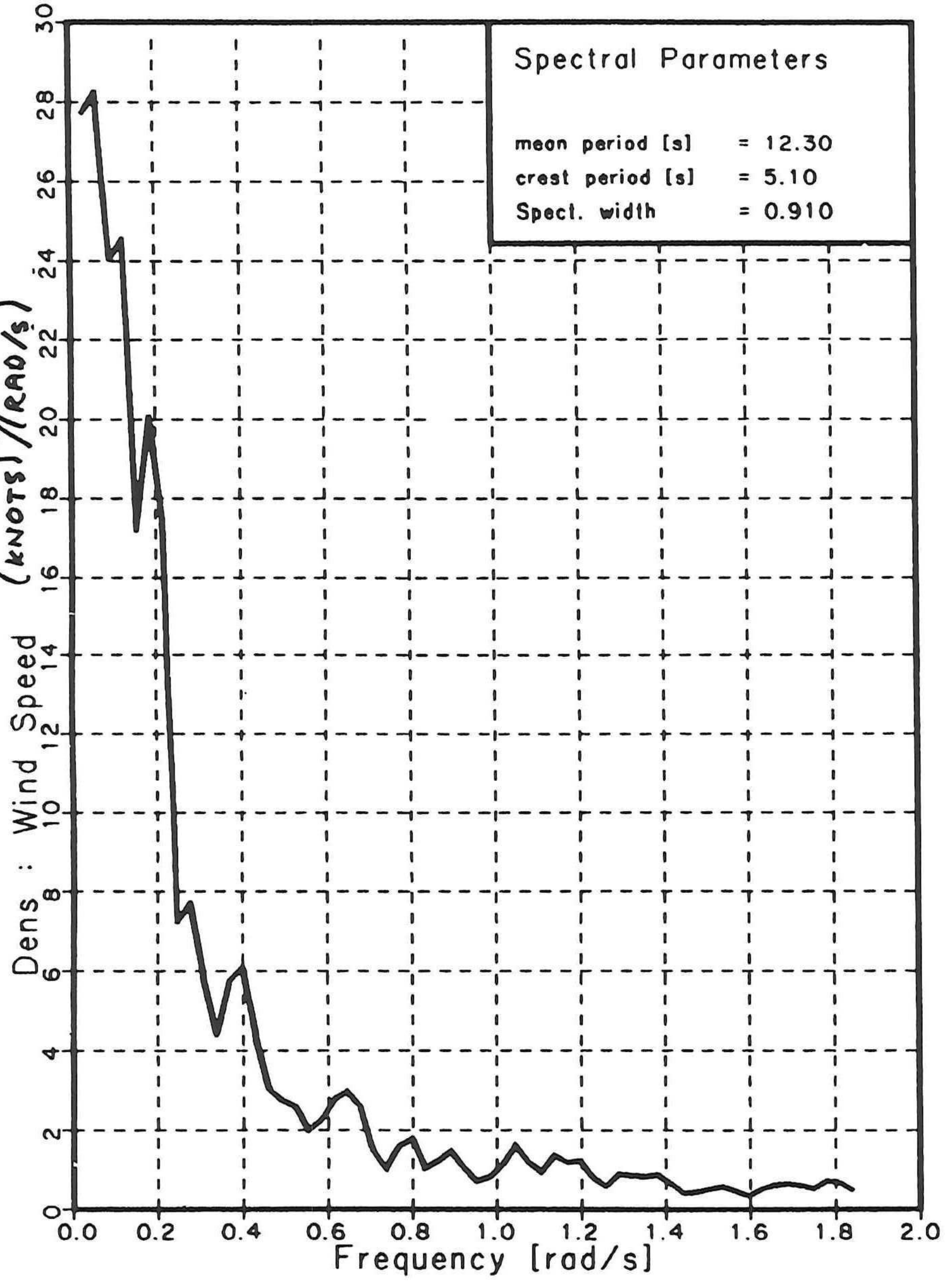

Spectral Density

Wind Speed (knots)

MAERSK: Feb.4, 89, 21:00

Fig. 28 ,1st. int., wind speed spectrum.

DAMPING : 3%

——— : DYNAL SIMULATION

------ : MEASUREMENTS

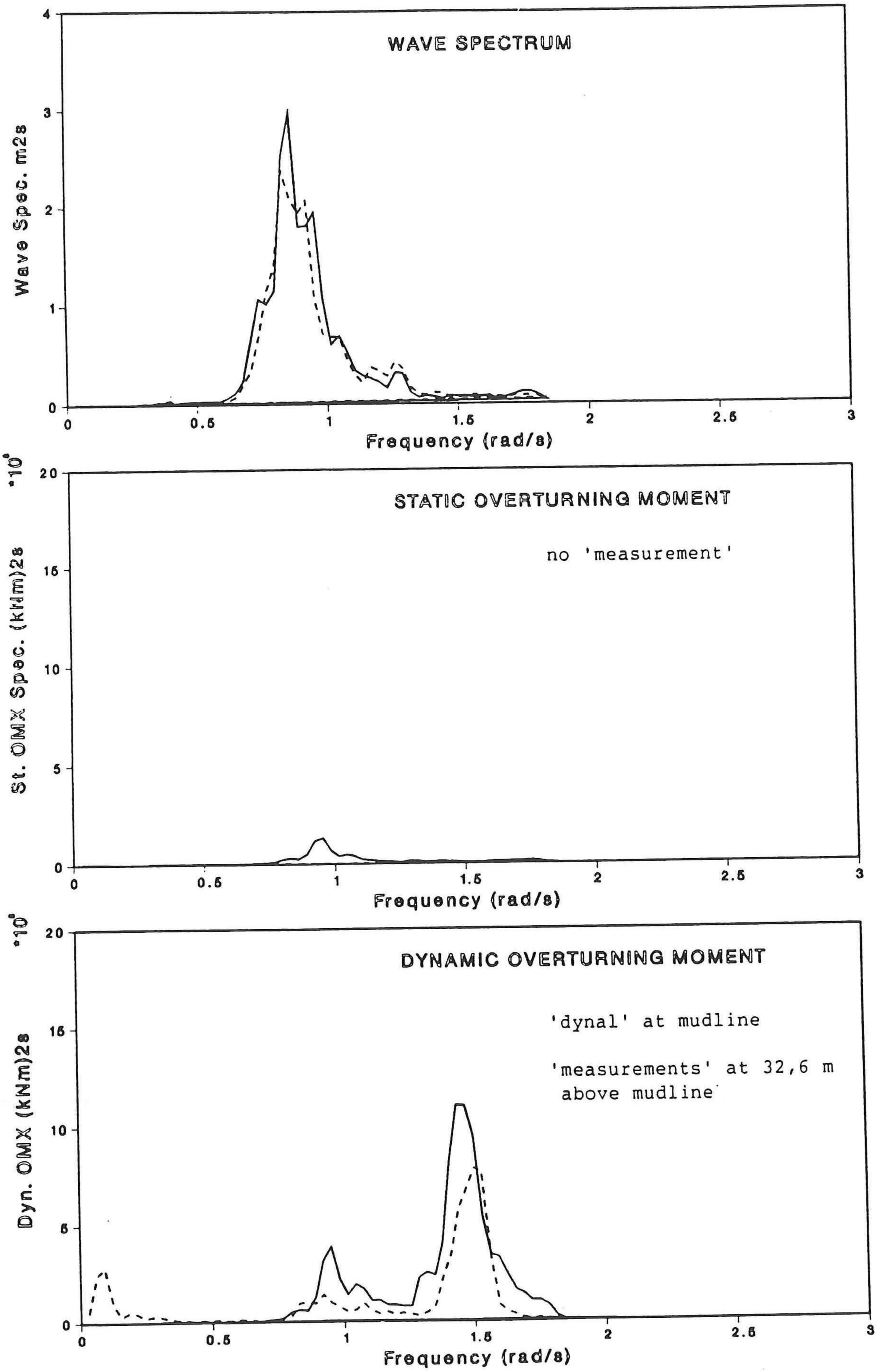

Fig. 29 ,OTM spectra, 3% damping

DAMPING : 2%

——— : DYNAL SIMULATION

------ : MEASUREMENTS

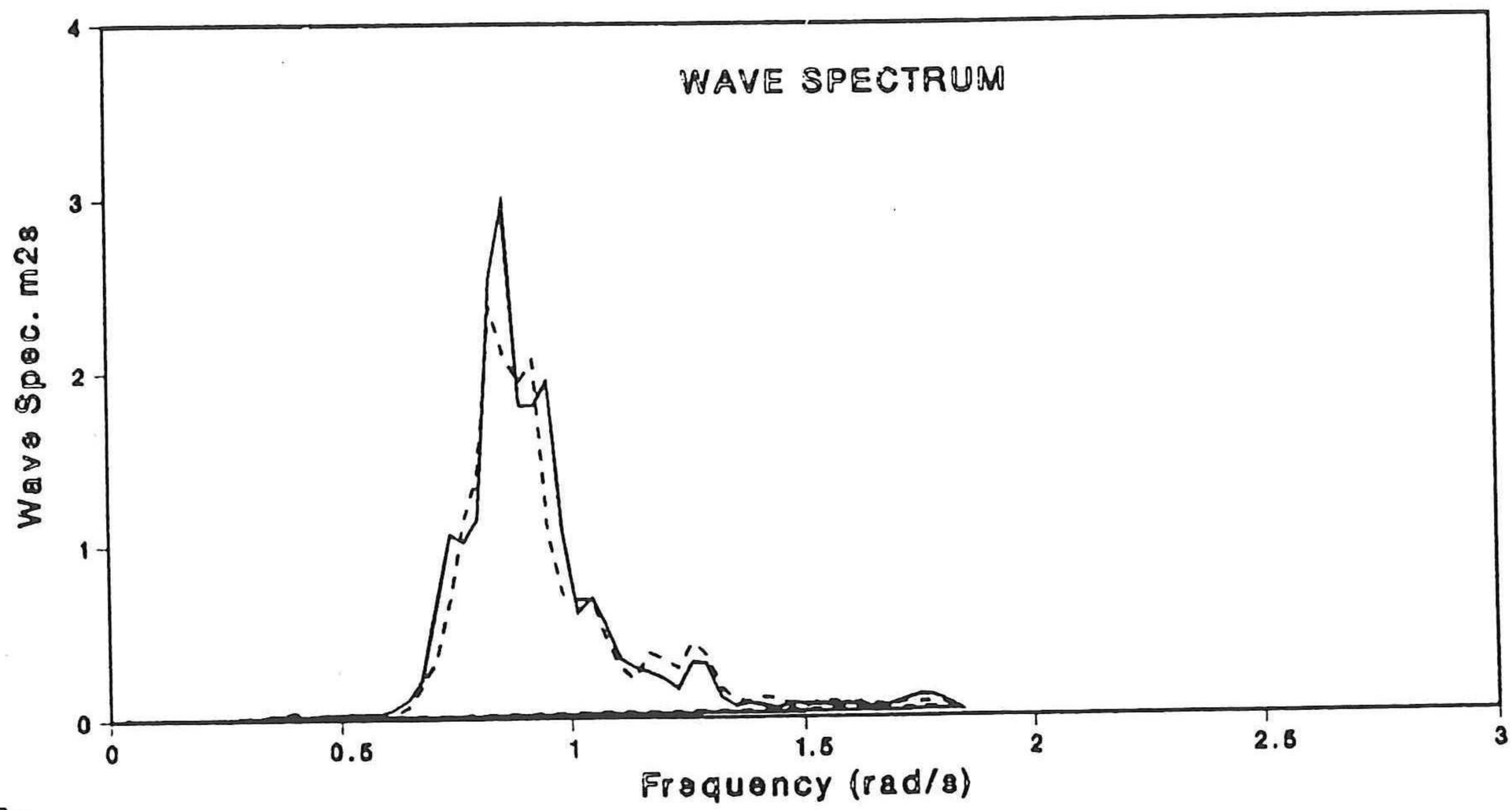

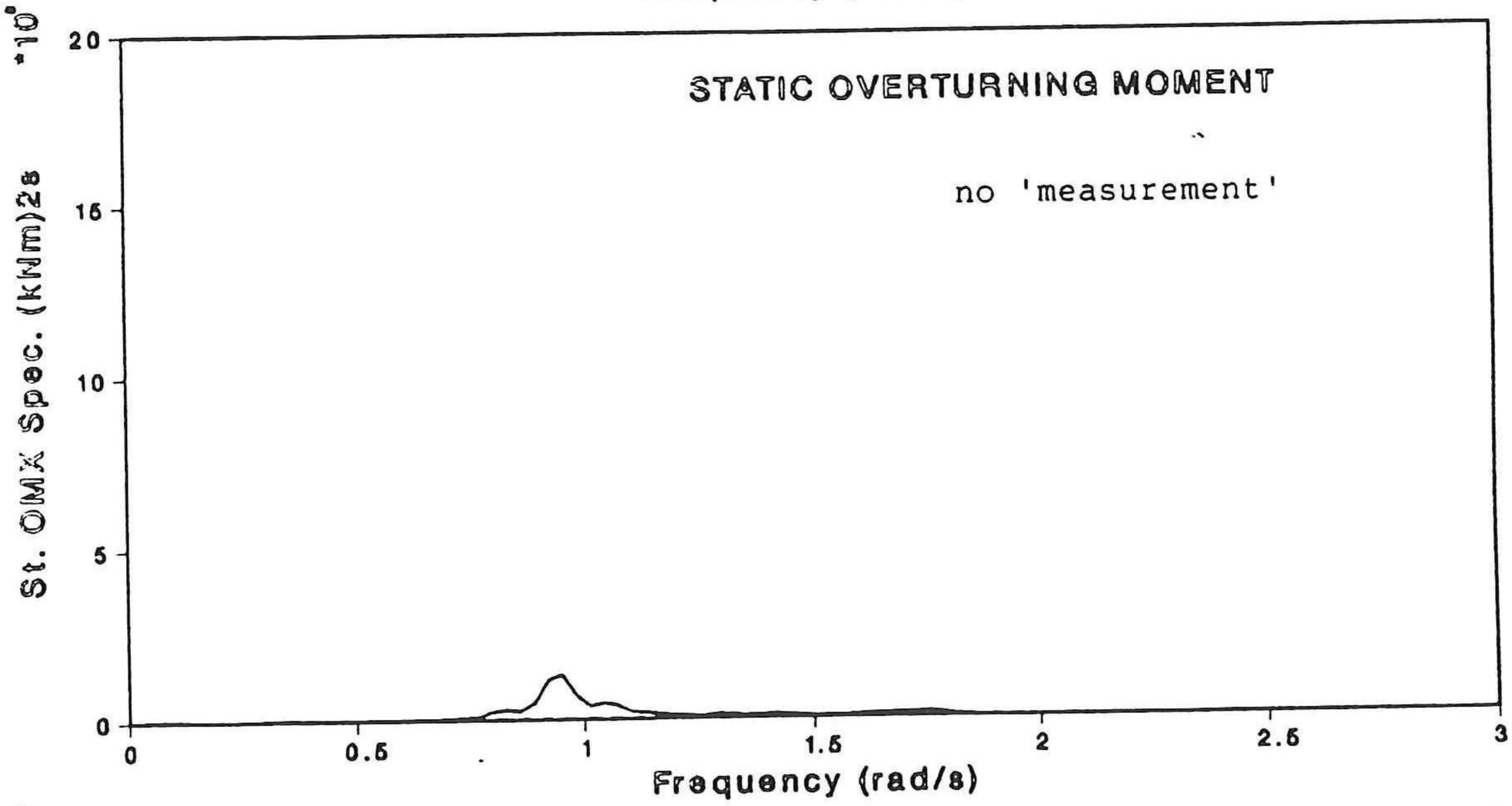

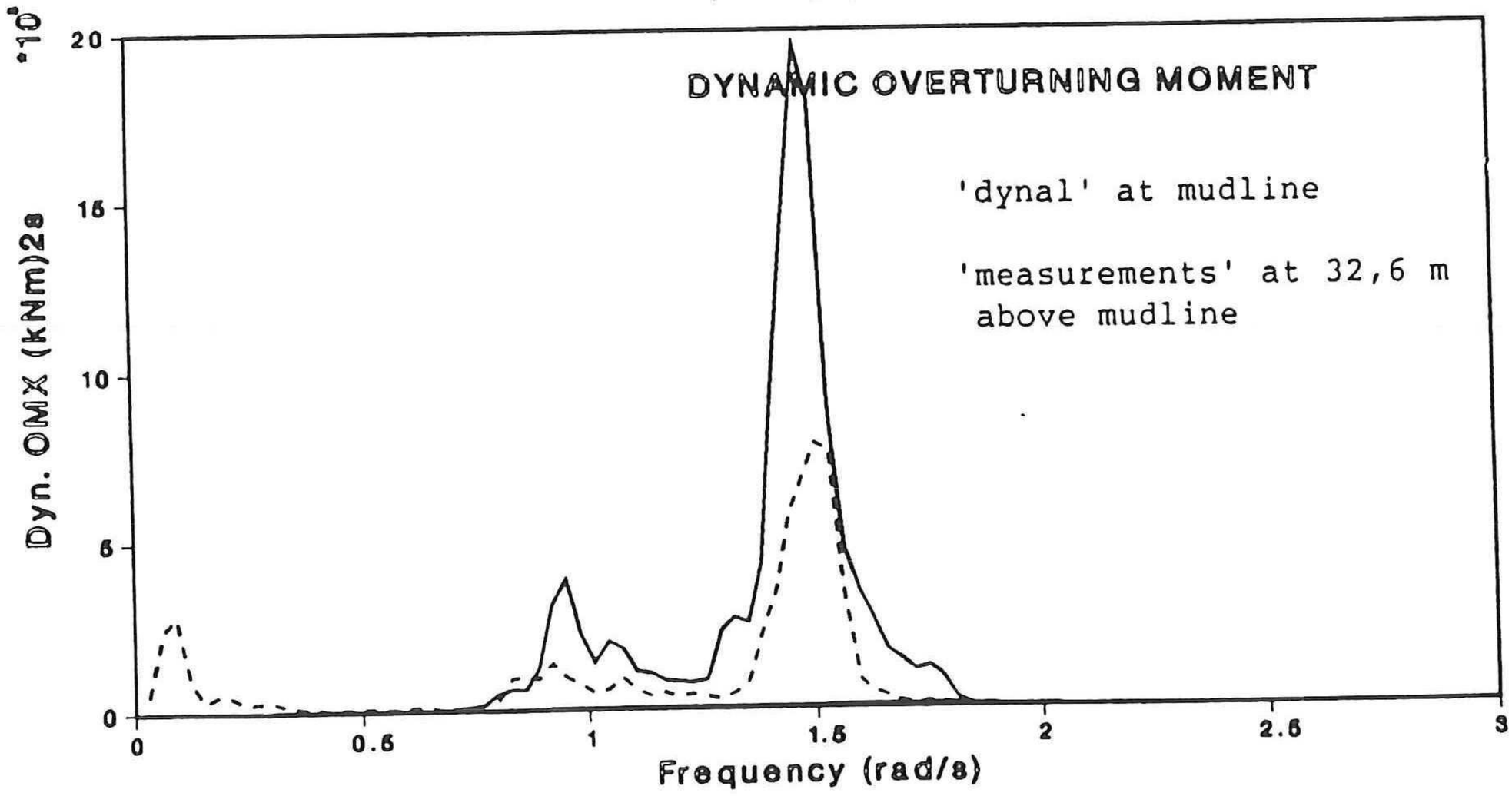

Fig. 30 ,OTM spectra, 2% damping

MEASURED

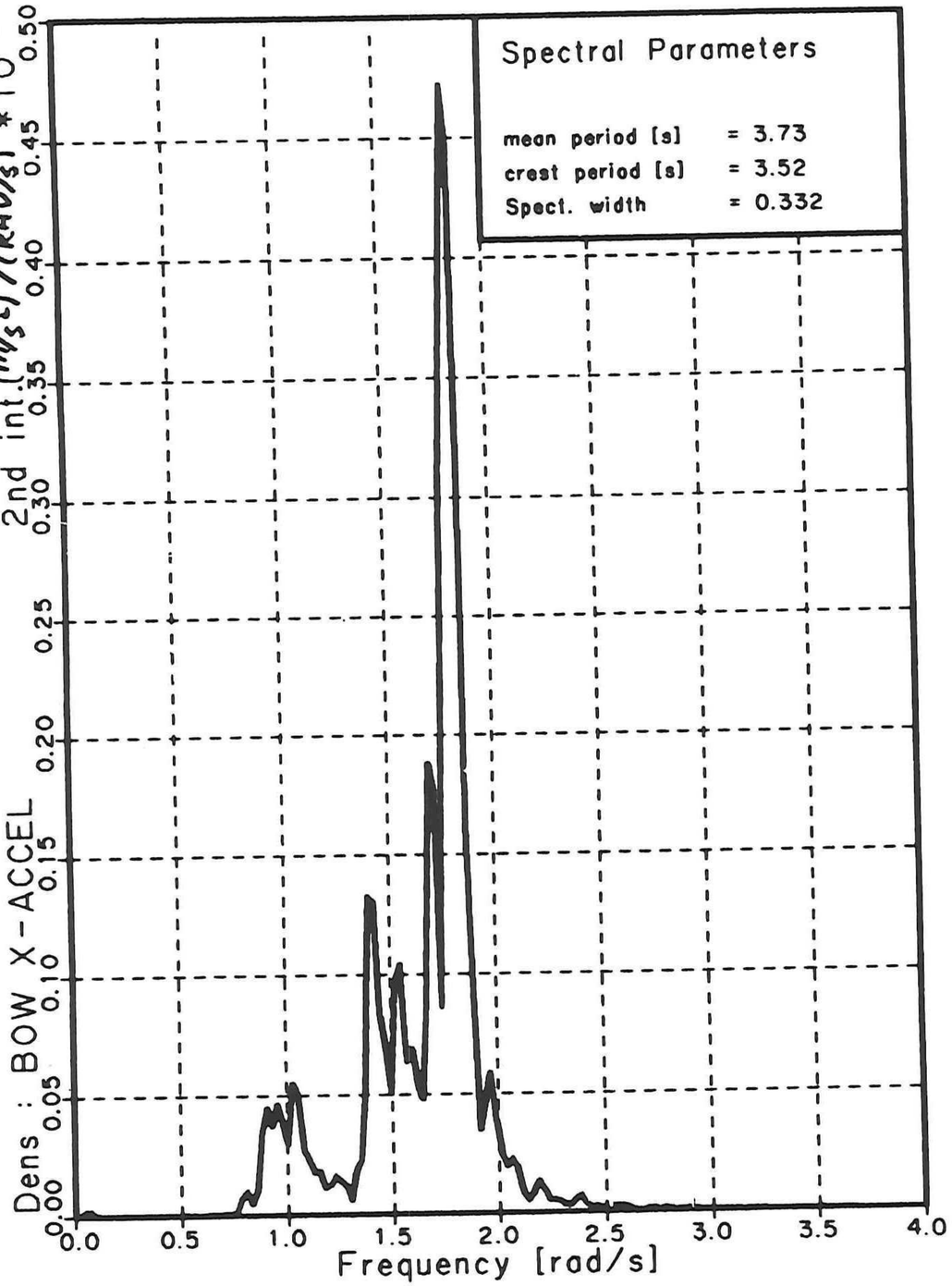

Spectral Density

BOW X-ACCEL (M/SEC**2) 2nd int.

SIMULATED

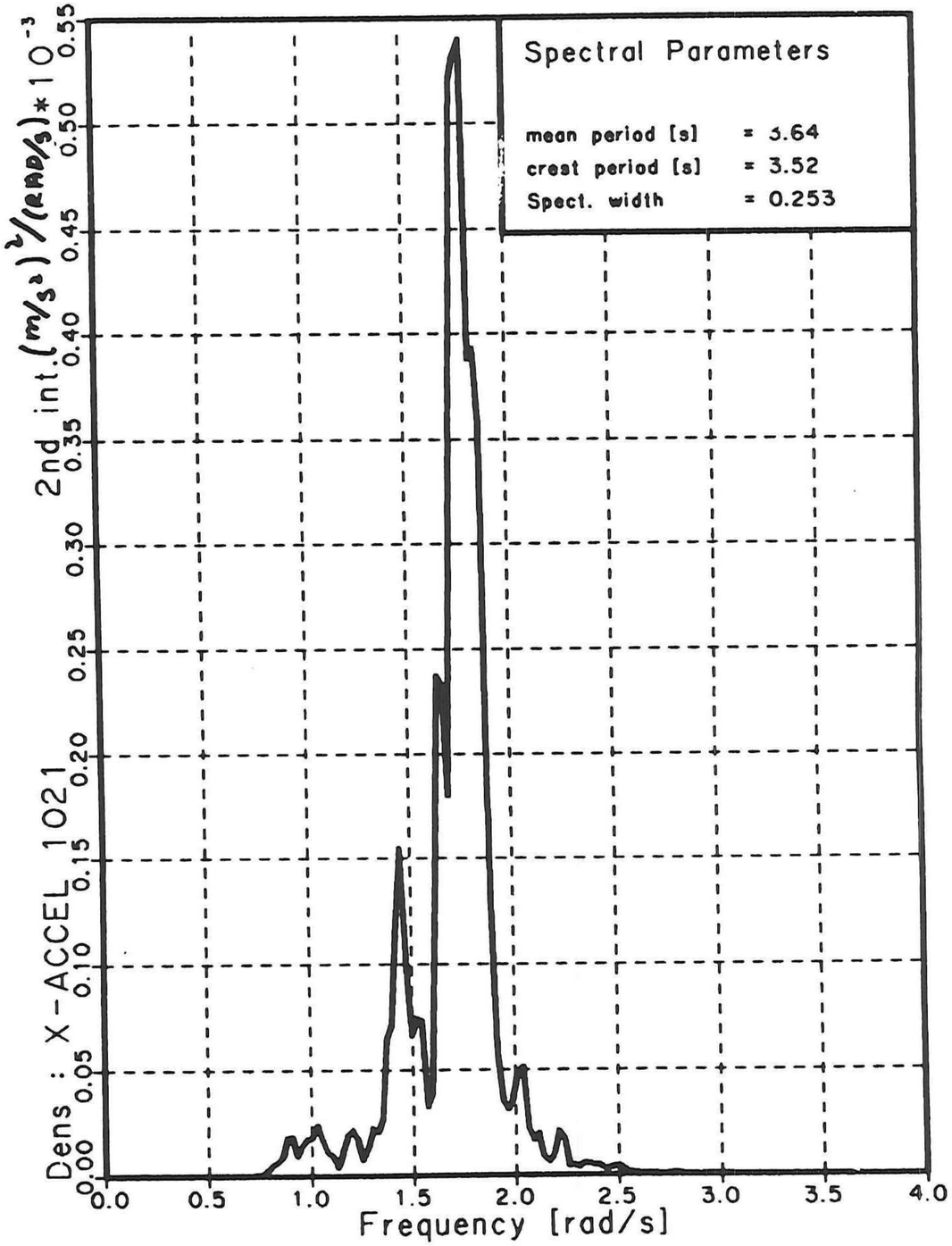

Spectral Density

X-ACCEL 1021 (M/SEC**2, 2nd int

Fig. 31 , 2nd. int., bow x acceleration spectra

MEASURED

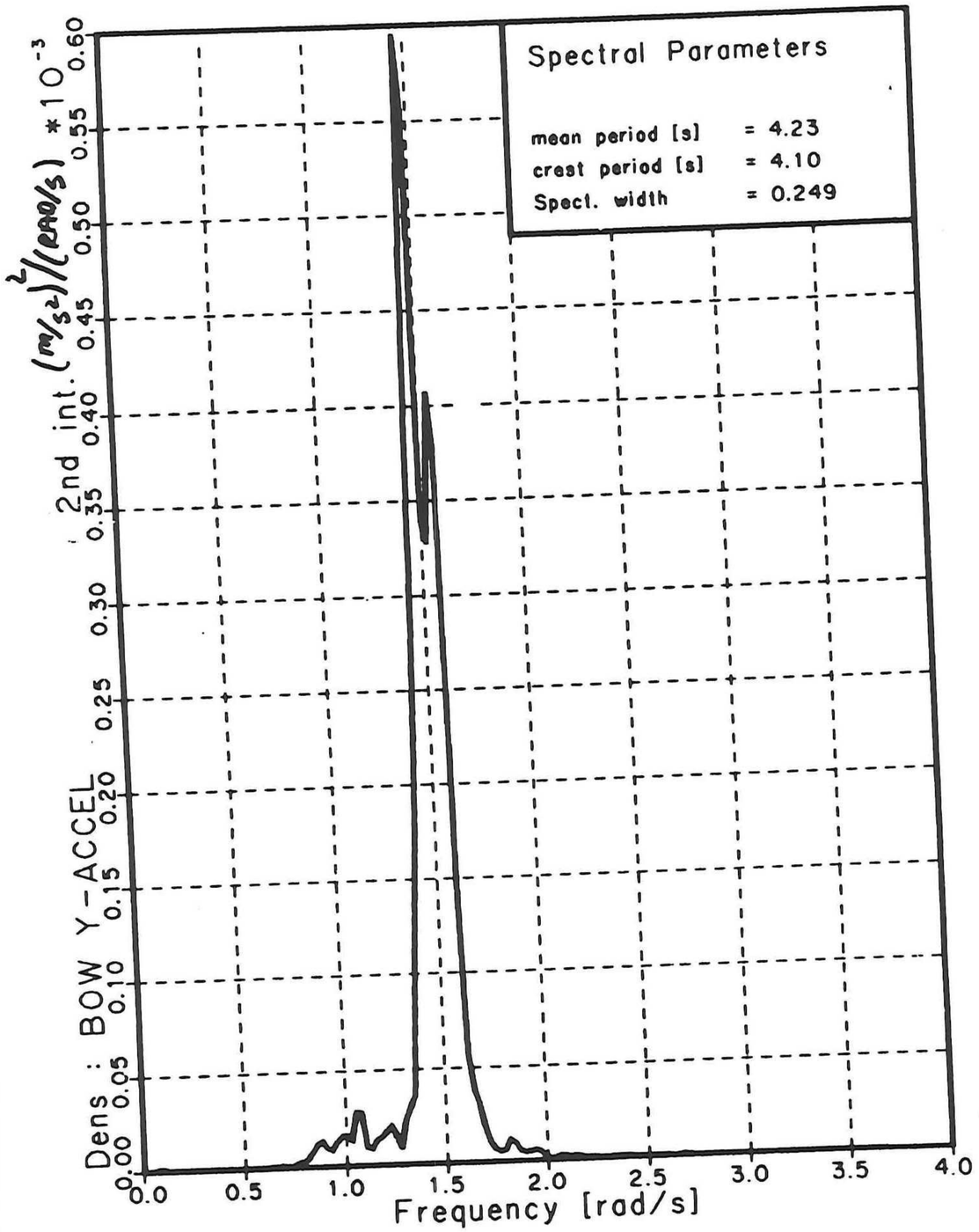

BOW Y-ACCEL (M/SEC**2) 2nd int.

SIMULATED

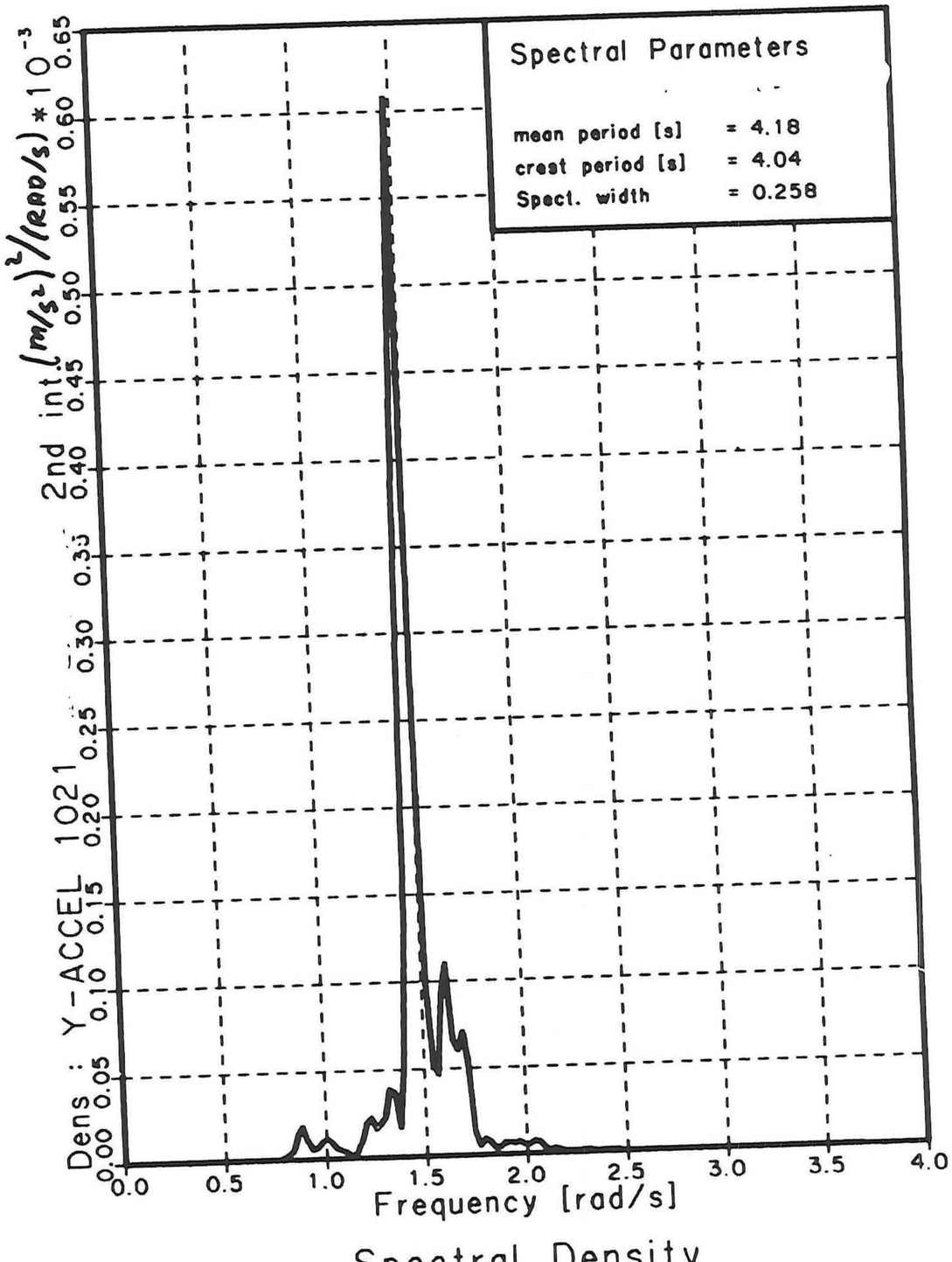

Y-ACCEL 1021 (M/SEC**2) 2nd int

Fig. 32 , 2nd. int., bow y acceleration spectra

MEASURED

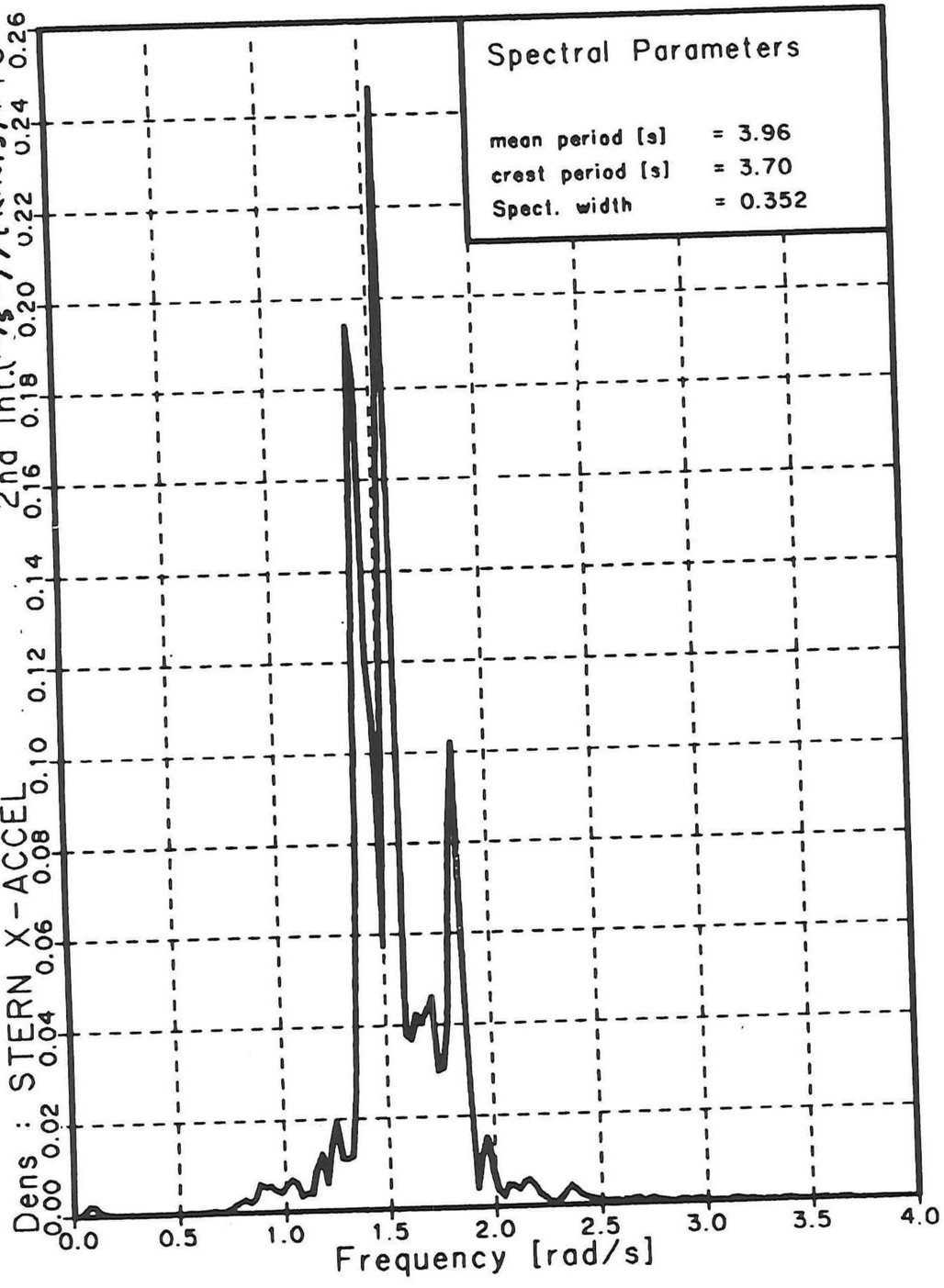

Spectral Density

STERN X-ACCEL (M/SEC**2) 2nd int.

SIMULATED

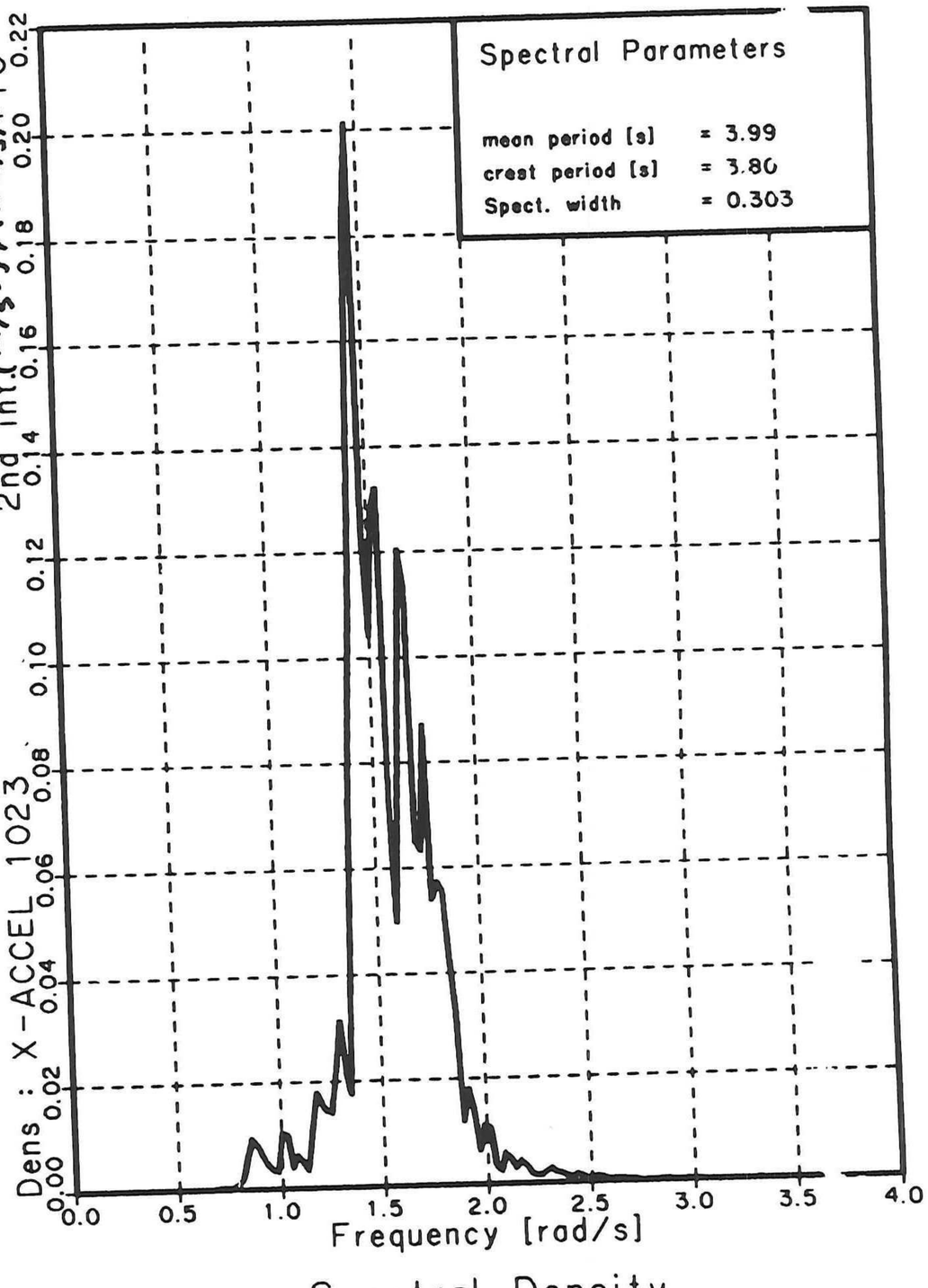

Spectral Density

X-ACCEL 1023 (M/SEC**2) 2nd int.

Fig. 33 , 2nd. int., stern x acceleration spectra

MEASURED

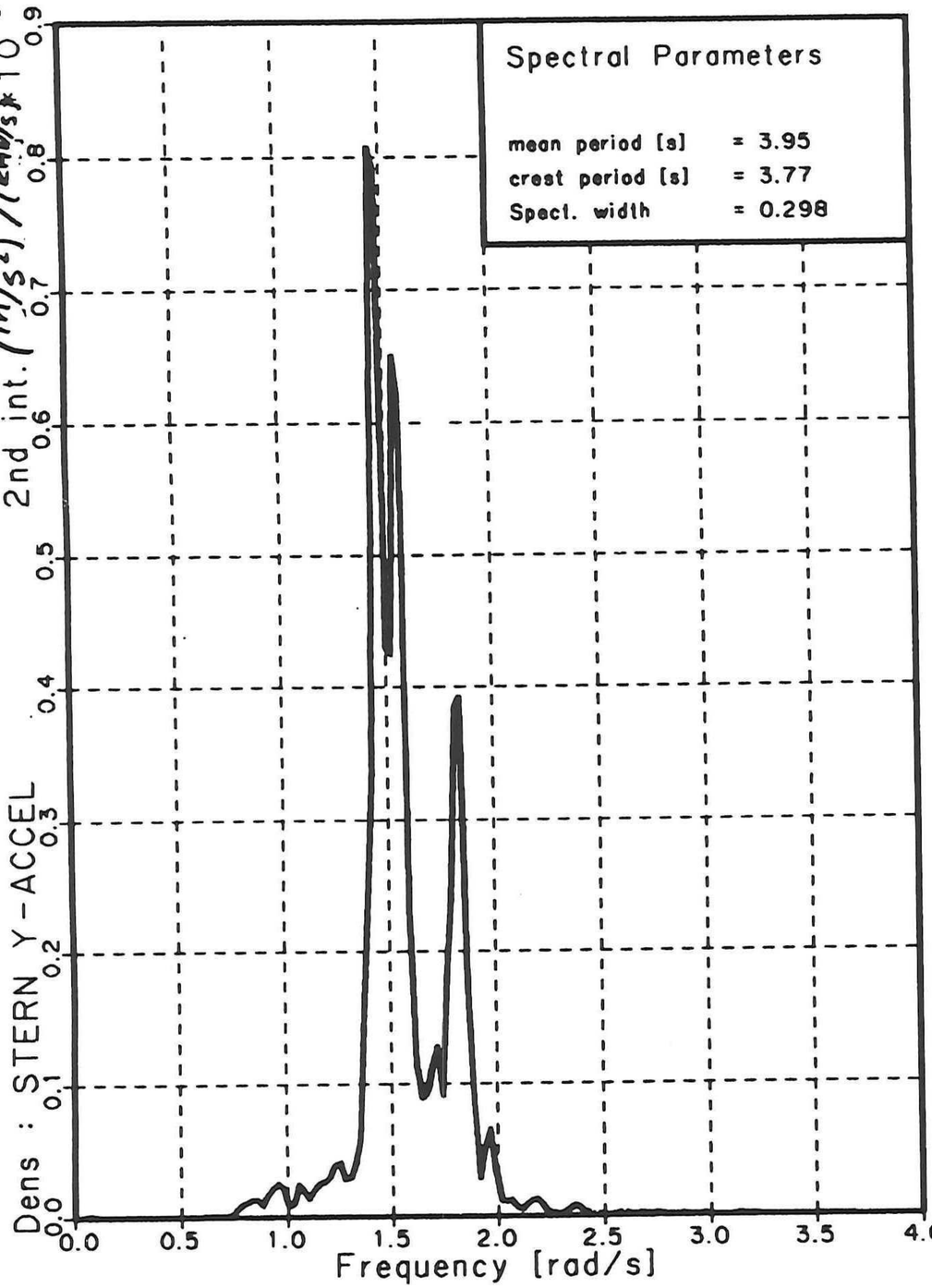

STERN Y-ACCEL (M/SEC**2) 2nd int

SIMULATED

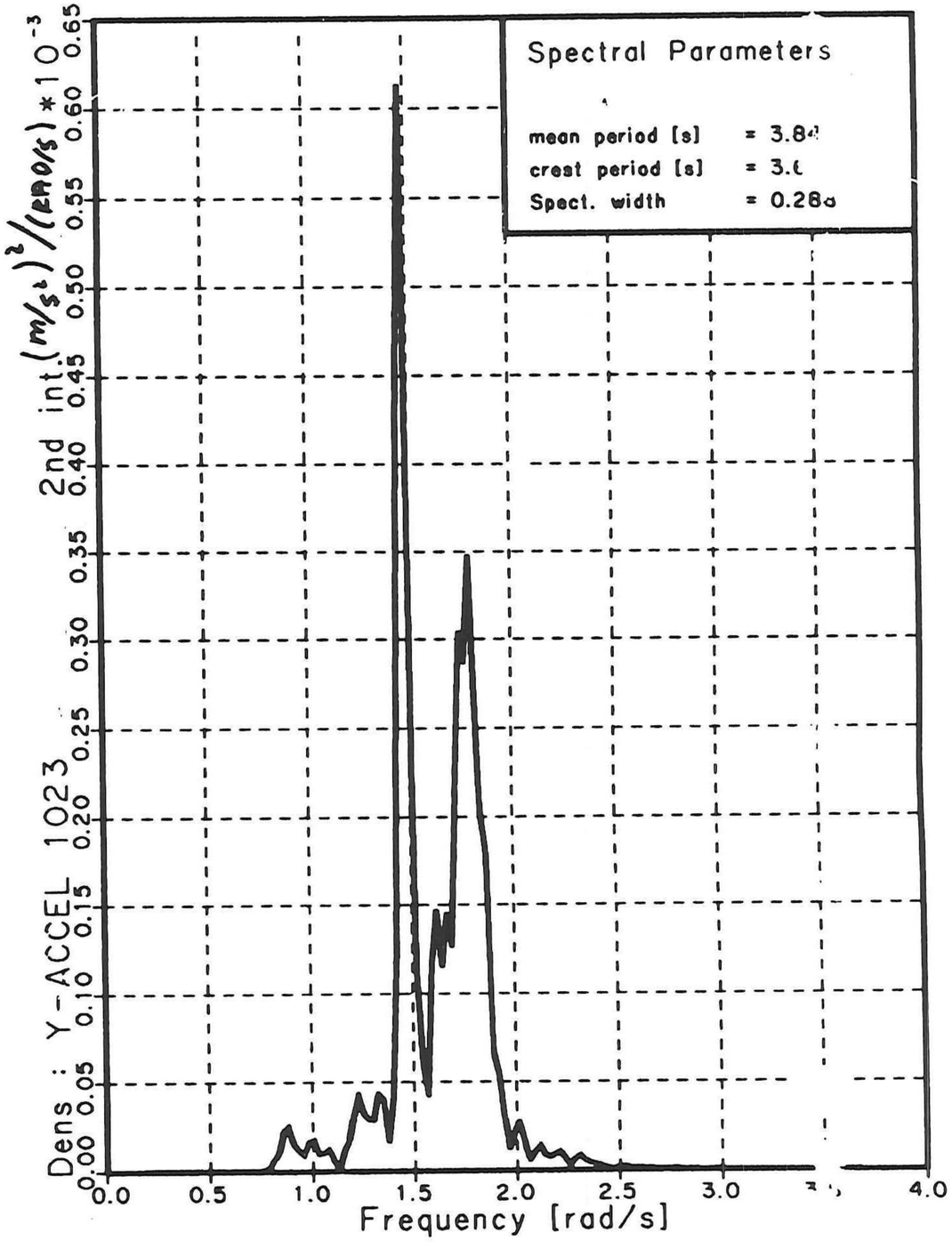

Y-ACCEL 1023 (M/SEC**2) 2nd in

Fig. 34 , 2nd. int., stern y acceleration spectra

SURFACE ELEVATION (BAY #19)

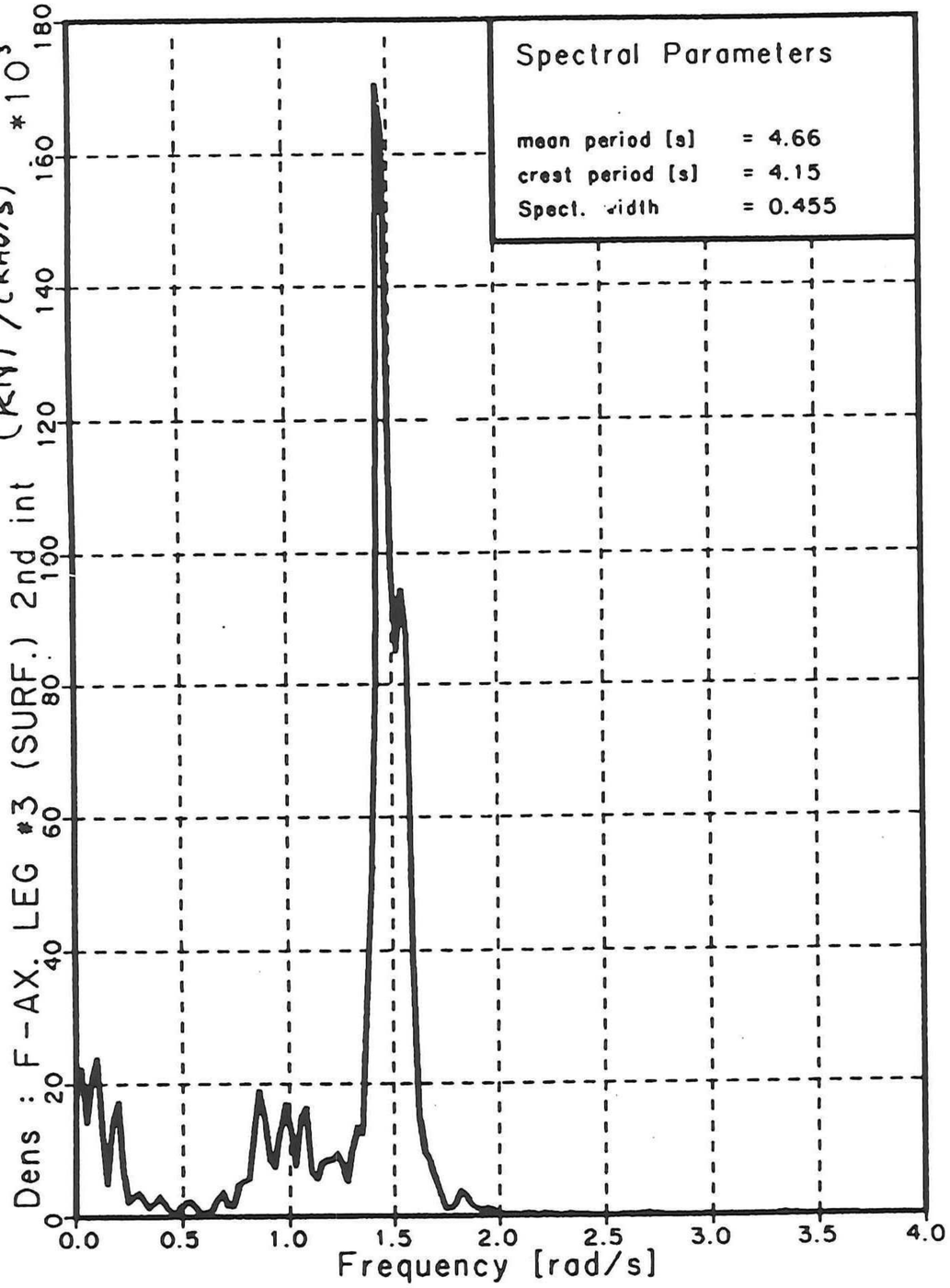

Spectral Density

SUBSEA ELEVATION (BAY #7)

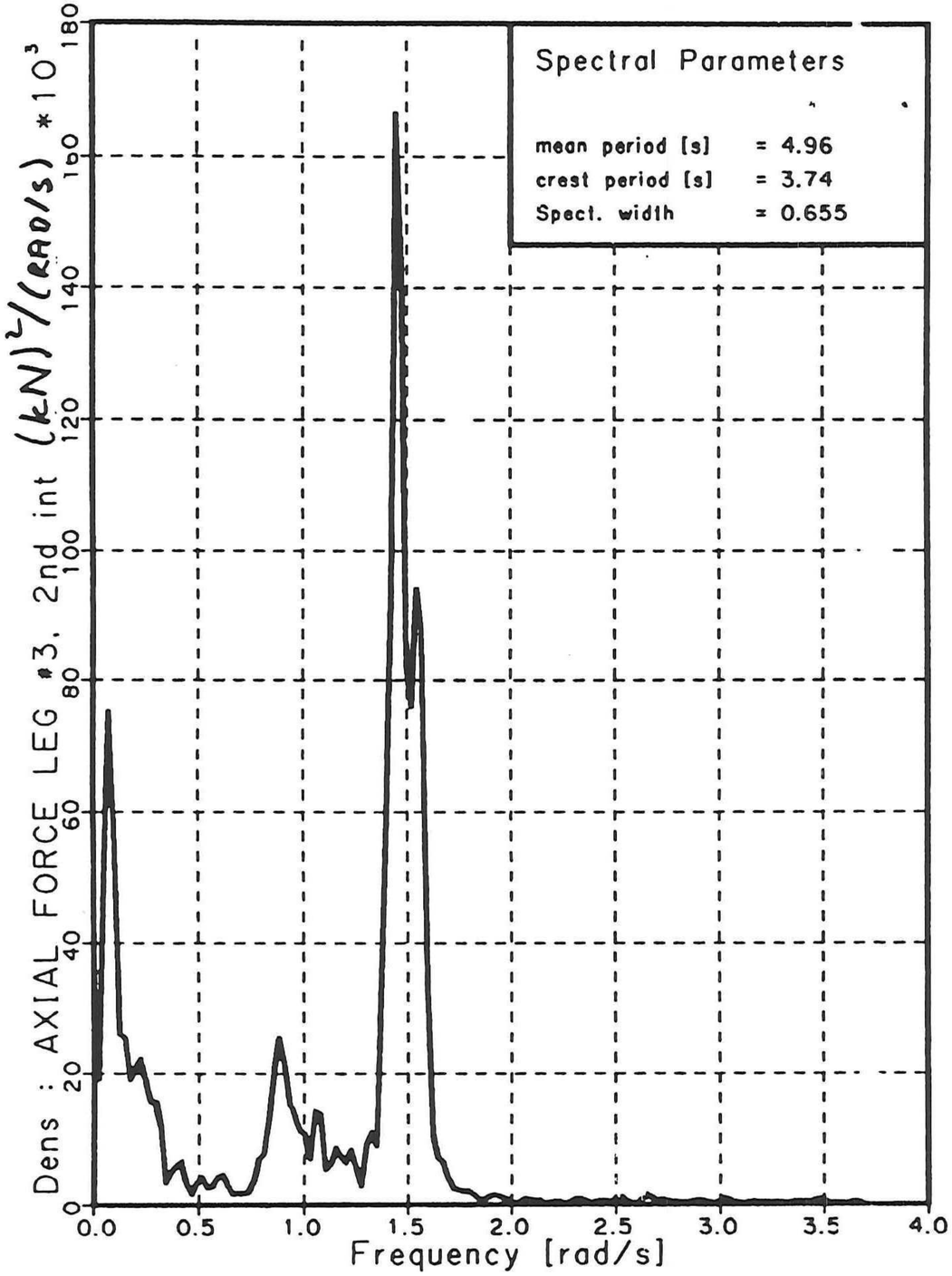

Spectral Density

Fig. 35 , 2nd. int., leg #3 axial force spectrum

FIG.

AXIAL FORCE IN LEG #3, 2ND INTERVAL

MAERSK: Feb.4, 89, 21:00

MEASURED

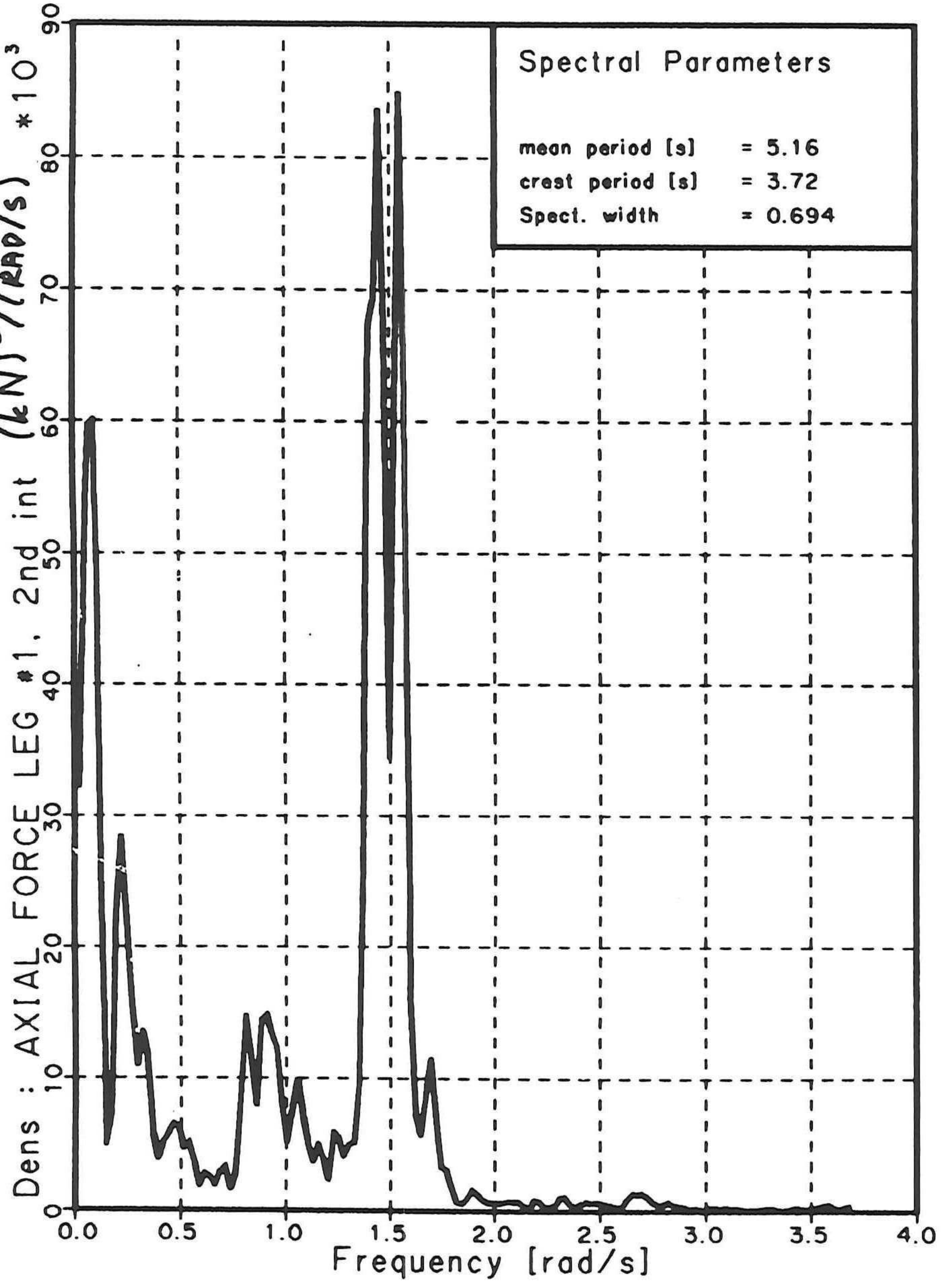

Spectral Density

AXIAL FORCE LEG #1, 2nd int (kN)

SIMULATED

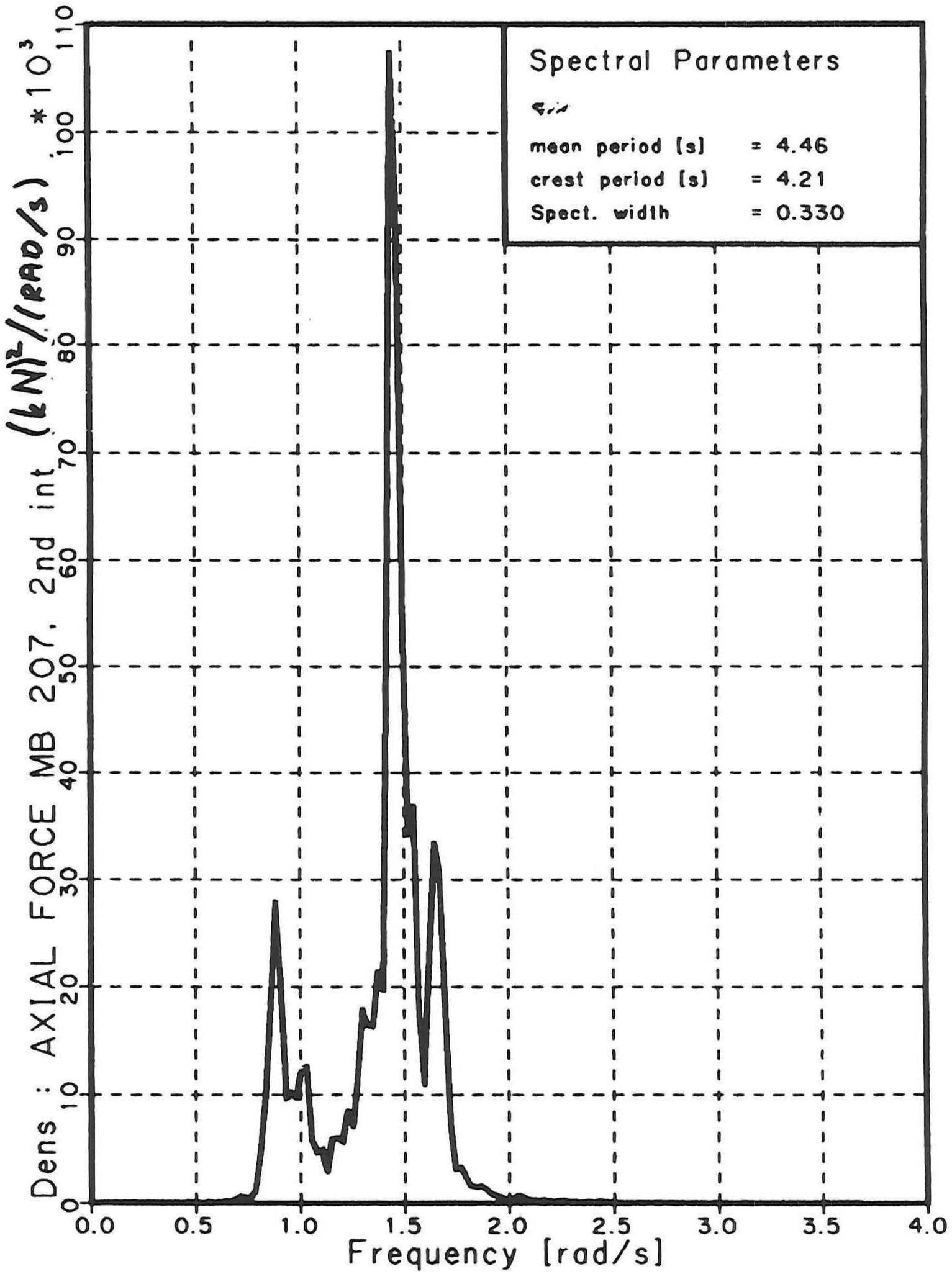

Spectral Density

AXIAL FORCE MB 207, 2nd int (kN)

Fig. 36 , 2nd. int., leg #1 axial force spectra

MEASURED

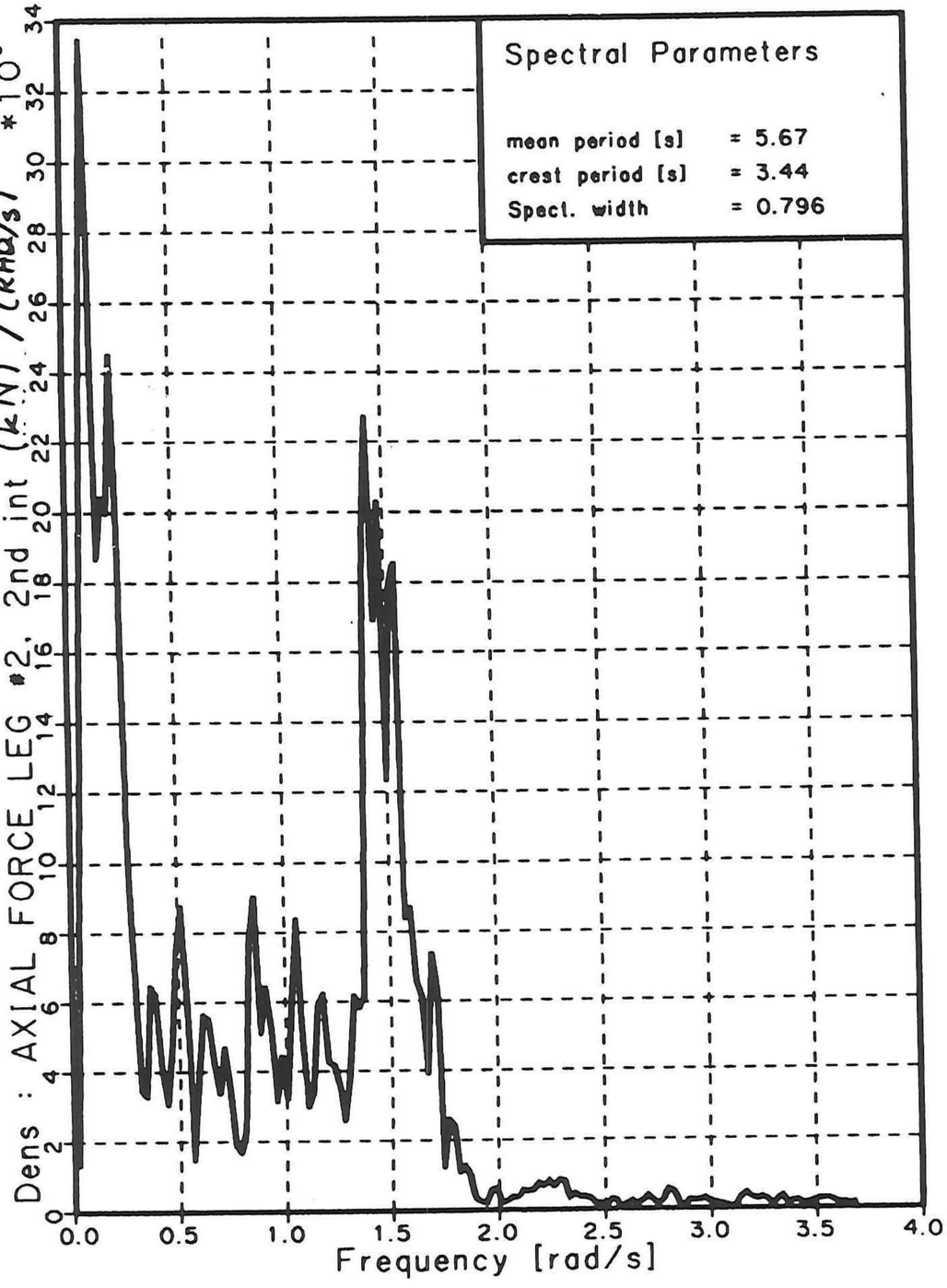

Spectral Density

AXIAL FORCE LEG #2, 2nd int (kN)

SIMULATED

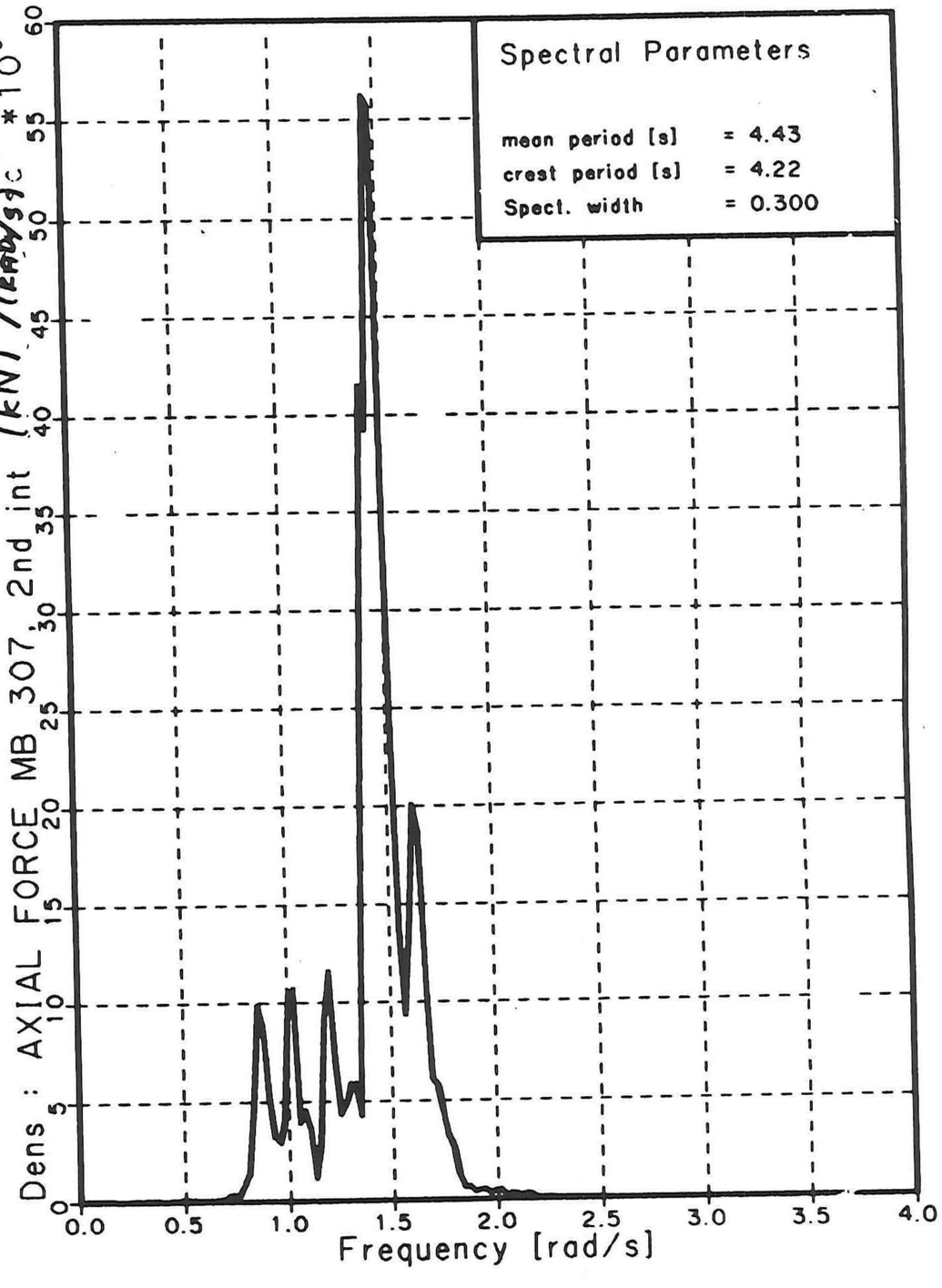

Spectral Density

AXIAL FORCE MB 307, 2nd int (kN)

Fig. 37, 2nd. int., leg #2, axial force spectra

MEASURED

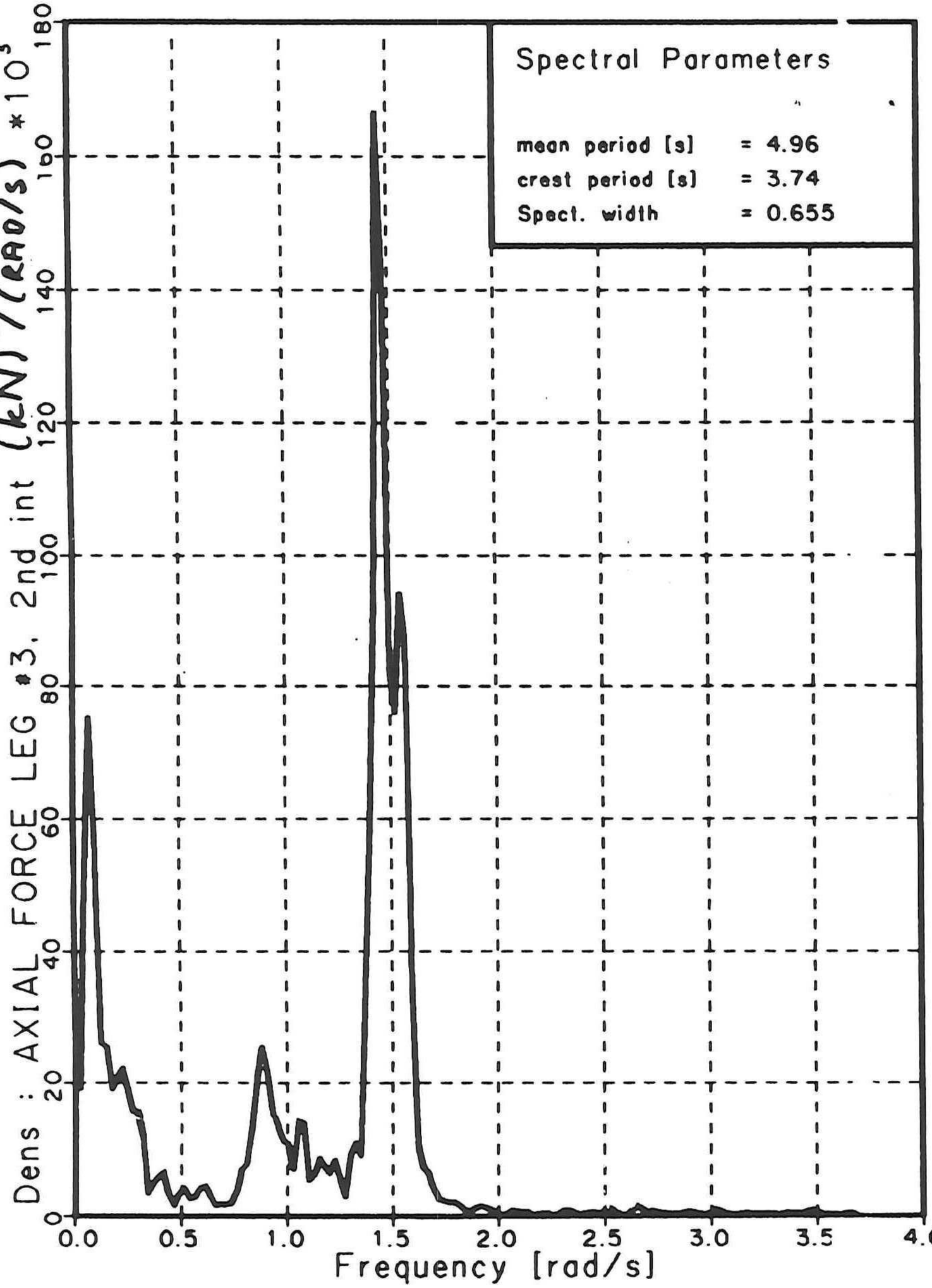

Spectral Density

AXIAL FORCE LEG #3, 2nd int (kN)

SIMULATED

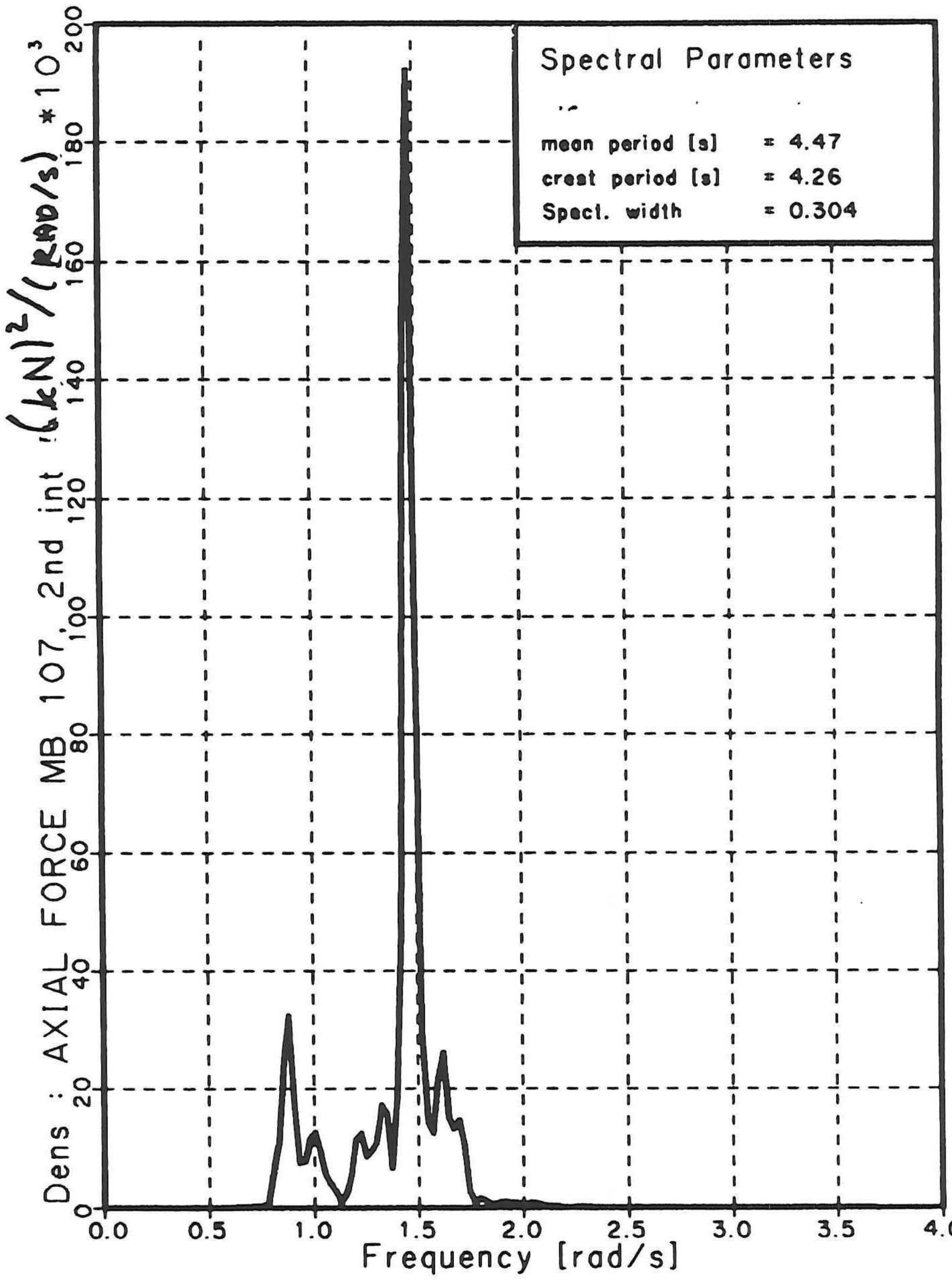

Spectral Density

AXIAL FORCE MB 107, 2nd int (kN)

Fig. 38 ,2nd. int., leg #3, axial force spectra (subsea elevation)

MEASURED

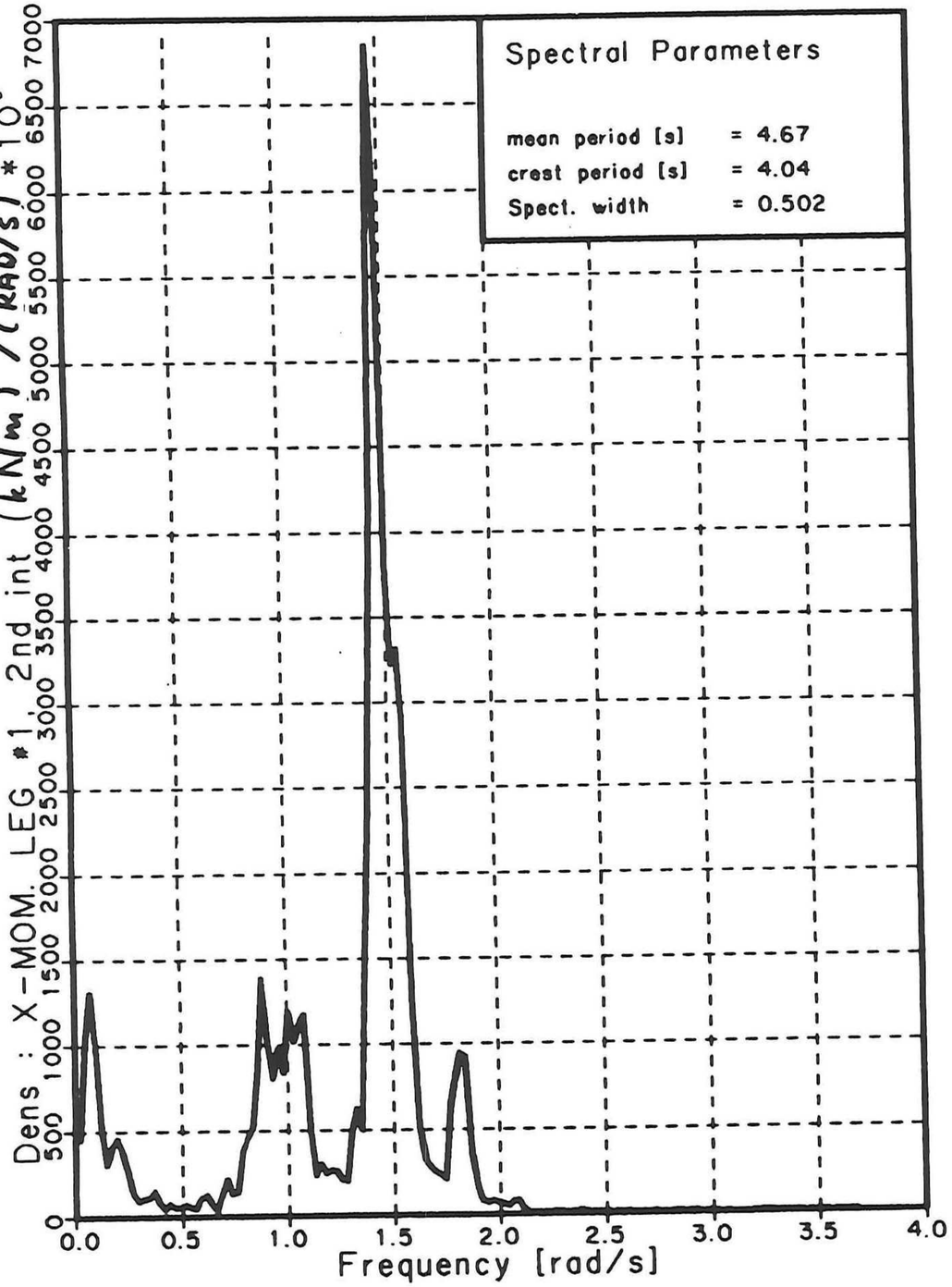

Spectral Density

X-MOM. LEG #1, 2nd int (kNm)

SIMULATED

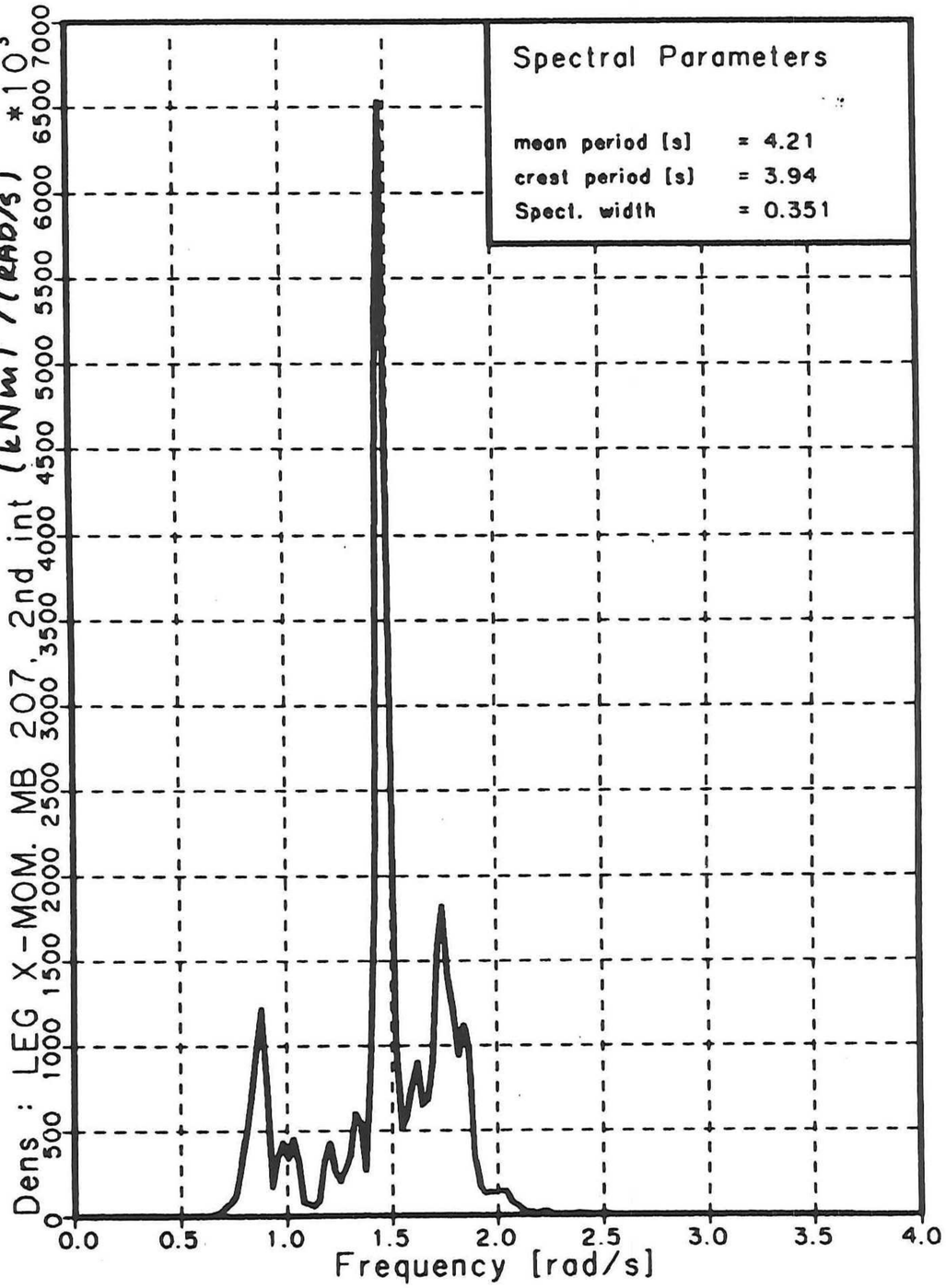

Spectral Density

LEG X-MOM. MB 207, 2nd int (kNm)

Fig. 39 , 2nd. int., leg #1 x moment spectra

MEASURED

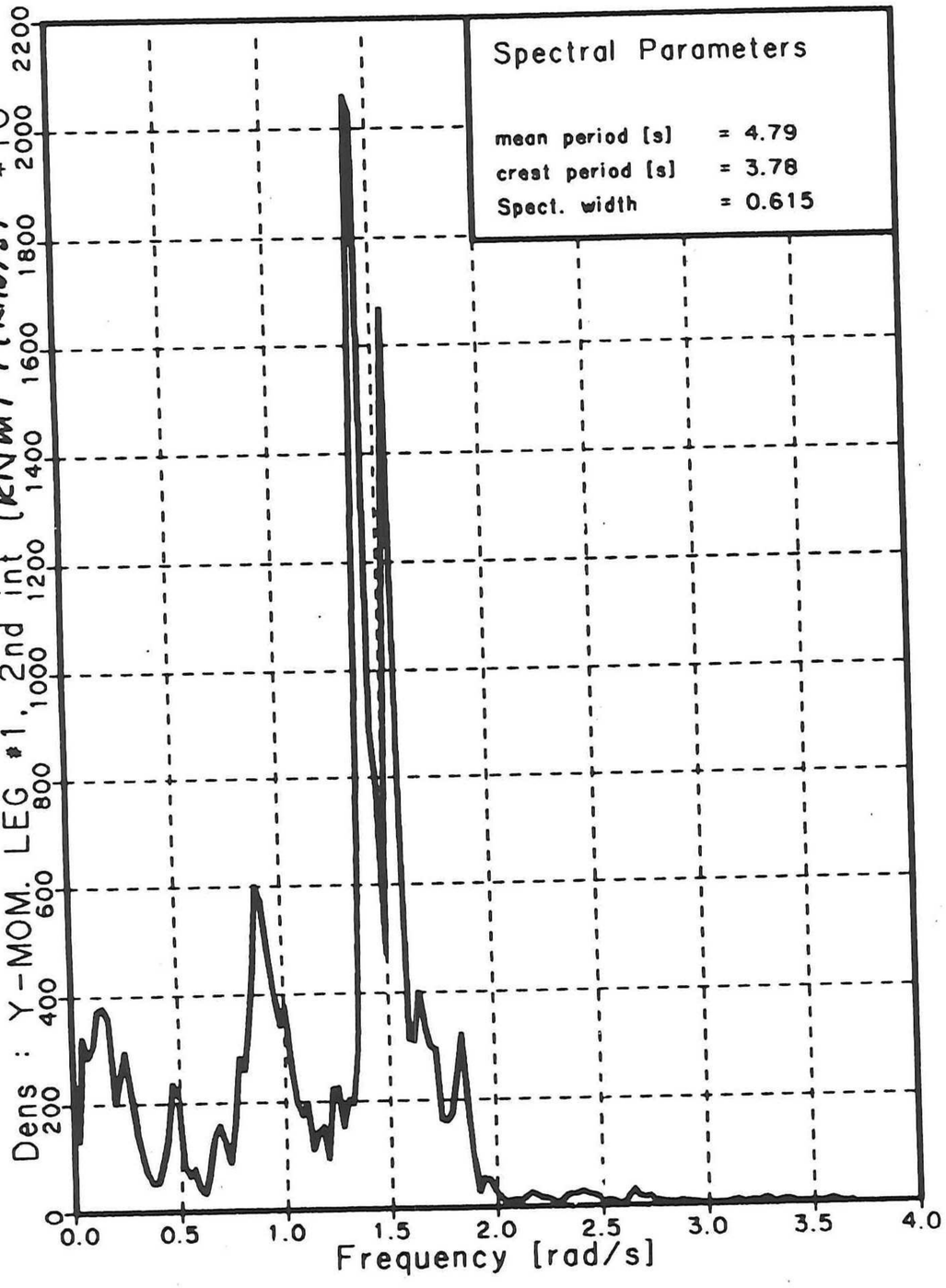

Spectral Density

Y-MOM. LEG #1, 2nd int (kNm)

SIMULATED

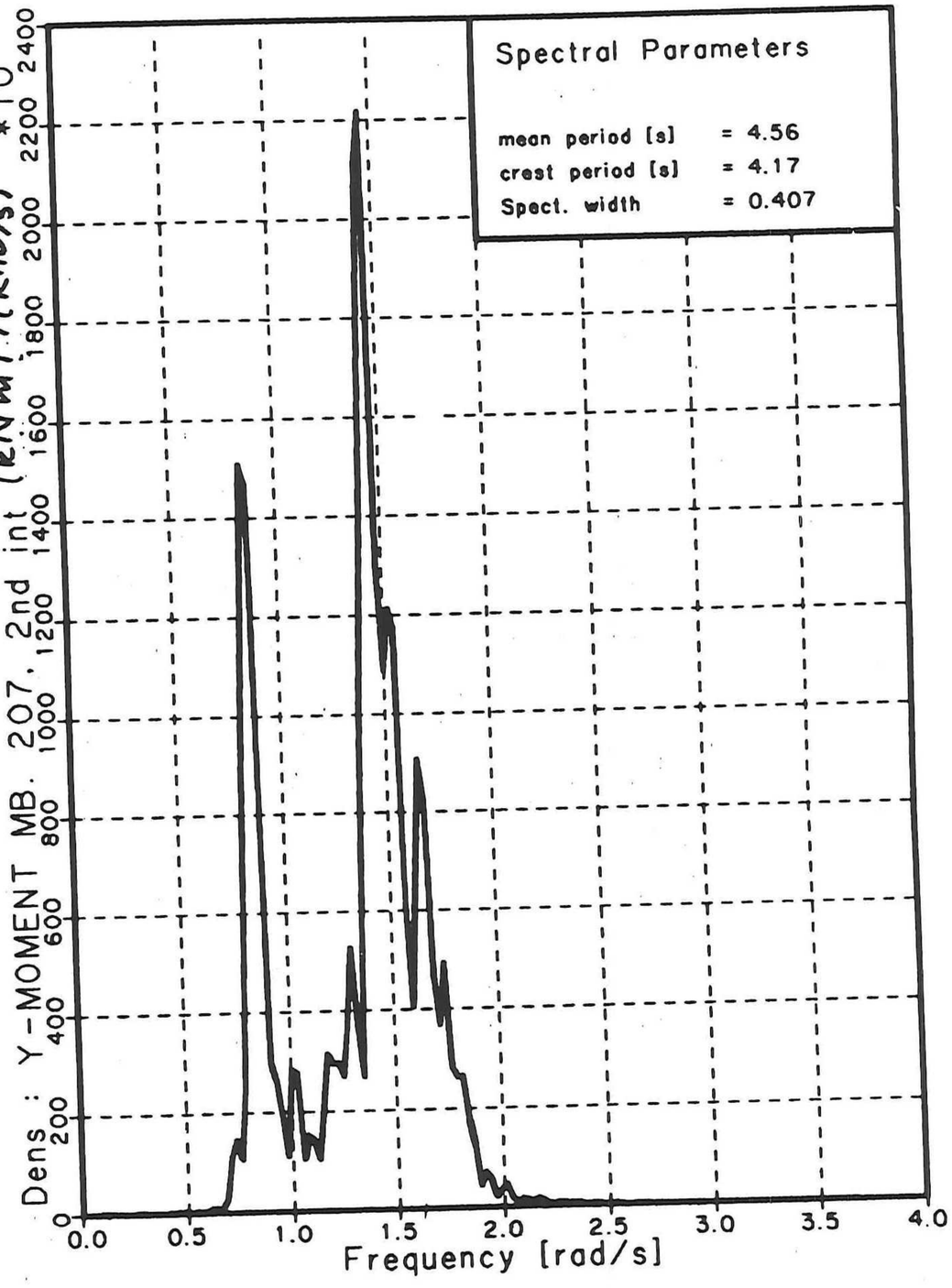

Spectral Density

Y-MOMENT MB. 207, 2nd int (kNm)

Fig. 40 ,2nd. int., leg #1, y moment spectra

MEASURED

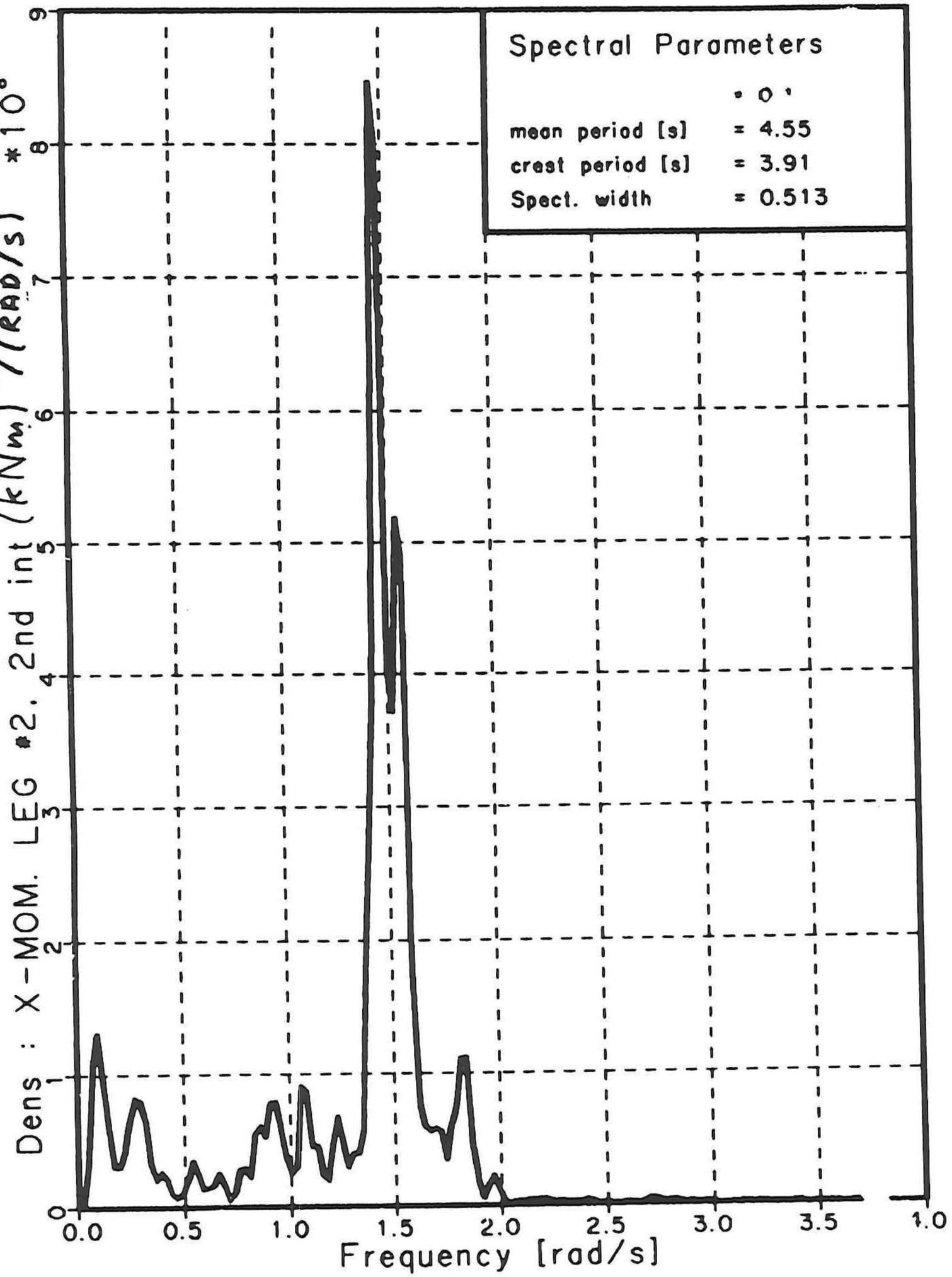

Spectral Density

X-MOM. LEG #2, 2nd int (kNm)

SIMULATED

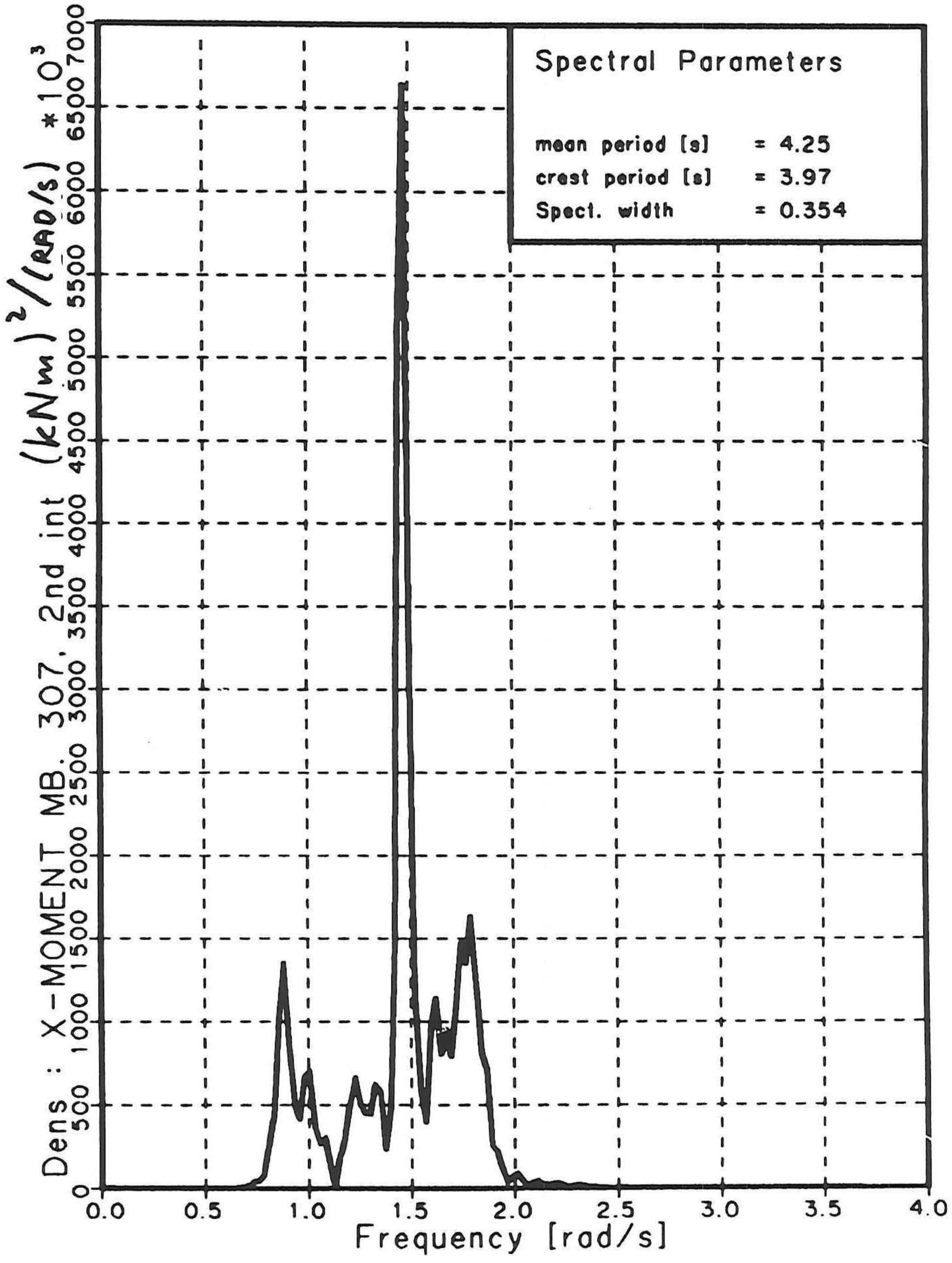

Spectral Density

X-MOMENT MB. 307, 2nd int (kNm)

Fig. 41 , 2nd. int., leg #2, x moment spectra

MEASURED

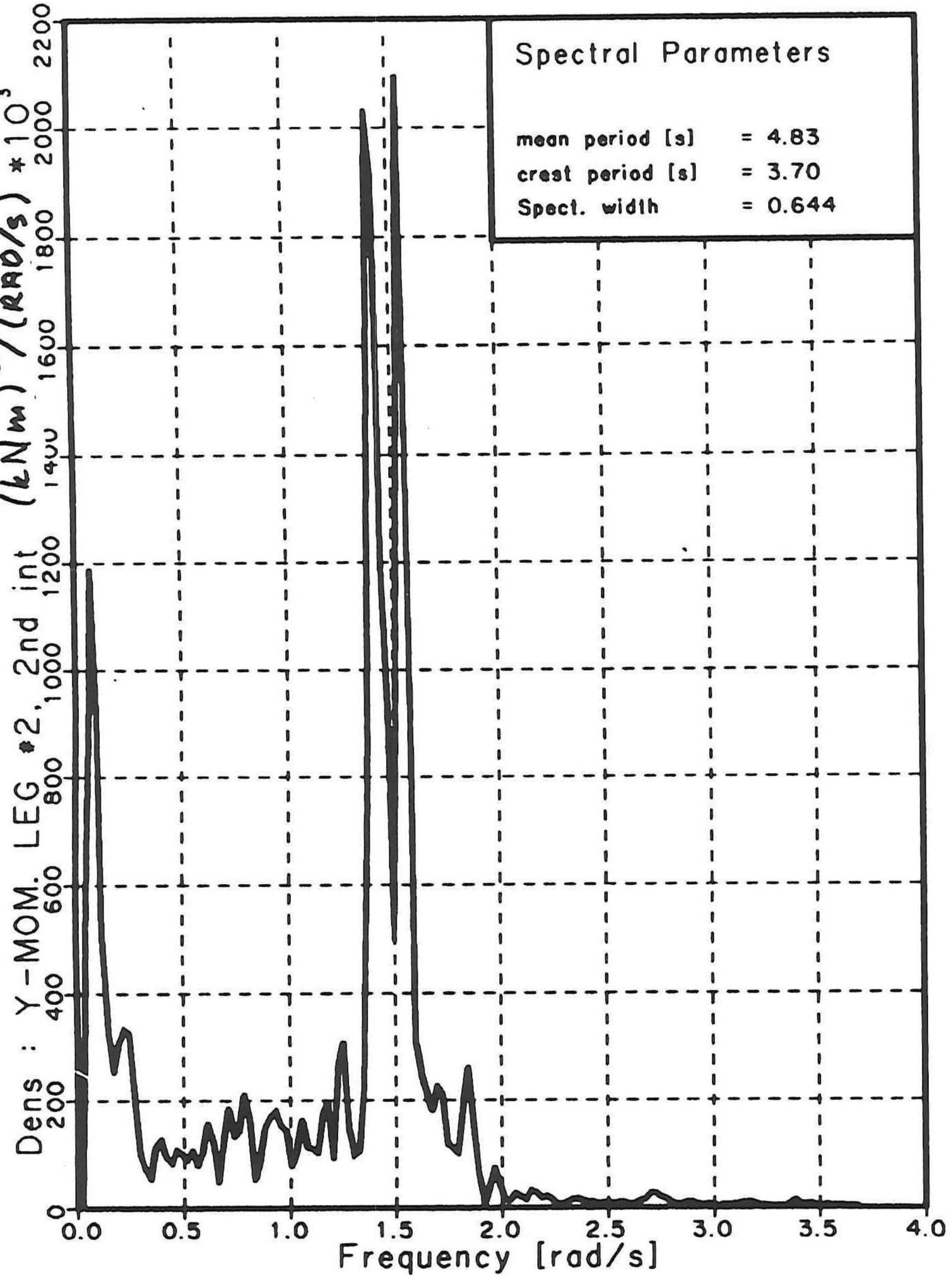

Spectral Density

Y-MOM. LEG #2, 2nd int (kNm)

SIMULATED

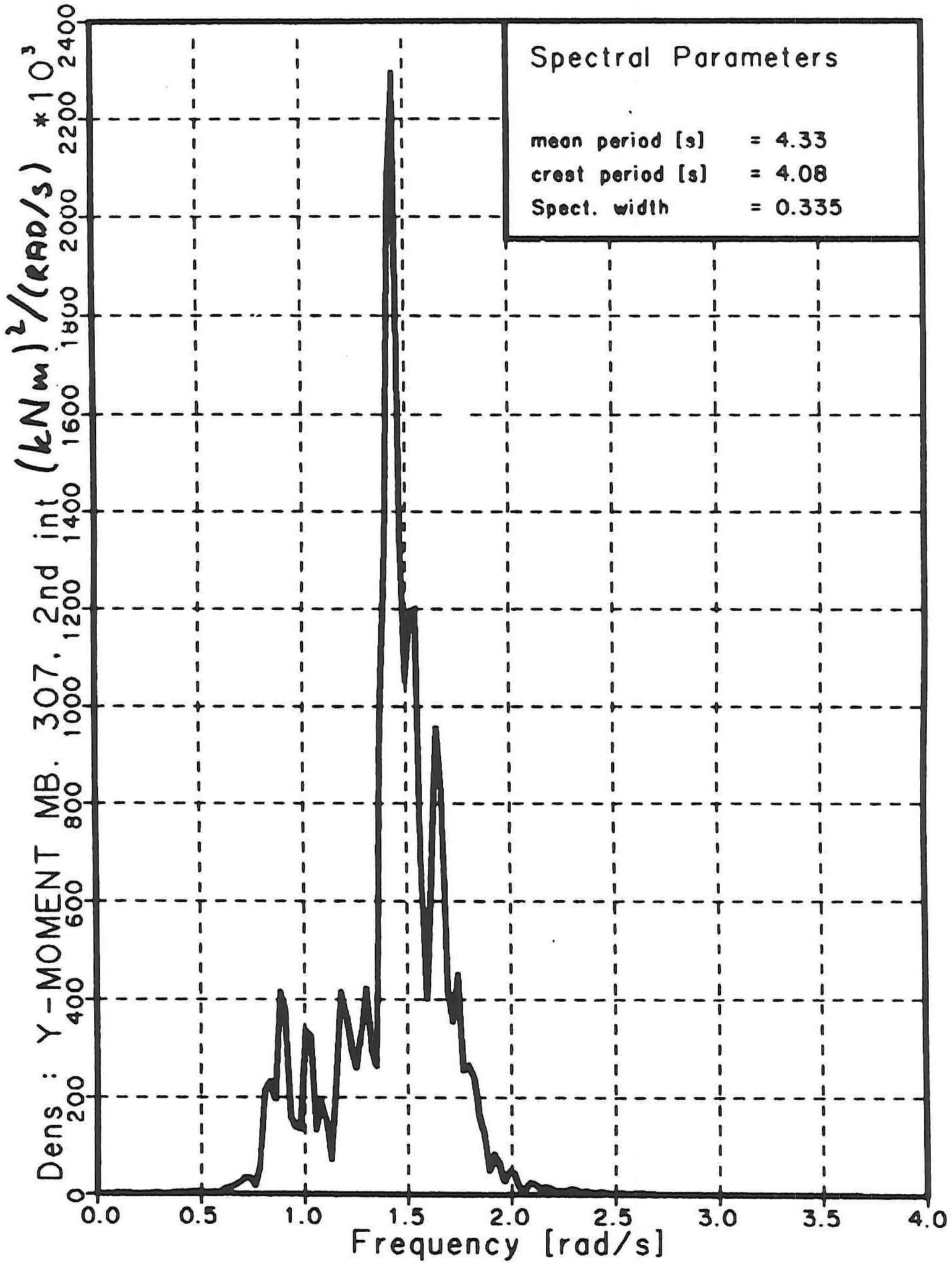

Spectral Density

Y-MOMENT MB. 307, 2nd int (kNm)

Fig. 42 , 2nd. int., leg #2, y moment spectra

MEASURED

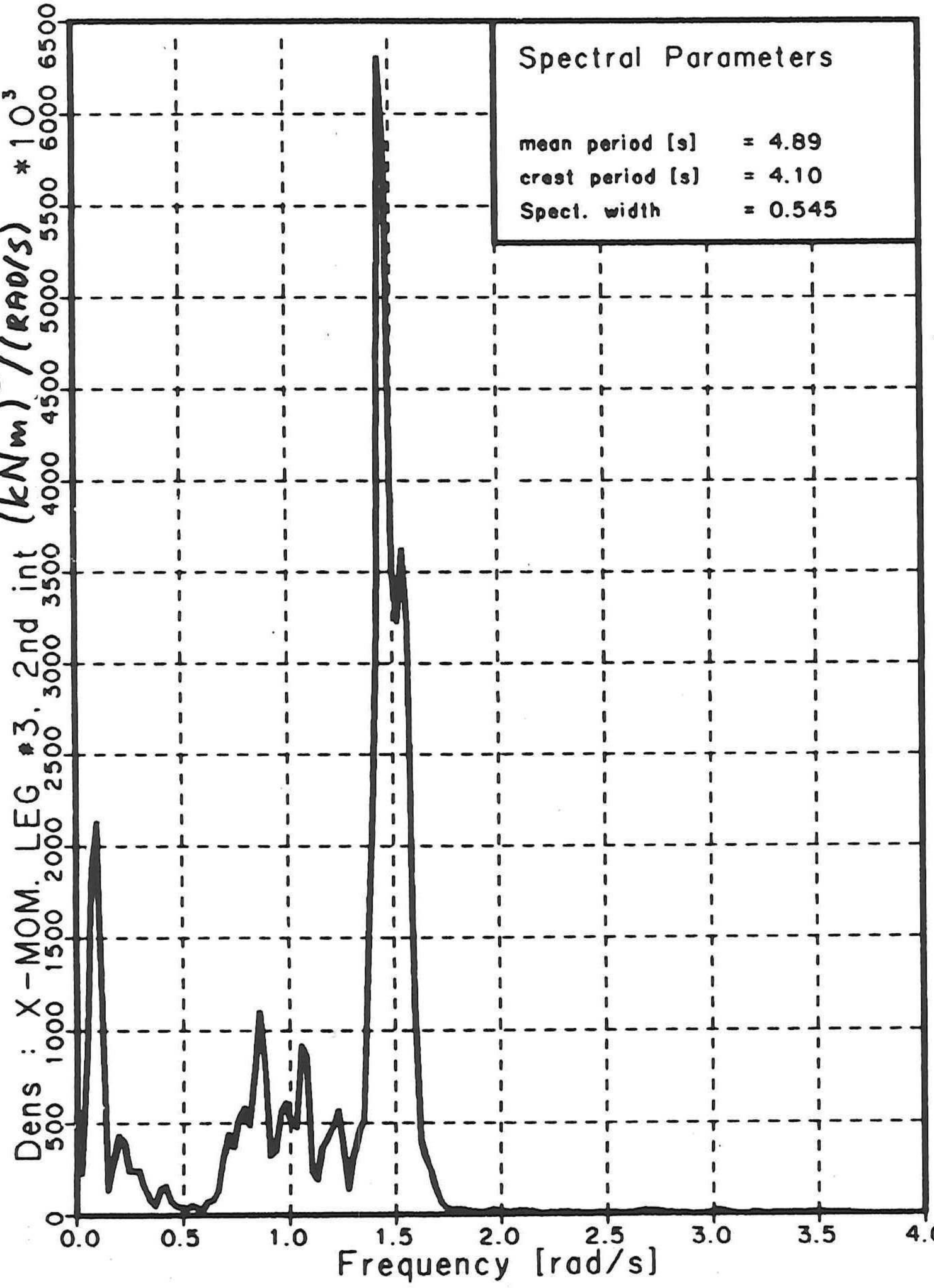

Spectral Density

X-MOM. LEG #3, 2nd int (kNm)

SIMULATED

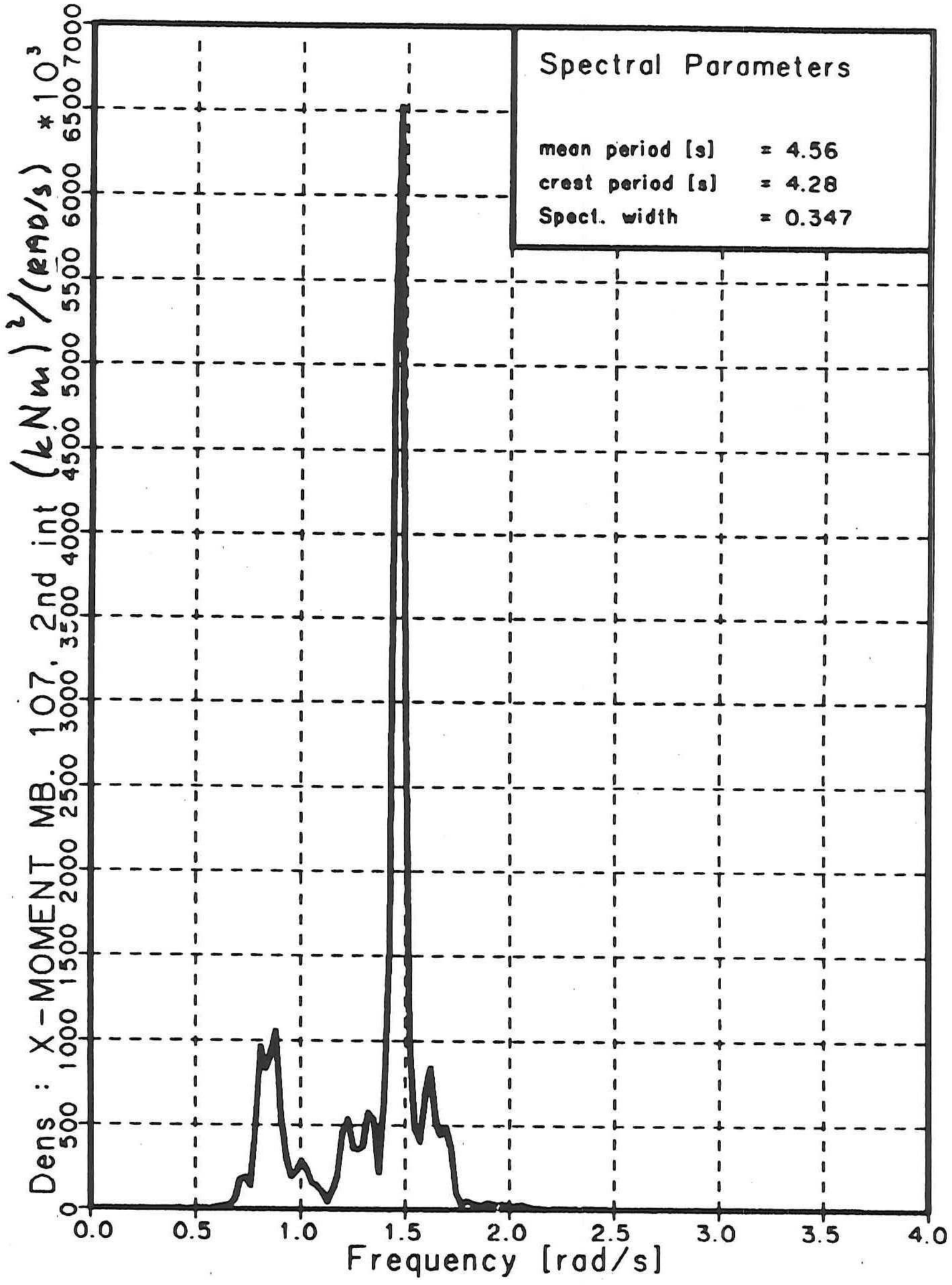

Spectral Density

X-MOMENT MB. 107, 2nd int (kNm)

Fig. 43 , 2nd. int., leg #3, x moment spectra

MEASURED

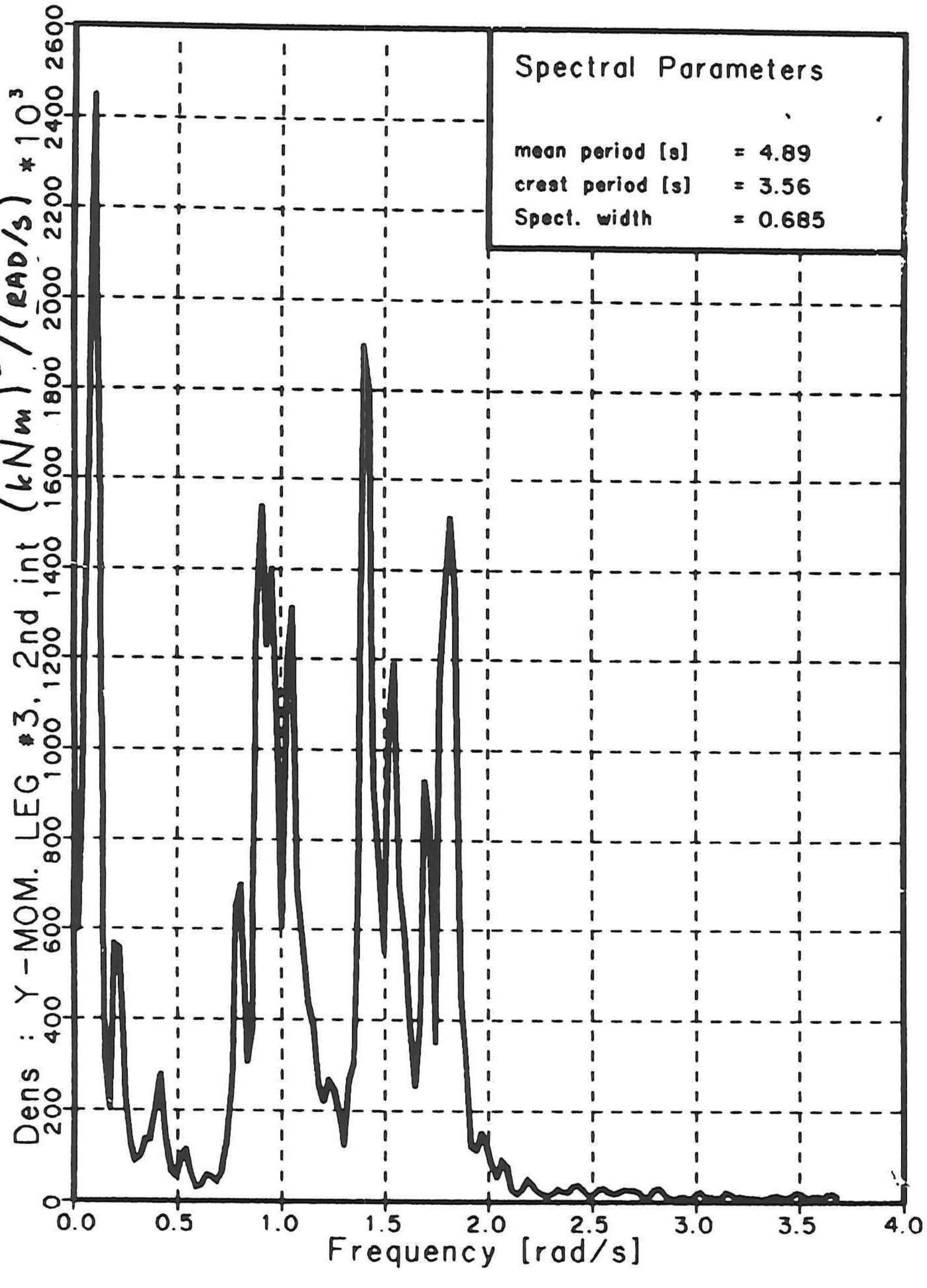

Spectral Density

Y-MOM. LEG #3, 2nd int (kNm)

SIMULATED

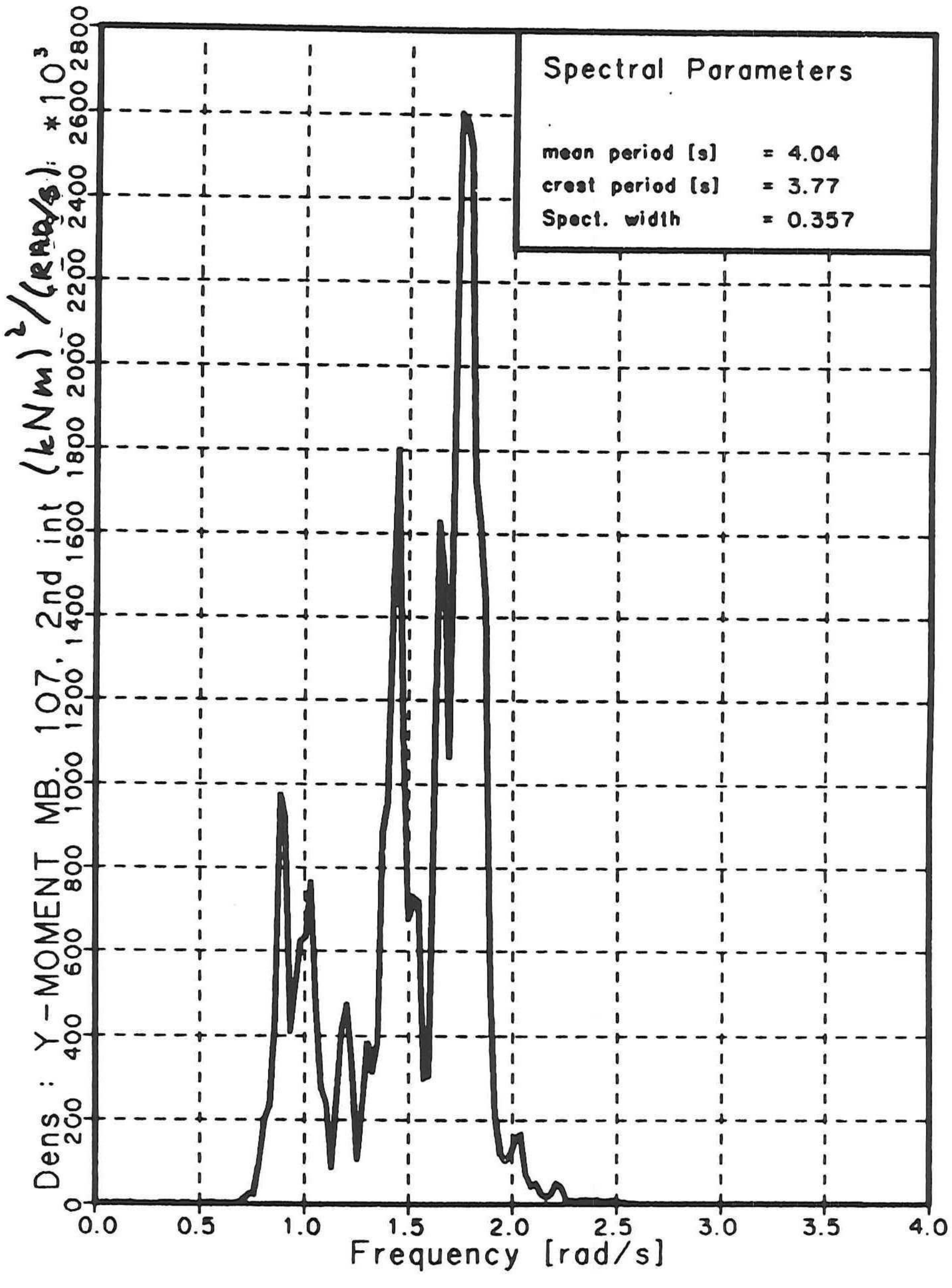

Spectral Density

Y-MOMENT MB. 107, 2nd int (kNm)

Fig. 44 , 2nd. int., leg #3, y moment spectra